FOCUS

ELECTRICAL ENGINEERING SERIES

Advanced Control of AC/DC Power Networks

System of Systems Approach Based on Spatio-temporal Scales

Abdelkrim Benchaib

iSTE

WILEY

Advanced Control of AC/DC Power Networks

FOCUS SERIES

Series Editor Nouredine Hadj-Saïd

Advance Control of AC/DC Power Networks

System of Systems Approach Based on Spatio-temporal Scales

Abdelkrim Benchaib

ISTE

WILEY

First published 2015 in Great Britain and the United States by ISTE Ltd and John Wiley & Sons, Inc.

Apart from any fair dealing for the purposes of research or private study, or criticism or review, as permitted under the Copyright, Designs and Patents Act 1988, this publication may only be reproduced, stored or transmitted, in any form or by any means, with the prior permission in writing of the publishers, or in the case of reprographic reproduction in accordance with the terms and licenses issued by the CLA. Enquiries concerning reproduction outside these terms should be sent to the publishers at the undermentioned address:

ISTE Ltd
27-37 St George's Road
London SW19 4EU
UK

www.iste.co.uk

John Wiley & Sons, Inc.
111 River Street
Hoboken, NJ 07030
USA

www.wiley.com

© ISTE Ltd 2015
The rights of Abdelkrim Benchaib to be identified as the author of this work have been asserted by him in accordance with the Copyright, Designs and Patents Act 1988.

Library of Congress Control Number: 2015944964

British Library Cataloguing-in-Publication Data
A CIP record for this book is available from the British Library
ISSN 2051-2481 (Print)
ISSN 2051-249X (Online)
ISBN 978-1-84821-802-4

Contents

FOREWORD ix

PREFACE xi

LIST OF FIGURES xiii

LIST OF TABLES xvii

INTRODUCTION xix

CHAPTER 1. MODELING CONTROL OF VSCS 1

1.1. Introduction 1
1.2. Steady state voltage control systems – multi-terminal direct current (VSC-MTDC) model 3
1.2.1. Convention 4
1.2.2. DC side model 5
1.2.3. DC power flow calculation 5
1.2.4. AC side model 6
1.3. Control system of VSC based on VOC 8
1.3.1. Inner current controller 10
1.3.2. Outer power controller 11
1.3.3. DC voltage controller 13
1.4. Conclusion 15

CHAPTER 2. TIME SCALE TOOLS: A CONTROL SOLUTION FOR MTDC COMPLEX SYSTEMS WITH PLUG-AND-PLAY REQUIREMENTS 17

2.1. Introduction 17

2.2. Recalling VSC-HVDC control objectives 18
2.3. DC voltage control strategies for MTDC grids 20
2.3.1. Slack bus control (master/slave control) 21
2.3.2. Voltage margin control 22
2.3.3. Droop control 24
2.3.4. Dead-band-droop control 28
2.3.5. Undead-band-droop-control. 29
2.3.6. Priority control 30
2.3.7. Ratio control. 30
2.3.8. DC voltage control strategy summary. 31
2.4. DC grid steady state modeling. 32
2.5. Newton–Raphson technique 35
2.6. DC power flow. 36
2.6.1. The first method: for master/slave control strategy 37
2.6.2. The second method (for a droop control): generalized approach 42
2.6.3. Generalized power flow for multi-terminal DC grids with more than one slack bus. 45
2.7. Steady state control of multi-terminal DC grids 45
2.7.1. Normal operation (without fault). 46
2.7.2. Power-step-change with master/slave strategy of control 48
2.7.3. Voltage margin control 49
2.7.4. Power-step-change for a voltage/power droop control 51
2.8. Primary and secondary control strategies 52
2.9. Dynamic control of multi-terminal DC grids 54
2.10. Plug-and-play in interconnected systems: application to MTDC grids 55
2.11. Control of the actuators connected to the power system. 55
2.12. Concluding remarks 56

CHAPTER 3. FROM SMALL SIGNAL TO EXACT LINEARIZATION OF SWING EQUATIONS 57

3.1. Introduction. 57
3.2. Recalling stability analysis tools 62
3.2.1. Small signal analysis – first method of Lyapunov. 63
3.2.2. Transient stability. 63
3.2.3. Global stability 66
3.2.4. Summary of stability approaches. 66
3.3. Modeling of AC power network – swing equation. 67
3.3.1. Nonlinear swing equation 68
3.3.2. Linearized swing equation 70

3.3.3. Development of the electrical power term . . . 72
3.4. Simulation of AC swing equation . . . 74
3.4.1. Post-fault simulation case (transient response) . . . 77
3.5. Revisited swing equation for multi-machines power system modeling . . . 82
3.6. Exact linearization of swing equation . . . 83
3.7. Concluding remarks . . . 85

CHAPTER 4. SPACE SCALE PROPERTIES FOR AC/DC POWER NETWORK CONTROL AND OPERATIONS: NEW AGGREGATION METHODS IN POWER SYSTEMS . . . 87

4.1. Introduction . . . 87
4.2. Inter-area oscillation damping: locally intelligent substation . . . 88
4.3. Free of space-scale model for AC systems: model reduction . . . 92
4.3.1. Average model for N station multi-terminal systems: aggregated power system . . . 92
4.3.2. Free of space-scale model for inter-region application . . . 94
4.4. Modeling of DC power networks . . . 99
4.4.1. Mathematical approach of two-terminal DC grid modeling . . . 99
4.4.2. Multi-terminal DC (MTDC) grid modeling: generalized MTDC model . . . 101
4.4.3. Toward DC swing equation . . . 102
4.4.4. Development of the electric power term P_e . . . 104
4.4.5. AC and DC "swing equations" equivalence . . . 104
4.5. AC/DC converter control to mimic synchronous generators . . . 105
4.6. Concluding remarks . . . 107

CONCLUSION . . . 109

APPENDICES . . . 113

APPENDIX 1 . . . 115

APPENDIX 2 . . . 117

APPENDIX 3 . . . 121

BIBLIOGRAPHY . . . 123

INDEX . . . 129

Foreword

At the end of the 19th Century, Thomas Edison and Nikola Tesla were very invested in the famous AC versus DC power battle for the power networks development, i.e. *War of the Currents*.

During the 20th Century and today, power networks are mainly based on an AC supply.

Now, at the beginning of the 21st Century, the continuous development of the increasingly renewable energy sources (RESs) interconnected into power networks may reveal the following strategic question:

– *What do we see as the future of AC and DC power networks?*

The author of this book tries to answer this fundamental question to ensure security of the electricity supply in the world by providing an in-depth thinking based on a new approach called "Systems of Systems", using advanced control algorithms. Moreover, the concept of "Plug and Play" is also introduced by the author to satisfy industrial objectives in relation with the development of new electric power grids integrated massive RESs and plug-in electric vehicles (PEVs).

The large experience of the author in R&D in the industry, supplemented by a significant background in academic research and executive teaching, give to this book a particular attractiveness.

The multi-terminal direct-current (MTDC) grids, using power electronics-based systems, are investigated by the author in terms of

modeling, analysis and advanced control in order to define the optimized building blocks requested for "mixed" AC & DC future power networks.

From the theoretical point of view, fully in relation with the stability analysis of AC and DC grids, the equivalence of the AC "swing equation" and the DC "swing equation" is described. This new analytical tool appears as a major added value of the presented works.

This book has also the ambition to bring together the academic and industrial communities in the areas of:

– power networks,

– automatic control,

– power electronics,

– electrical machines,

in order to propose new disruptive technologies to build the future mixed AC and DC power networks.

Many fields of scientific investigations are present in this work and open the door for future debates on transmission and distribution grids, guaranteeing the security of the electricity delivery and minimizing the risk of blackouts.

To conclude, this book is certainly a reference for the advanced control of "mixed" AC and DC power networks in the future.

Prof. Dr. Ing. Jean-Luc THOMAS
Chair Professor in Electrical Engineering
Conservatoire national des arts et métiers, Paris, France
President, European Power Electronics and Drives Association (EPE)

Preface

Nowadays, more than ever, the power engineering domain is facing huge challenges. It is showing an increasing interest in intermittent renewable energies which are imposing major technical limitations. The use of these resources must be accompanied by secure, indigenous, sustainable, clean and competitive operation. A realistic solution is wind power. Many countries are now starting to install wind turbines offshore. In Europe, the offshore wind potential is able to cover seven times the whole demand. High-voltage alternating current (HVAC) provides the simplest and most economic connection method for short distances. Because the distance of the offshore farms exceeds 100–150 km, the transmission with high-voltage direct current (HVDC) is economically inevitable. Thus, HVDC systems offer interesting prospects if the power grid is well controlled.

For power transmission, the DC grid would overlay the existing AC grid, like a national motorway system connects to smaller local road systems. In power distribution, DC grids will emerge from more constrained grid codes as they will be imposed by distribution operators for PV integration. One of the main challenges for DC deployment is the handling of multi-terminal DC (MTDC) grids. At the heart of the thinking behind the MTDC grids is, precisely, the notion of "system of systems". Indeed, a key component of systems of systems control and operations is the notion of time scales. For example, the primary control in AC grids is a global but distributed control in which the notion of "Think Globally and Act Locally" (TGAL) is applied. This time scales control philosophy will enable the "plug-and-play" property which is mandatory when dealing with networked systems. For example, in a flock of birds or school of fish, each individual keeps a certain distance and follows the congener in front. The result is that each individual acts like the

whole group, while the whole group acts like an individual (droop control: global but distributed control). The individual can leave or join the group without altering its global behavior (plug-and-play). In addition to time scales, space scale considerations need to be taken into account with new modeling, control and observation tools and techniques.

Abdelkrim BENCHAIB
July, 2015

List of Figures

INTRODUCTION

I.1. Blackouts in power networks. xix
I.2. Blackout in Western Europe, 4th November 2006: frequency split and resynchronization process (source: ENTSOE) xx
I.3. Challenges for power network of the future xxi
I.4. Cost of HVDC link compared to HVAC xxiii
I.5. New highways for power grid of the future, courtesy of Desertec xxiii
I.6. Power profile provided to the network xxiv
I.7. PV production unit with energy storage system (ESS) xxiv
I.8. DC grid for PV integration with ESS connected to the power grid xxv
I.9. Hybrid (AC and DC) power network of the future. xxvi
I.10. French power network hierarchization xxvii

CHAPTER 1

1.1. Two-terminal VSC system 2
1.2. Power and current directions. 4
1.3. Monopolar symmetrically grounded VSC-MTDC system 5
1.4. Single-phase VSC representation 7
1.5. PQ closed-loop VOC implemented on the dq synchronous frame 9
1.6. Current controller structure – VOC based on dq synchronous frame 10

1.7. V_{dc}-Q closed-loop VOC implemented on the dq synchronous frame 14
1.8. DC voltage control structure 14
1.9. DC voltage droop proportional controller 15

CHAPTER 2

2.1. Time scale control structure for multi-terminal DC grids 18
2.2. Three-terminal HVDC 21
2.3. Illustration of: a) slack bus and b) P-controller 22
2.4. Three-terminal HVDC under master/slave control strategy 22
2.5. Voltage margin strategy illustration 23
2.6. Operating point in voltage margin strategy 23
2.7. A second operating point in voltage margin strategy 24
2.8. Voltage droop characteristics: a) voltage/power and b) voltage/current 25
2.9. Voltage droop characteristics: a) voltage limitation and b) power limitation 28
2.10. Power limitation: a) for a node which is capable of working only as a generator ($P > 0$) and b) for a node which is capable of working only as a load ($P < 0$) 28
2.11. Voltage droop characteristics with dead-band: a) voltage dead-band and b) power dead-band 29
2.12. Voltage droop characteristics with undead-band: a) voltage undead-band and b) power undead-band 30
2.13. Monopolar symmetrically grounded VSC substation connected to an MTDC network 32
2.14. *i, j* connection 33
2.15. Current flowing to the shunt resistance 33
2.16. Geometrical illustration of the Newton–Raphson technique 36
2.17. Chart of the power flow calculation: first method 37
2.18. NR flow chart for the first power flow resolution method 41
2.19. Chart of the power flow calculation with droop characteristics: second method 42
2.20. NR flow chart for power flow calculation taking into account voltage/power droop 44
2.21. Three-terminal DC grid 46
2.22. Three-terminal HVDC before the power flow resolution 46

2.23. Illustration of the power flow results of a three-terminal HVDC 48
2.24. DC grid power response to power disturbance at node 1 with master/slave control strategy 48
2.25. DC grid voltage response to power disturbance at node 1 with master/slave control strategy 49
2.26. DC grid power voltage responses to power disturbance at node 1 with voltage margin control strategy 50
2.27. DC grid power response to power disturbance at node 1 with voltage/power droop control strategy 51
2.28. DC grid voltage response to power disturbance at node 1 with voltage/power droop control strategy 51
2.29. Power balancing of a three-terminal DC grid with primary and secondary control strategies 53

CHAPTER 3

3.1. Wide area monitoring system (WAMS) 58
3.2. PMU-based WAMS and network-model-based EMS hybrid solution 60
3.3. Real power flowing on a major transmission line during the Western North American power system breakup of 1996 61
3.4. Response to a fault cleared in t_{c1} seconds, stable case (left), in t_{c2} seconds unstable case (right) 64
3.5. Three-interconnected generators model with Simpower system 75
3.6. Interconnected generators model (swing equation) with Matlab/Simulink 78
3.7. Post-fault frequency responses of a) Simpower system, b) nonlinear swing equation model and c) linearized swing equation model 79
3.8. Post-fault electrical power of a) Simpower system, b) nonlinear swing equation model and c) linearized swing equation model 80
3.9. Post-fault angle differences of a) Simpower system, b) nonlinear swing equation model and c) linearized swing equation model 81
3.10. Three-node interconnected AC power network 82
3.11. Simulation results for a nonlinear model and linearized model 85

CHAPTER 4

4.1. Simulation results of the linear model without/with command 91
4.2. Simulation results for the three-machine system and average model 94
4.3. Interconnection of two power systems – regions r_1 and r_2. 95
4.4. Power transfer between regions 1 and 2 (nonlinear model) 97
4.5. Power transfer between regions 1 and 2 (average model) 97
4.6. Frequency (rd/s) in region 1: nonlinear model a), average model b) 98
4.7. Frequency (rd/s) in region 2: nonlinear model a), average model b) 98
4.8. Time derivative of the frequency in regions 1 and 2 98
4.9. Two-terminal DC grid 99
4.10. Three-terminal DC grid 101
4.11. DC station 102
4.12. Two-terminal DC grid for electric power term calculation 104
4.13. Power part of a synchronverter – a three-phase inverter, including LC filter 106
4.14. Electronic (control) part of a synchronverter 106

CONCLUSION

C.1. School of fish 111

APPENDIX 3

A3.1. Simulation of generator (2) with Simpower system 121
A3.2. Power flow computation with PowerGUI 122

List of Tables

CHAPTER 2

2.1. Summary of the control strategy gain settings 31
2.2. Lineic resistance and the length of the cables (links) 46
2.3. DC power injections and DC voltage values at different nodes 47
2.4. Transmitted DC power between the connected nodes 47
2.5. Power losses in the shunt resistance at the different nodes 47

CHAPTER 3

3.1. Summary of stability approaches 67
3.2. Generator parameters 76
3.3. Transformer parameters 76
3.4. Transmission line parameters 76
3.5. Load parameters 76

CHAPTER 4

4.1. Simulation data for three interconnected machines 94
4.2. Simulation scenario for inter-region connection 97
4.3. Similarities between AC and DC systems 105

Introduction and Problem Positioning

I.1. Today's power network conditions

Operating closer to their limits, AC power grids are more vulnerable and subject to instabilities than ever before. Controlling and operating them with a given degree of reliability will be our main challenge in power networks of the future. The warning signs are shown in Figure I.1.

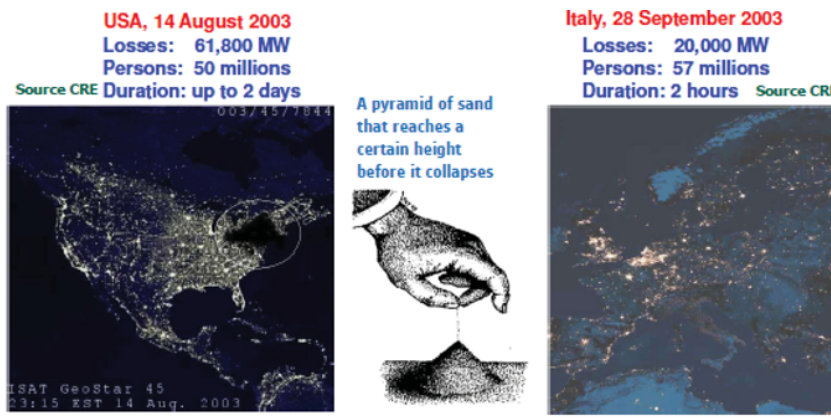

Figure I.1. *Blackouts in power networks*

In 2003, blackouts cost the US economy $6 billion. In the same year, they were responsible for four deaths in Italy. The power failures across Western Europe in 2006 caused by a transmission line shutdown in Germany underlined the risks of outages crossing national boundaries (see [ALS 14] and references therein).

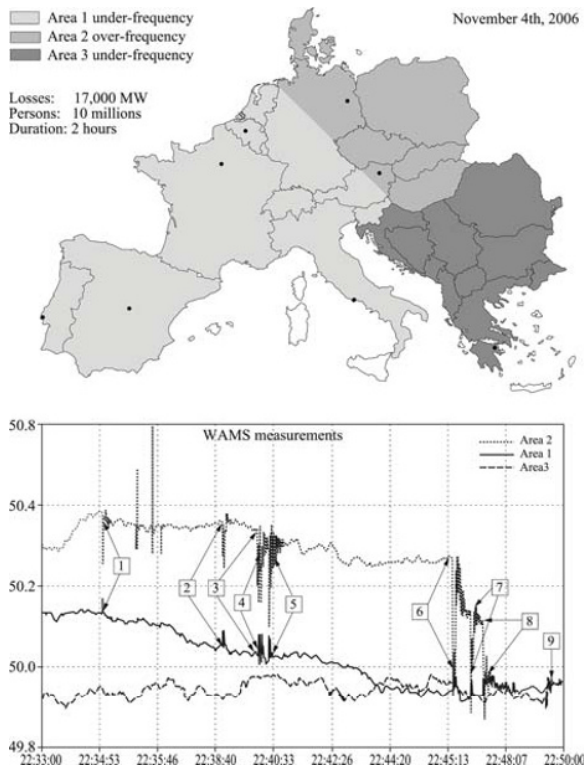

Figure I.2. *Blackout in Western Europe, 4th November 2006: frequency split and resynchronization process (source: ENTSOE)*

During this latter event, the UCTE grid was split into three islands at different frequencies. In the 2 hours, it took to resynchronize, some 15 million people were affected, and some 17,000 MW of power generation had to be curtailed.

Yet a certain school of thought contends that blackouts are natural network behavior: "It's like a pyramid of sand that reaches a certain height before it collapses, because that's the nature of sand (see Figure I.1 and references in [DOB 12]). There have been serious attempts to develop blackout prevention strategies, but blackouts and brownouts still occur and will continue to do so. Prevention is merely containment." Sooner or later, the variety and complexity of loads and operations will reach AC network limits.

I.2. AC power network capabilities for more renewable energy penetration

The European Commission's energy trends show an exponential rise in energy demand from 2,800 TWh per year today to nearly 4,000 TWh by 2030. Electricity is the fastest rising demand – up 58% by 2030 and accounting for nearly 25% of the total energy demand. Higher production will require stronger protection, particularly as increasingly renewable energy sources (RESs) flow into the grid. Total gross RES power generation – under 500 TWh in 2009 – will reach almost 1,400 TWh by 2030. Ultimately, only a grid with a far higher power transmission capacity will be able to cope with burgeoning consumption, production and protection.

The integration of these large intermittent and stochastic quantities of RES power generation into power networks operating at their limits will heavily affect the stability and, consequently, will increase the probability of blackouts occurring.

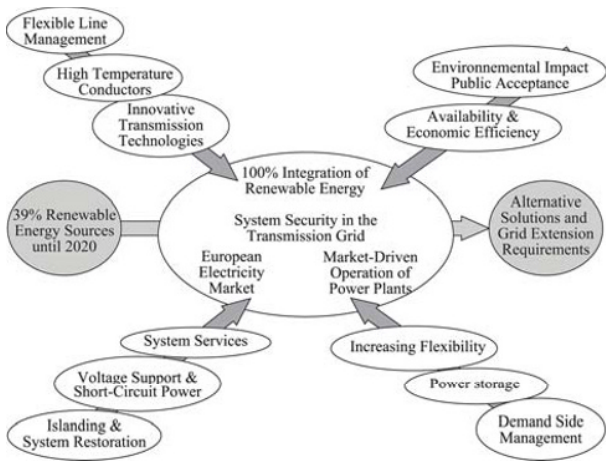

Figure I.3. *Challenges for power network of the future*[1]

In order to guarantee the network stability and consequently its availability, the grid operators impose rules and standards to all connected actors to the power network. This will be the case for power network of the

1 http://www.dena.de/en/publications/energy-system/dena-grid-study-ii.html.

future, whose main challenges are given in Figure I.3. At the systems level, the integration (or connection) standards describing the performances of the production units as well as their interaction with the power system are established by network operators. Those standards concern the connection constraints, manufacturing, modeling, tests, monitoring, as well as control and operations of production units (units commitment). Nowadays, the RES connection standards exist at national and/or operators levels.

Based on their own experience or other operators, many countries or electricity companies have updated their connection codes, or developed standard documents specifically to satisfy the connection requirements for wind farms and photovoltaic (PV) productions in order to increase these RES penetrations in a reliable manner.

Some supplementary speculations are under discussion (for example, high voltage ride through (HVRT) or inertial responses). Of course, these additional specifications will impose constraints on power operators, but at the same time increase the pressure and costs on the actors who will want to connect to the power network. The connection codes which are applied today to transmission networks will necessarily be needed for distribution networks and even for residential power grid (low voltage).

However, the hardening of these connection standards will constitute a great opportunity for power electronics-based converters and measurement sensors manufacturers, as well as control and communication solution providers

I.3. The future gird: toward DC grid development

I.3.1. *HVDC for electrical power transmission: integration of offshore wind energy*

From an economical point of view, the high voltage direct current (HVDC) seems the most efficient solution when the offshore distance is over 50 km.

In order to optimize the connection costs and increase the reliability of the system, an association of wind production sources could be considered giving birth to a multi-terminals meshed DC grid. Other RES types could be connected via a DC power grid making the new highways for power networks of the future (see Figure I.5).

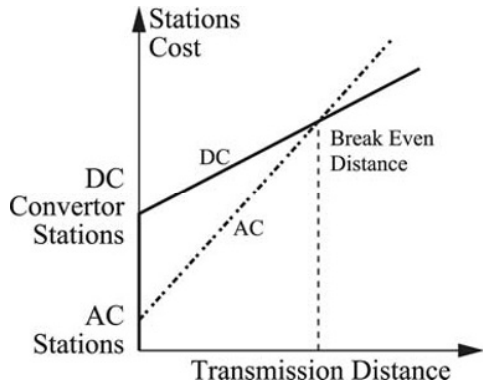

Figure I.4. *Cost of HVDC link compared to HVAC*

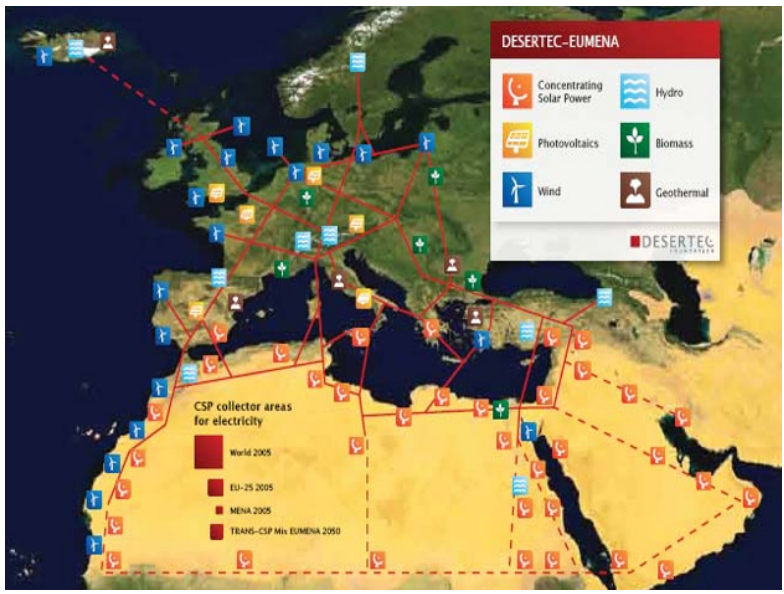

Figure I.5. *New highways for power grid of the future, courtesy of Desertec. For a color version of the figure, see www.iste.co.uk/benchaib/control.zip*

I.3.2. *MPDC for electrical power distribution: PV integration*

In the medium power direct current (MPDC) system, and due to the hardening of the grid connection codes, PV production unit owners will

probably consider the use of storage system in order to cope with these new requirements (as asked in the call for tenders provided by the *Commission de Régulation de l'Énergie* (CRE) for islanded power network for production units over 250 kWC), as shown in Figure I.6. It was requested to start injecting power into the AC network before the start of the PV production (before sunrise) and continue injecting the power after the sun sets (t3). In normal operation, the power should be maintained at 40% of the nominal power. It is obvious that a storage system is needed in order to address such requirements.

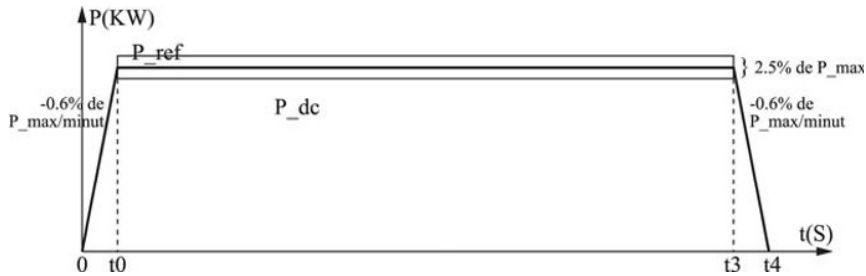

Figure I.6. *Power profile provided to the network. For a color version of the figure, see www.iste.co.uk/benchaib/control.zip*

The configuration given in Figure I.7 is then imposed by the connection requirements in which the storage system becomes mandatory.

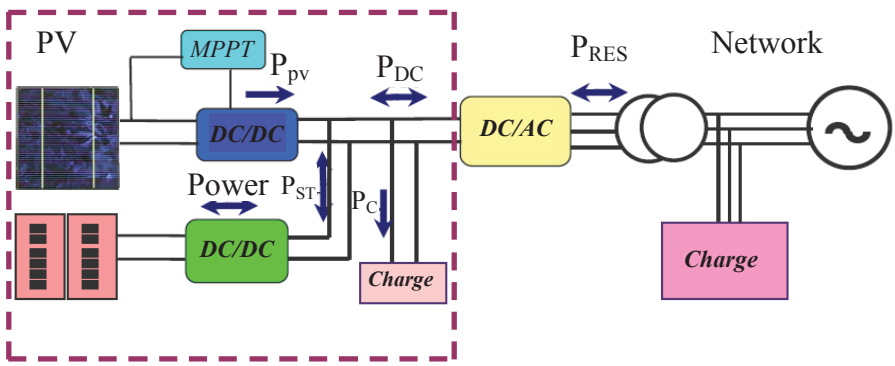

Figure I.7. *PV production unit with energy storage system (ESS)*

The association of PV and ESS could constitute the foundation for medium voltage direct current (MVDC).

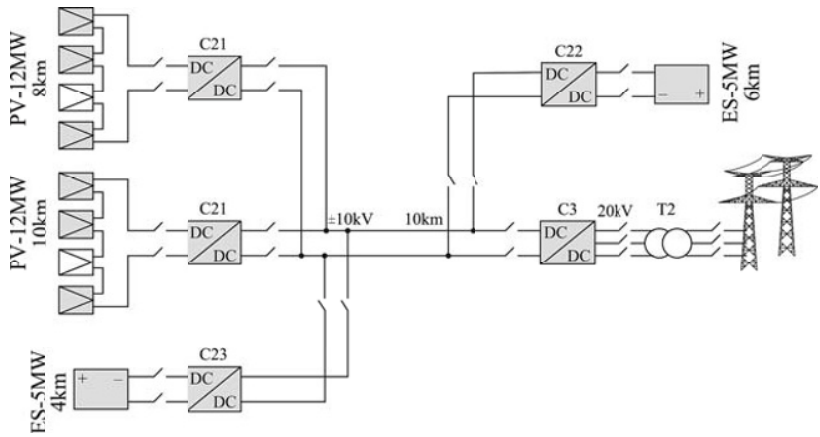

Figure I.8. *DC grid for PV integration with ESS connected to the power grid*

In order to decrease the PV energy connection cost and facilitate its penetration, an energy storage system sharing between production units could be considered, as shown in Figure I.8. For an equivalent cost of installation with an AC connection, the configuration given in Figure I.8 allows to fulfill the existing grid code requirements and anticipate the constraint related to the inertia response which could rise in the near future.

I.3.3. *DC grid deployment*

The future power networks will be developed at first with high voltage DC (HVDC) system in order to connect the offshore wind energy. However, MPDC will be proposed more specifically for PV systems and also for storage, car charging and other applications, as shown in Figure I.9.

However, in order to address the future requirements for power networks, such as reliability and performances, bigger integration amounts of renewable energy and availability of new components, a huge R&D effort needs to be performed.

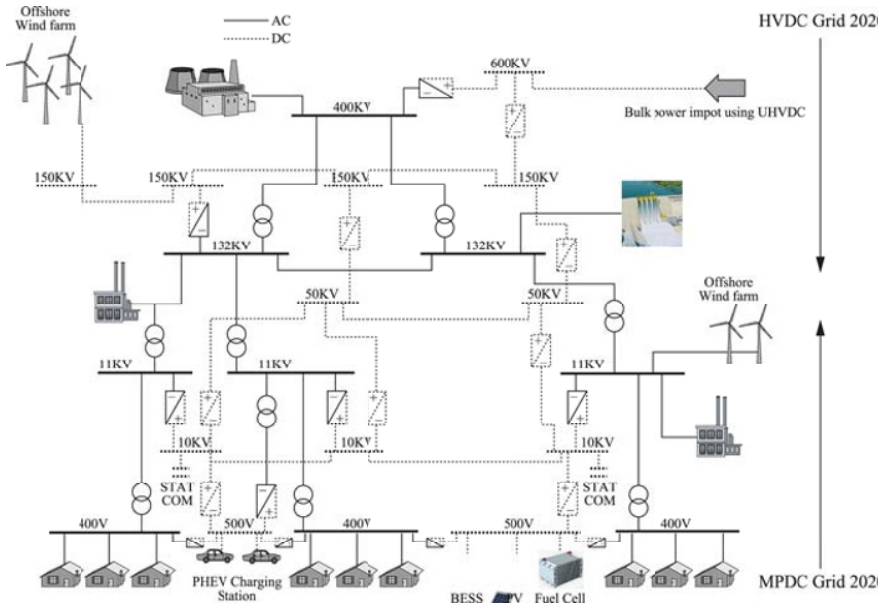

Figure I.9. *Hybrid (AC and DC) power network of the future. For a color version of the figure, see www.iste.co.uk/benchaib/control.zip*

I.4. DC system of systems: time and space scale tools for power network control

In an informal way, time and space scales tools have already been used for the control of the AC power system. A natural analogy appears between the AC frequency and the DC voltage since they both reflect the power balance in the grid. However, attention must be given to the fact that different frequencies at different points in an AC system indicate transient processes, while the DC voltage at each node is not the same in steady state due to the power flow.

In the same way, an analogy can be made between the aforementioned DC voltage control strategies, especially the DC voltage droop, and the primary speed control action used in AC generators, since they aim to restore the power balance of the network by acting locally following given characteristics, even if the "global" variable (frequency/DC voltage) strays from its specified value.

Local [BAC 14] and then distributed control will enable adjustments at different hierarchical levels and at different timescales to take place across the entire network. Indeed, a key component of system of systems thinking is the notion of scale. Flexibility comes from the ability to switch from long time scales and large space scales to small space scales, then back again. It should be possible to add a load to a system or to remove it without destabilizing the system in the DC power network of 2030, all of which points to the tantalizing prospect of plug-and-play. AC networks, of course, have that plug-and-play capability, developed piecemeal over the years. However, with mass RES, their control systems are unlikely to be able to cope.

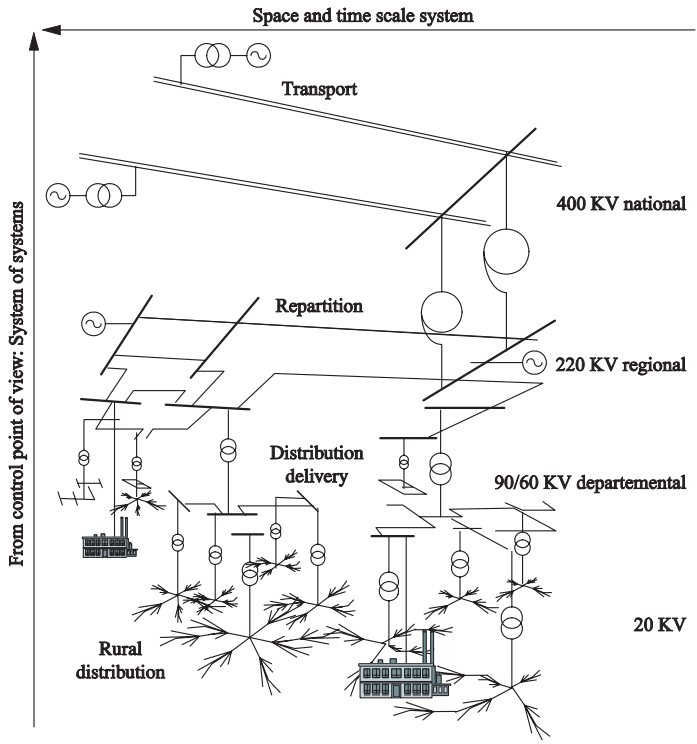

Figure I.10. *French power network hierarchization (source: CRE)*

The time-dynamic response of the primary control should therefore be slower (longer timescale) than the controller of the converter, which is around a few milliseconds. This primary control "time constant" will not depend only on the reactivity of the converter but also on the power injection

ability of all connected nodes (production, storage, loads, etc.), which theoretically should be from a few hundred milliseconds to a few seconds, as for AC systems. Primary control is global but distributed. A primary control strategy that has proved itself in AC grids is the so-called droop control technique. This could be applied for multi-terminal DC (MTDC) power grids.

The section gives a quick overview of the research program to be developed through the next years in order to control new MTDC grid system and then to extend it in order to tackle the hybrid AC and DC power network. By applying a "system of systems" approach with its time and space dimensional aspects, new modeling, control and observation tools will be proposed to satisfy the requirements of such a huge and complex system.

I.5. Book organization

At the beginning of each chapter, some relevant literature reviews are undertaken in order build the context of the proposed results. The proposed book is organized as follows:

– In Chapter 1, modeling and control of VSC converters will be addressed taking into account future conditions and constraints for multi-terminal configuration. First of all, the DC side model will be built, followed by the DC power flow calculation, and then the steady state AC side model will be presented to obtain a VSC average model. Finally, control structures of VSC converters for MTDC grids taking into account normal as well as disturbed operations will be proposed considering only vector oriented control (VOC) methods.

– Chapter 2 will be organized in three main parts. The first part will review the principles, tools and control strategies present in the literature and necessary for the control of MTDC grid. The second part will concern some recent results on the control of the DC grid. Implementation and simulation of different control strategies in spite of power disturbance for the MTDC grid will be highlighted. Finally, primary and secondary control strategies for MTDC grids will be proposed. The third part concerns the present and future research activities in the area of multi-time scales-based control of MTDC grids. Next, an initial study of dynamic control of MTDC grids will be given. Thereafter, plug-and-play properties of networked systems will be

proposed. Finally, control of actuators for power network are shortly discussed.

– In Chapter 3, we recall stability analysis tools. Thereafter, a detailed modeling of AC power network dynamics with swing equations will be derived. Next, an exact linearized model for swing equation will be proposed. It is one of the main results presented in this book.

– In Chapter 4, space dimensions of power networks will be addressed. Then, considering the new expression of the swing equation, an inter-area oscillations damping controller will be proposed. Thereafter, the free of space-scale model for an AC system will be given using new averaging-based technique. The second aspect of the considered chapter is the modeling of DC technology as what has been developed for AC systems. Finally, and in order to have a global view of interconnected AC and DC power systems via converters, a proposed technique proposed in the literature for VSCs will be discussed. It should be noted that the cited references are selected due to their vicinity to the proposed state of the art. This is a non-exhaustive list and for more details, the reader should refer to the references in the papers, books and reports given at the end of the book.

– Finally, Chapter 5 will highlight some concluding remarks and the research direction proposed by the author.

1

Modeling Control of VSCs

1.1. Introduction

In recent years, the technical possibility has matched the market opportunity given that the National Energy Policies (associated with the exploitation of renewable energy sources) and the Electricity Sector Reforms (deregulation) demand higher efficiencies, such as power flow (PF) control capabilities and growing interconnections, with asynchronous features for more economic or reliable system operation.

Under this scenario, the widely deployed alternating current (AC) transmission technology presents limitations, since higher efficiencies, PF control capabilities and growing interconnections with asynchronous features are required for a more economical and reliable system operation [HAM 00]. Moreover, the long-distance bulk-power transmission and the synchronous connections between AC networks are claimed to deteriorate the overall dynamic behavior of the AC systems, while the submarine cable crossing length is limited by the management of the reactive power [HAM 00].

These applications among others, together with the development of power semiconductors, microprocessors and new insulation materials, have spurred the advancement of high voltage direct current (HVDC) technology as an alternative for power transmission [BAH 07], notwithstanding the technological challenges that remain, such as the improvement of Direct Current (DC) breakers and cables rating.

More recently, the advent of the high-power insulated gate bipolar transistor (IGBT) and its turn-off capability has given rise to a new converter technology: the voltage source converter (VSC) or forced-commuted

Advance Control of AC/DC Power Network: *System of Systems Approach Based on Spatio-temporal Scales*, First Edition. Abdelkrim Benchaib.
© ISTE Ltd 2015. Published by ISTE Ltd and John Wiley & Sons, Inc.

converter (FCC) that is capable to provide reactive power support and control the active PF, the reason why it is considered to outmatch its predecessor, the well-known current source converter (CSC) or line-commuted converter (LCC) [FLO 09].

Traditionally, when considering an HVDC link, only two converters are taken into account, connected through a DC cable. In this scenario, significant research has been carried out, such as [BAJ 08a] and [BON 06]. A basic configuration of a VSC-based HVDC transmission system is presented in Figure 1.1, where the converter is represented by a six-pulse bridge equipped with self-commutating switches and diodes connected in antiparallel.

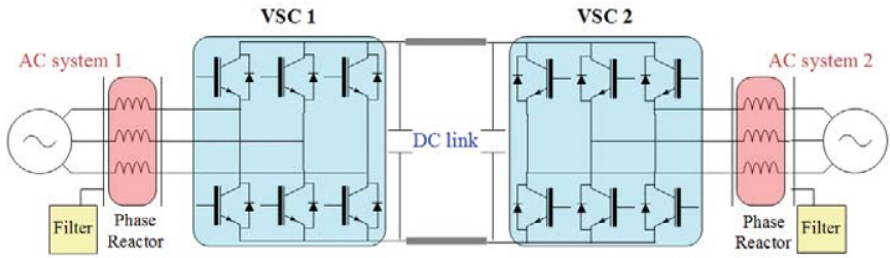

Figure 1.1. *Two-terminal VSC system*

It is worth mentioning that this point-to-point connection may be achieved using both aforementioned technologies (CSC and VSC). Nevertheless, an outstanding difference, from the control point of view, appears. When thyristor-based converters (CSC) are used, only one degree of freedom is available at each terminal and its operating principle is based on keeping a constant DC current (reason why it is called CSC), while both magnitude and direction of the PF are controlled by changing the magnitude and direction of DC voltage as the control system acts through firing angle adjustments of the valves and through tap changer adjustments on the converter transformers [BAJ 08a]. Thus, the power reversal in CSC-based HVDC links is obtained by reversing the polarity of the direct voltages at both ends, which represents an issue when considering multi-terminal operation [BAJ 08a].

In contrast, VSC converters offer two degrees of freedom at each terminal, which allows the independent control of the active and reactive power. Moreover, each converter can be used to synthesize a balanced set of

three phase voltages like inertia-less synchronous machine, provided that the DC voltage is free from oscillations during disturbances and fault occurrences on the AC sides of the VSC-HVDC stations [HAI 08].

Furthermore, unlike conventional HVDC transmission (CSC), the transistor-based converters (VSC) themselves have no reactive power demand and can actually control their reactive power to regulate AC system voltage. The dynamic voltage support of the AC voltage offered at each VSC terminal improves the voltage stability and can increase the transfer capability of the sending and receiving AC systems without much need for AC system reinforcement.

Moreover, the PF direction in the VSCs is controlled by changing the direction of the current, which makes them suitable for multi-terminal operation.

In this chapter, modeling and control of VSC converter will be addressed taking into account future conditions and constraints for multi-terminal configuration.

1.2. Steady state voltage control systems – multi-terminal direct current (VSC-MTDC) model

The steady state of a system refers to an equilibrium condition, where the effect of transients is no longer relevant. In power systems, any specific steady state operating point can be determined through an analytical technique called PF analysis (also known as load-flow), where the loads are modeled as bulk power delivery points and the voltages of the transmission network can be determined [KUN 94].

An analogous study for a VSC-MTDC system was conducted in [BEE 12]. The DC power flow (DC PF) calculation can be used to find the starting point for dynamic analysis, considering that the VSC-MTDC system is operating under a centralized DC voltage control such as master/slave (M/S), where only one converter (known as slack converter) is designated to keep the DC voltages in a close band around its rated value through active power compensation.

Once more, an outstanding difference between the AC and DC systems must be kept on sight. In an AC transmission system, where the line

resistances are neglected given the inductance higher values, the active PF is dominated by the angle differences between different buses, while the reactive PF is mainly associated with the voltage magnitude deviation of different nodes [KUN 94].

When considering a DC grid, there is no reactive PF; therefore, the PF calculation is solely concerned with the active power, which, contrary to the AC case, is dictated by the differences in the voltage magnitudes between the different nodes. Another specification of the DC grid is the absence of the frequency; hence, only resistances are introduced in the nodal admittance matrix (Y_{dc}).

In the following, the selected sign convention is defined. Afterward, the DC side model is built, followed by the DC PF calculation. Then, the steady state AC side model is presented, where the filter and other station equipment are not considered, and the VSC is represented by its average model, approximation consistent with the phenomena of interest. Finally, control structures of VSC converters for multi-terminal DC grids taking into account normal as well as disturbed operations will be proposed. For the sake of understanding, vector control method will be used with adequate references.

1.2.1. *Convention*

DC power and current are assumed to be positive when they are flowing away from the VSC, as shown in Figure 1.2. Therefore, DC power (and current) are considered as positive when they are being injected into the DC grid.

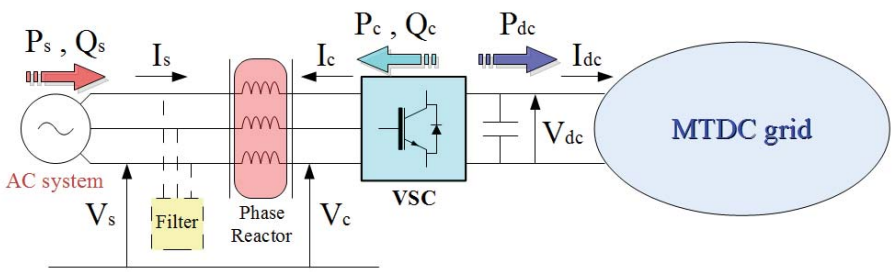

Figure 1.2. *Power and current directions*

1.2.2. *DC side model*

In steady state, the DC network is modeled by the link resistances (R_{ij}). It is a common practice to add a shunt resistance to represent the converter losses as shown in Figure 1.3.

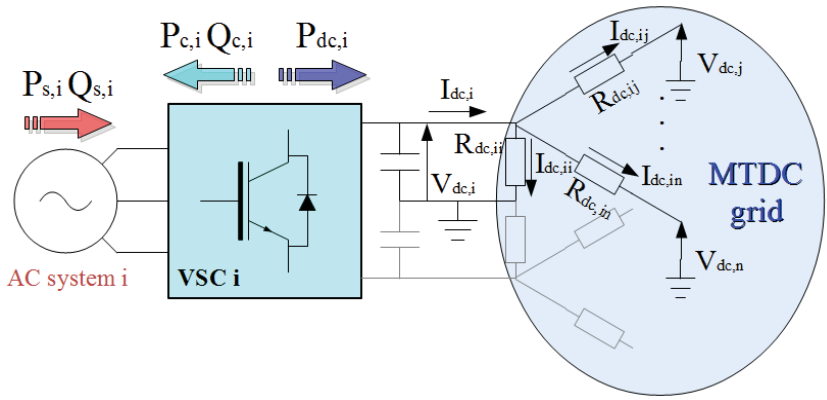

Figure 1.3. *Monopolar symmetrically grounded VSC-MTDC system*

In a MTDC system of n DC nodes, the current injected in a node i is calculated as the sum of all the currents flowing to the other (n-1) interconnected nodes and the current going into the shunt resistance ($R_{dc,ii}$), as written in equation [1.1].

$$I_{dc,i} = \left(\sum_{\substack{j=1 \\ j \neq i}}^{n} \frac{1}{R_{dc,ij}} \cdot (V_{dc,i} - V_{dc,j}) \right) + \frac{V_{dc,i}}{R_{dc,ii}} \qquad [1.1]$$

1.2.3. *DC power flow calculation*

The active power in each node is the product of its DC voltage and DC current. For a monopolar symmetrically grounded converter, as the one shown in Figure 1.3, and for bipolar converters the power injection is given by equation [1.2].

$$P_{dc,i} = 2V_{dc,i}I_{dc,i} \qquad [1.2]$$

Substituting equation [1.1] into [1.2], it is possible to calculate the power injection into each DC node, when the DC voltage values are known beforehand as shown in equation [1.3].

$$P_{dc,i} = 2V_{dc,i} \cdot \left(\left(\sum_{\substack{j=1 \\ j \neq i}}^{n} \frac{1}{R_{dc,ij}} \cdot (V_{dc,i} - V_{dc,j}) \right) + \frac{V_{dc,i}}{R_{dc,ii}} \right) \quad [1.3]$$

However, in a VSC-MTDC system under a centralized DC voltage control (M/S), the DC voltage is only known for the slack converter, while it remains as an unknown in the other nodes where the VSCs are operating in a constant active power injection mode ($P_{dc,i}$ known); giving rise to a nonlinear equations system that should be rewritten as equation [1.4].

$$Y_{dc}\mathbf{V_{dc}} - \left[\frac{P_{dc,i}}{2V_{dc,i}} \right] = 0 \quad [1.4]$$

where Y_{dc} is the DC nodal admittance matrix, since

$$\mathbf{I_{dc}} = Y_{dc}\mathbf{V_{dc}} \quad [1.5]$$

The solution of the equation system given in equation [1.4] gives the power injection at the slack converter and the DC voltages of all the VSCs operating in a constant active power injection mode. Therefore, after performing the DC power flow (PF), the voltage and active power injection of all the DC nodes in the MTDC grid will be perfectly specified.

1.2.4. *AC side model*

VSC converters are considered to be connected to the AC system through a phase reactor as shown in Figure 1.4. It is a common practice to include a transformer, but for the purposes of this study (where filters and other station equipment are not model), its representation is omitted.

The phase reactor is represented by a resistance (R_{pr}) and an inductance (L_{pr}). In the following, the perunit system is adopted as defined. The basic equation of this circuit, following the Kirchhoff's voltage law (KVL), is:

$$V_c - V_s = R_{pr} I_c + L_{pr} \frac{dI_c}{dt} \qquad [1.6]$$

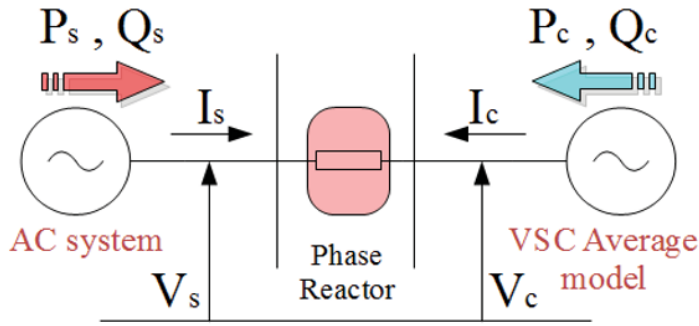

Figure 1.4. *Single-phase VSC representation*

HYPOTHESIS.–

– If a balanced three-phase system is considered, equation [1.6] can be transformed into a rotating *dq0* reference frame, using the Park–Clarke transformation (P) defined as:

$$P = \frac{2}{3}\begin{bmatrix} \cos(\theta) & \cos\left(\theta - \frac{2\pi}{3}\right) & \cos\left(\theta + \frac{2\pi}{3}\right) \\ -\sin(\theta) & -\sin\left(\theta - \frac{2\pi}{3}\right) & -\sin\left(\theta + \frac{2\pi}{3}\right) \\ \frac{1}{2} & \frac{1}{2} & \frac{1}{2} \end{bmatrix}$$

Such that, in steady state,

$$V_{cd} - V_{sd} = R_{pr} I_d - X_{pr} I_q \qquad [1.7]$$

$$V_{cq} - V_{sq} = R_{pr} I_q + X_{pr} I_d \qquad [1.8]$$

– Then, if the converter losses are not considered ($R_{ii} = \infty$),

$$P_c = -P_{dc} \quad [1.9]$$

– And the phase reactor resistance and losses are neglected,

$$P_c = -P_s \quad [1.10]$$

The active power at the system node and both sides of the VSC are the same.

– Moreover, if the AC system voltages (V_s) are considered as known (from the AC PF).

– The voltage-oriented control (VOC) method [TEO 11] is applied ($V_{sq} = 0$):

$$P_s = \frac{3}{2} V_{sd} I_{sd} \quad [1.11]$$

$$Q_s = -\frac{3}{2} V_{sd} I_{sq} \quad [1.12]$$

If the active and reactive powers injected by any AC system are defined as set points by the associated transmission system operators (TSO); then, the converter's AC side currents (I_d and I_q) can be determined by equations [1.11] and [1.12], since no filter is considered (thus, I_s = - I_c). Finally, the converter's AC side voltages (V_{cd} and V_{cq}) are given by equations [1.7] and [1.8].

1.3. Control system of VSC based on VOC

In response to the forthcoming massive renewable energy integration, which will be connected to the existing AC electrical network through power converters, great efforts have been devoted to the development of a greater performing control system that, alongside others, will contribute to mitigate the inherent problem of intermittent but clean renewable energy sources (RES).

In the literature, special attention has been given to the controllers design, including classical proportional integral (PI), hysteresis regulators and the development of customized adaptive algorithms [MIL 13, CHA 13]. Also, robust nonlinear control techniques based on Lyapunov and backstepping

methodologies have been proposed, in which the system decoupling is obtained via a cascade structure and using the inherent time scales of the studied system [ELO 06]. Finally, the dead-beat (DB) control including current and voltage limitations has been suggested when high dynamic response is mandatory [BEN 04].

Additionally, available control methods have been evaluated for Voltage Source Converter (VSC)-HVDC transmission systems applications, such as direct power control (DPC) and vector control in different reference frames such as the VOC in *dq0* or alpha-beta [SOO 10]. However, in this study, the well-known closed-loop vector control method in conjunction with PI controllers in cascade structure is adopted according to [TEO 11], since this work aims to offer a contribution in the understanding of the overall VSC-MTDC system behavior in order to establish a DC voltage control philosophy, when further contributions regarding stability analysis as well as robustness properties to obtain effective control scheme can be subsequently included.

Therefore, in this section, only the control structure is presented, considering their integral and proportional gains as known. In practice, the inner (current) loop was tuned according to "modulus optimum" technique, while the outer (power/voltage) loop was tuned following the "symmetrical optimum" criteria as suggested in [BAJ 08b].

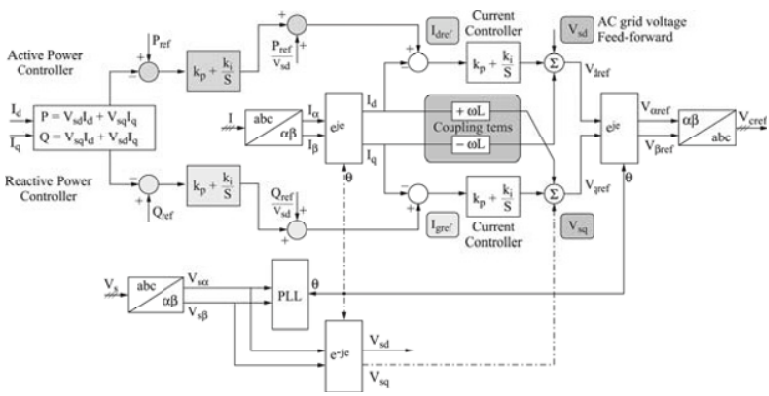

Figure 1.5. *PQ closed-loop VOC implemented on the dq synchronous frame*

The active and reactive power control structure, based on a closed-loop structure under synchronous frame VOC, is shown in Figure 1.5, as presented in [TEO 11], where PI-based controllers decide the reference

current d and q components from the error between the actual injected powers and their reference values, resulting in a four loops control structure.

1.3.1. *Inner current controller*

The converter's AC side current can be controlled by two parallel inner loops using PI controllers that transform the current errors into voltage signals as shown in Figure 1.6.

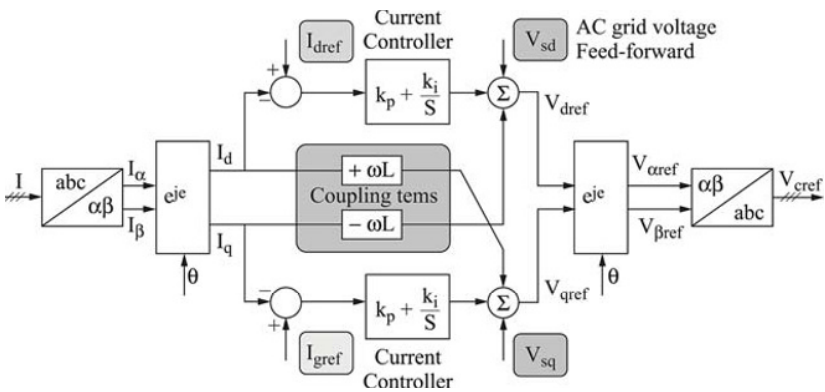

Figure 1.6. *Current controller structure – VOC based on dq synchronous frame*

The representative equation of the PI regulator is:

$$G_{PI}(s) = K_p + \frac{K_i}{s} = K_p\left(\frac{1+\tau_i S}{\tau_i S}\right) \qquad [1.13]$$

where the proportional gain K_p and integral time constant τ_i or the integral gain K_i are the design parameters calculated according to [BAJ 08b].

Using separate current controller loops for I_d and I_q, the converter reference voltage signals for the two axes (V_{dref} and V_{qref} in Figure I.6) are generated from the current error and the PI regulator transfer function.

$$V_{cdref} = \left(K_{p1} + \frac{K_{i1}}{s}\right)\left(I_{dref} - I_d\right) \qquad [1.14]$$

$$V_{cqref} = \left(K_{p1} + \frac{K_{i1}}{s} \right) \left(I_{qref} - I_q \right) \quad [1.15]$$

In equations [1.16] and [1.17], the grid voltage has been feed-forwarded and the cross-coupling terms between the two control loops are added to compensate the ones introduced by the transformation to the rotating reference frame [TEO 11].

$$V_{cdref} = V_{sd} - \omega L_{pr} I_q + \left(K_{p1} + \frac{K_{i1}}{s} \right) \left(I_{dref} - I_d \right) \quad [1.16]$$

$$V_{cqref} = V_{sq} + \omega L_{pr} I_d + \left(K_{p1} + \frac{K_{i1}}{s} \right) \left(I_{qref} - I_q \right) \quad [1.17]$$

1.3.2. *Outer power controller*

An active and reactive power closed-loop control structure is employed; hence, the reference currents for the inner loop (I_{dref} and I_{qref}) are calculated in an outer power loop where the active and reactive powers injected are estimated using measurements (of three-phase voltages and currents) at the point of common coupling (PCC) and their values are compared to the set points.

Special attention must be given to the selected convention. If the power set points (P_{set_point} and Q_{set_point}) are defined by the TSO as injected by the AC system into the VSC station, while the controlled current (I_d and I_q) has been defined as injected by the VSC into the AC grid, the power reference value given to the control system (P_{ref} and Q_{ref} in Figure 1.5) must be defined in the same direction of the current, such that:

$$P_{ref} = -P_{set_point} \quad [1.18]$$

$$Q_{ref} = -Q_{set_point} \quad [1.19]$$

1.3.2.1. *Active power controller*

When the M/S DC voltage control strategy is implemented in a VSC MTDC system with an n DC nodes, $n - 1$ converters control the active

power, and one controls the DC voltage. Therefore, the variable I_{dref} is calculated from the active power set point of all converters, except for the slack converter, through a combination of an open loop and a PI controller as expressed in equation [1.20]:

$$I_{dref} = \frac{P_{ref}}{V_{sd}} + \left(K_{pp} + \frac{K_{ip}}{s} \right) \left(P_{ref} - P \right) \qquad [1.20]$$

A feed-forward term representing the *d*-axis current (I_d) that should be generated when the injected power is equal to its reference is added to minimize the disadvantage of slow dynamic response of cascade control. Additionally, this contributes to improve stability since the load variation can be greatly reduced and, with it, the gain of voltage controller [BAJ 08b].

According to equation [1.11], it should be a 3/2 factor in the feed-forward term, but it has disappeared due to the chosen per unit system: the power and voltage bases have been set as the rated three-phase power of the converter [VA] and the peak value of rated line-to-neutral voltage [V].

1.3.2.2. *Reactive power controller*

Analogously, the *q*-axis current reference (I_{qref}) is calculated from the reactive power reference value (Q_{ref}), where a combination of an open loop and a PI controller is used to drive the reactive power to its desired value, leading to:

$$I_{qref} = -\frac{Q_{ref}}{V_{sd}} + \left(K_{pq} + \frac{K_{iq}}{s} \right) \left(Q_{ref} - Q \right) \qquad [1.21]$$

Alternatively to the reactive power, the magnitude of the AC grid voltage could be controlled; however, an extra control loop is needed to provide the reactive power reference to the reactive power control loop. In computer models, the reactive power injection necessary to keep the AC system's voltage in a given value can be calculated by an AC PF, where the converter is considered as a photo-voltaic (PV) node [KUN 94]. A sequential AC/DC PF has been proposed in [BEE 10a] and [BEE 10b].

In [COL 10], it is proposed to calculate the *q*-axis current reference directly from the voltage reference using a PI controller as in equation [1.22], but this scenario is not considered in this work since no further

models of the AC grid have been so far included; thus, the evolution of the grid voltage (V_{sd}) in response to the control q-axis current is unknown.

$$I_{qref} = \left(K_{pv} + \frac{K_{iv}}{s} \right) \left(V_{acref} - V_{sd} \right) \quad [1.22]$$

1.3.3. *DC voltage controller*

1.3.3.1. *Master/slave DC voltage control*

When the M/S DC voltage control strategy is implemented, one converter of the VSC MTDC system controls the DC voltage. The control of the DC voltage could act directly on the d-axis reference current (i_{dref}) as shown in Figure 1.7. The design parameters of the controller are found through a linearization of the power equation [TEO 11]. Otherwise, in this work, the control of the DC voltage is considered to act on the DC current, here referred as i_{dcref}, and the d-axis reference current (i_{dref}) is found directly from the power balance equation, as represented in Figure 1.8. Therefore, a PI controller is used to keep the DC voltage of the slack converter at its reference value and the steady state DC current (as a function of the actual DC power injected by the slack converter into the DC grid, $P_{dc,slack}$, and the reference DC voltage) is feed-forwarded. Subsequently, the reference DC current of the slack converter can be expressed as:

$$I_{dcref,slack} = \frac{P_{dc,slack}}{2V_{dcref}} + \left(K_{pdc} + \frac{K_{idc}}{s} \right) \left(V_{dcref} - V_{dc,slack} \right) \quad [1.23]$$

where $P_{dc,slack}$ could be calculated using measurement at the DC bus [1.24], or, if the converter losses have been neglected, as a function of the calculated AC side converters voltage and current [1.25].

$$P_{dc,slack} = 2I_{dc,slack}V_{dc,slack} \quad [1.24]$$

$$P_{dc,slack} = -P_{c,slack} = -I_d V_{cd} - I_q V_{cq} \quad [1.25]$$

Finally, the d-axis reference current ($I_{dref,slack}$) is defined as:

$$I_{dref,slack} = -\frac{2I_{dcref,slack}V_{dc} + I_q V_{cq}}{V_{cd}} \quad [1.26]$$

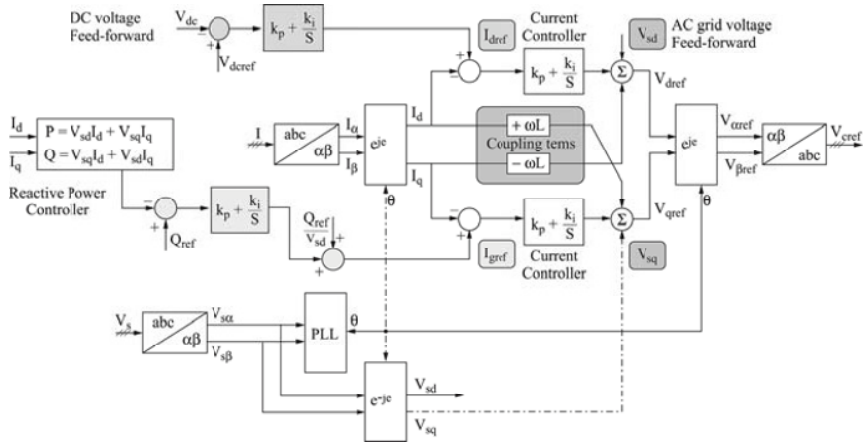

Figure 1.7. *V_{dc}-Q closed-loop VOC implemented on the dq synchronous frame*

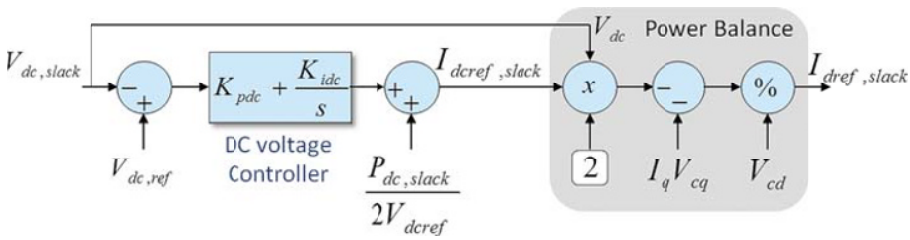

Figure 1.8. *DC voltage control structure*

1.3.3.2. *DC voltage: active power droop (VD)*

When the control of the DC voltage is considered to be distributed implementing a control strategy such as the DC voltage droop (VD), a group of converters may have a third control loop where the active power reference is generated as a function of a active *power set-point* (P_{dc0}) and the error between the actual DC voltage and its *set-point* (V_{dc0}) by a proportional controller, as shown in Figure 1.2, such that:

$$P_{ref_droop} = P_{dc0} + K_{pd}\left(V_{dc0} - V_{dc}\right) \qquad [1.27]$$

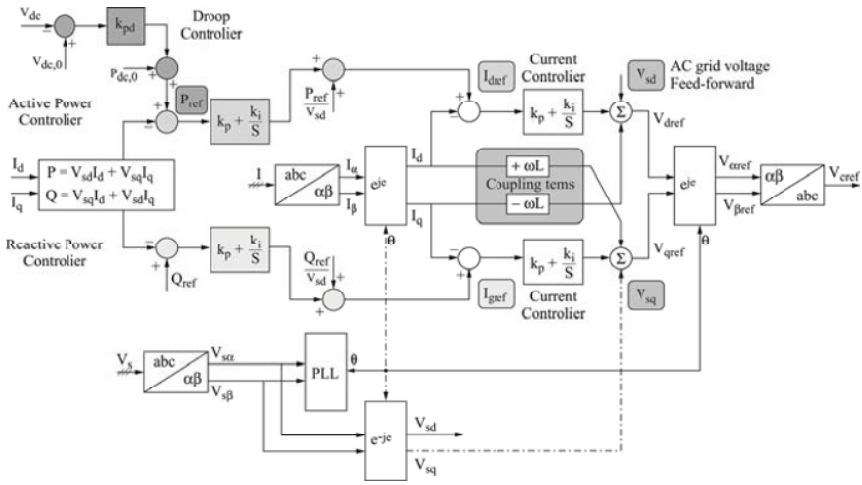

Figure 1.9. *DC voltage droop proportional controller*

1.4. Conclusion

In this chapter, having defined the adopted convention, the DC side model is built followed by the DC PF calculation (for more details see [CAR 12]). Then, the steady state AC side model has been presented, where the filter and other station equipment are not considered, thereafter the VSC has been modeled by its average model, approximation consistent with the phenomena of interest. Finally, control structures of VSC converter for multi-terminal DC grid taking into account normal as well as disturbed operations have been proposed considering only VOC method.

2

Time Scale Tools: a Control Solution for MTDC Complex Systems with Plug-and-Play Requirements

2.1. Introduction

This chapter proposes a global control strategy for Voltage Source Converter–Multi-Terminal Direct Current (VSC-MTDC) grids connected to alternating current (AC) networks, taking into account not only the direct current (DC) grid intrinsic dynamics but also interconnected systems and subsystems time variations. To achieve this goal, different time scales, as shown in Figure 2.1, are imposed to manage the DC grid, given that they are a key element when moving toward *system of systems* approaches. Hence, both steady state and dynamic models for high-voltage direct current multi-terminal systems based on voltage source converters (VSC-MTDC), suitable for studying slow transients due to operating point changes, are introduced, in order to represent the energy balance recovery in the DC grid after a perturbation. It is beyond the scope of this chapter to develop new efficient local control law algorithms, but it will consider the ones already used in power system engineering. The major contribution of this work is in presenting a cascaded primary and secondary control, with different time constants, which is able to manage and secure the VSC-MTDC grid recovery after disturbances, similarly to what has been developed for meshed AC power network. Thus, a DC voltage control philosophy that ensures an adequate redistribution of the power unbalance among the selected converters (AC systems) through a primary control action is proposed. Such control philosophy will also consider a secondary control, where the DC voltages are

Advance Control of AC/DC Power Network: *System of Systems Approach Based on Spatio-temporal Scales*, First Edition. Abdelkrim Benchaib.
© ISTE Ltd 2015. Published by ISTE Ltd and John Wiley & Sons, Inc.

taken back to values around their nominal operating points. As shown in Figure 2.1, the time scales methodology could be extended even beyond the tertiary control layer in a "plug-and-play" property for connected subsystems with their control algorithms. At a different stage of the proposed strategies, simulation results will be shown to highlight the feasibility and effectiveness of such a philosophy. The main results of this chapter have been shown in [CAR 12, GHO 12] and [BEN 14] and references therein.

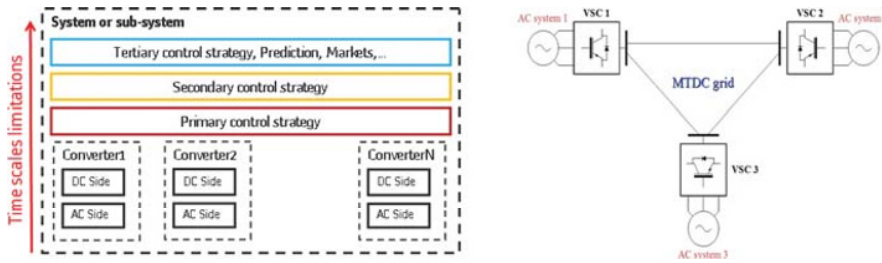

Figure 2.1. *Time scale control structure for multi-terminal DC grids*

This chapter is organized as follows. In section 2.2, voltage source converter – high voltage direct current (VSC-HVDC) control principles will be given. The control strategies of MTDC grids will be detailed in section 2.3. In section 2.4, DC grid steady state modeling is shown. Thereafter, the optimization technique based on the Newton–Raphson (NR) method and DC power flow are described in sections 2.5 and 2.6. After reviewing different principles, tools and control strategies for MTDC grid system, a first application on steady state control of such systems will be proposed in section 2.7. Then, primary and secondary control of meshed DC grid will be described in section 2.8. From this point, some research directions will be discussed. Section 2.9 will discuss the dynamic control of MTDC grid. Section 2.10 will concern the "plug-and-play" properties of networked system and more specifically MTDC grid. Section 2.11 will discuss the control of associated actuators where the control actions are performed. Finally, some concluding remarks will end this chapter.

2.2. Recalling VSC-HVDC control objectives

Unlike conventional HVDC converters, VSCs can operate at very low power. As the active and reactive powers are controlled independently, even at zero active power, the full range of reactive power can be utilized.

Active power transfer can be quickly reversed without any change of control mode, and without any filter switching or converter blocking. Furthermore, the power reversal is obtained by changing the direction of the DC current and not by changing the DC voltage as for conventional HVDC. VSC converters are very suitable for creating a DC grid with a large number of converters (multi-terminal HVDC), since very little coordination is needed between the interconnected VSCs. Nowadays, the use of VSC technology is assumed for the implementation of multi-terminal HVDC.

Each of the terminals should be able to adopt different strategies of control depending on its specific needs, [THO 01]. VSC-HVDC should have the capability to control DC side parameters as well as AC side parameters. On the DC side, the VSC-HVDC may operate in constant DC voltage mode, constant power mode or constant DC current mode, while on the AC side the VSC-HVDC may operate in constant AC voltage mode or constant reactive power mode depending on the type of the AC grid connection. Frequency droop could also be added optionally in the AC bus control:

– *Constant active power injection operating mode*:

This kind of control is applied when the VSC-HVDC is connected to a weak grid where the power flow needs to be kept constant.

– *Constant DC voltage operating mode*:

This kind of control is applied when the VSC-HVDC is connected to a strong grid where the DC must be regulated by active power compensation.

– *Constant reactive power injection operating mode*:

This type of control is adopted when the reactive power has to be specifically controlled. The reactive power reference could be assigned to zero to guarantee optimal power factor (1) if the control of the reactive power is not required.

NOTE.– A small amount of active power could be assigned to compensate for losses.

– *Constant AC voltage operating mode*:

This type of control is applied, when the VSC-HVDC is connected to a weak network, therefore, AC side voltage regulation is required by reactive power compensation.

2.3. DC voltage control strategies for MTDC grids

One of the most important elements of the DC grid is the capacitor. It discharges when the power demand of the converter AC side is increased. In this case, the DC voltages drop as the converter requests more active power. Contrarily, when additional power is injected into the DC grid, the capacitors are charged and the DC voltages increase. In steady state, the active power distribution is balanced.

The DC voltage control is definitely one of the main tasks of the VSC in an HVDC transmission system. The DC voltage is required to be well controlled within rigid limits under all conditions in order to guarantee the power balance between all MTDC network transmission terminals.

In a point-to-point HVDC transmission system, one of the terminals controls the DC voltage of the transmission link while the other terminal controls the active power sent to the interconnection. This kind of control is called master/slave control strategy.

Nevertheless, when an MTDC network is considered, it may be complicated to operate the system with just one converter station controlling the DC voltage. This is mainly due to two reasons: limited power rating of the VSC station controlling the DC voltage and the possibility of faults in the AC network connected to this station which could trigger the protection equipment within only a few cycles of the AC network. Hence, distributing the DC voltage control responsibility to more than one VSC station seems to be an improved option to operate MTDC systems.

In this section, different DC voltage control strategies, which are proposed in the literature, will be analyzed and compared. Using these strategies, the coordination of the multiple HVDC systems with a minimum or without an explicit communication has to be accomplished. Figure 2.2 shows a three-terminal HVDC system on which one of the following control strategies could be applied.

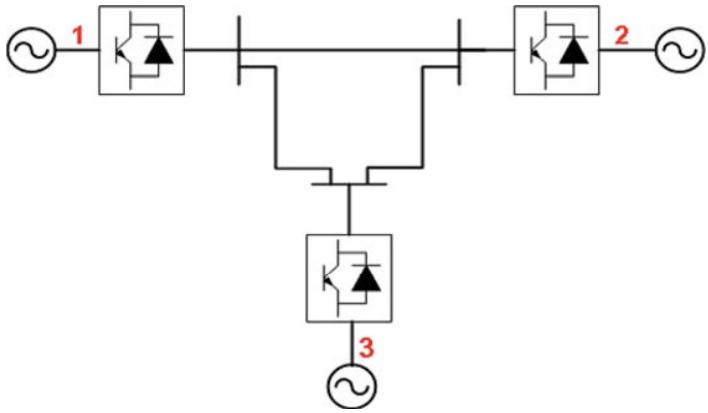

Figure 2.2. *Three-terminal HVDC*

2.3.1. *Slack bus control (master/slave control)*

Within this strategy of control, all converters except one operate in a fixed power injection mode. The function of the remaining converter is to keep the voltage of the DC bus to its reference value. The converter controlling the DC voltage will act as a "battery" or "slack bus", which means that, it will provide or absorb sufficient active power to achieve a power balance of the DC system [BAR 10]. Consequently, it adapts the output power to compensate all the losses in the DC system. This converter has to be connected to a strong node in the AC system and must have sufficient DC power rating; therefore, it needs to be oversized, reacting fast on DC grid transient such as a loss of converters or DC line [BEE 11]. In addition, an outage of this converter cannot be tolerated because it will entail the losing of the DC voltage control.

A possible solution is to control the DC voltage at different nodes of the DC grid simultaneously. However, even though such multiplication could increase the overall reliability of the system, it also gives rise to suboptimal operating points (statically) and to voltage and power oscillations [BEE 11]. An additional inconvenience of the master/slave strategy is the problem of the geographic location of the slack bus converter. The system operator assuming this responsibility will be requested to cope with all the problems in the DC grid. Figure 2.3 shows a P_{dc}-V_{dc} characteristic (the DC voltage/DC power) of slack bus converter (constant DC voltage) and a P-controller (constant power injection).

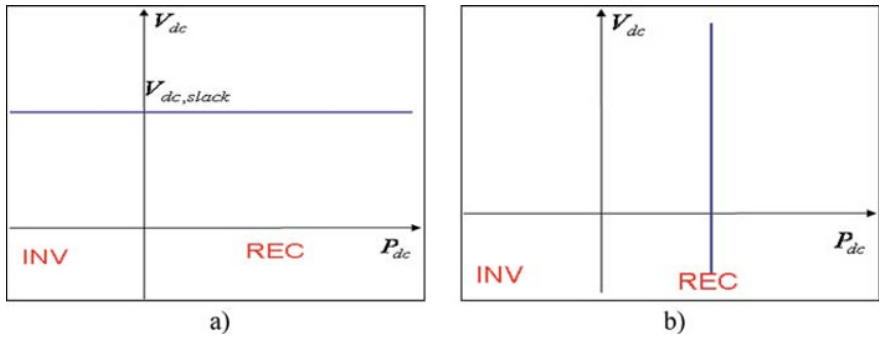

Figure 2.3. *Illustration of: a) slack bus and b) P-controller*

Figure 2.4 presents an example of role distributions following this control strategy over the nodes of a three-terminal HVDC grid. In the illustrated case, the first and second converters are P-controllers and the third converter is the slack bus converter, which is responsible to deal with all the problems in the DC grid.

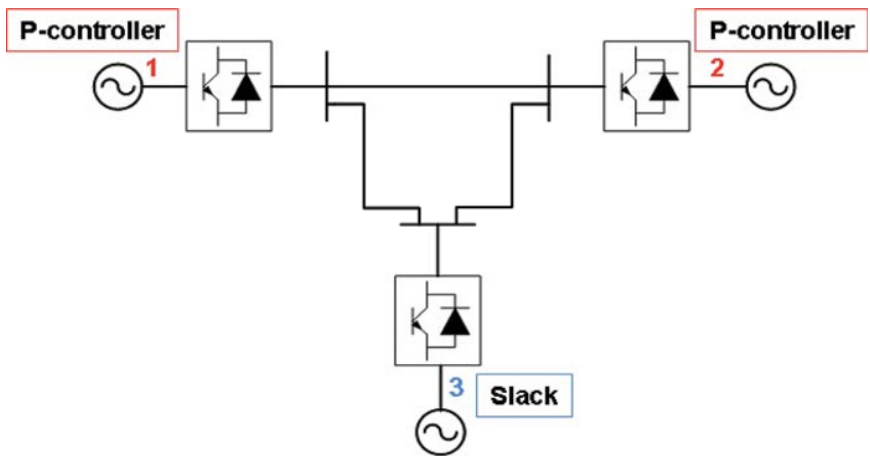

Figure 2.4. *Three-terminal HVDC under master/slave control strategy*

2.3.2. *Voltage margin control*

This type of control follows a P_{dc}-V_{dc} characteristic as shown in Figure 2.5.

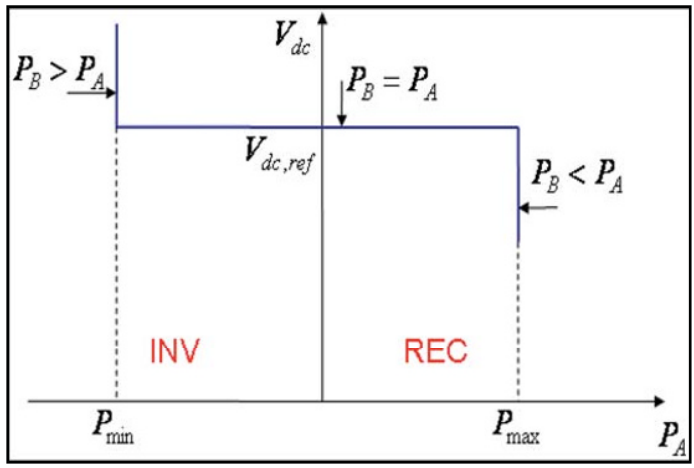

Figure 2.5. *Voltage margin strategy illustration [MEA 07]*

Figure 2.5 shows that the terminal A acts as DC voltage controller (slack) as long as it does not reach the upper or lower limits of the power injection P_{max} or P_{min}, respectively. If the power injection is larger than the upper limit, the DC voltage decreases, however, if it is lower than P_{min}, then the DC voltage increases further. If the DC voltage rises, it will go up until the other terminal with next higher DC voltage reference setting takes over the duty of DC voltage regulation (terminal B). This is shown in Figure 2.6.

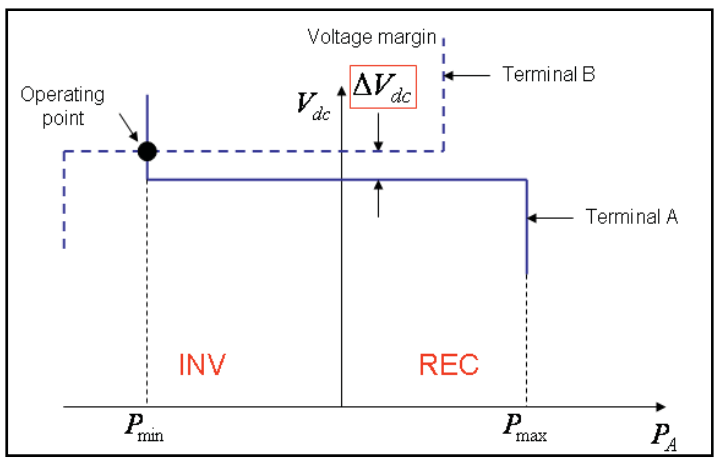

Figure 2.6. *Operating point in voltage margin strategy [NAK 99]*

However, if the DC voltage level is reduced, the terminal with the next lower DC voltage setting (terminal C) will start to act as a DC slack bus, see Figure 2.7.

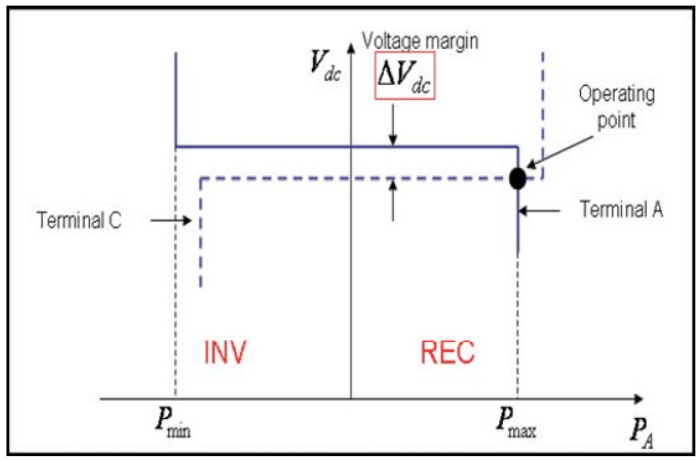

Figure 2.7. *A second operating point in voltage margin strategy*

The downside of the voltage margin is that only one converter is capable of controlling the system DC voltage at a given time [NAK 99]. Otherwise, in a MTHVDC network with a high number of nodes, the DC voltage is limited by ± 10% of the nominal voltage, limiting the amount of converter that could participate in this distributed DC voltage control strategy.

2.3.3. *Droop control*

An alternative control strategy is called droop control, where the DC voltage control is distributed over a number of converters, which *simultaneously* adapt their active power injections to deal with disturbed grid situations.

There are many similarities between the voltage droop control and the frequency droop used in AC systems, where the load-dependent frequency variation is used as an input signal for the control system to adjust the generated power to meet the demand in all times. However, the difference is that the frequency remains constant in the AC system and the DC voltage differs from one bus to another as a result of the power flows. The voltage

deviations at different nodes do not entail the existence of transient conditions.

From the control point of view, there is an outstanding particularity in this control strategy, where the concept of reference values of active power and DC voltage given by the operator of the system is changed by the idea of set points. The difference lies on the new steady state condition after a disturbance. In the droop control, although the set points are equally given by the operator as a result of an optimal power flow in a nominal condition, it is not expected that the power, neither the voltage, return to their initial values after a disturbance.

In other words, in a non-disturbed condition, identical to the one established by the operator as the nominal one, the converters will follow the set points as their reference values and the desired power flow will be achieved. However, when the active power balance is disturbed, the DC voltages deviate and the converters under droop control (as those operating in DC voltage control mode, if any) will change their active power injection *permanently* to regain the power balance. In this new condition, the DC voltages of droop and power controller converters have also moved away from the set points.

In MTDC networks, the control employs the droop mechanism to regulate the DC voltage by adjusting the converters' power injections or the current injections as shown in Figure 2.8.

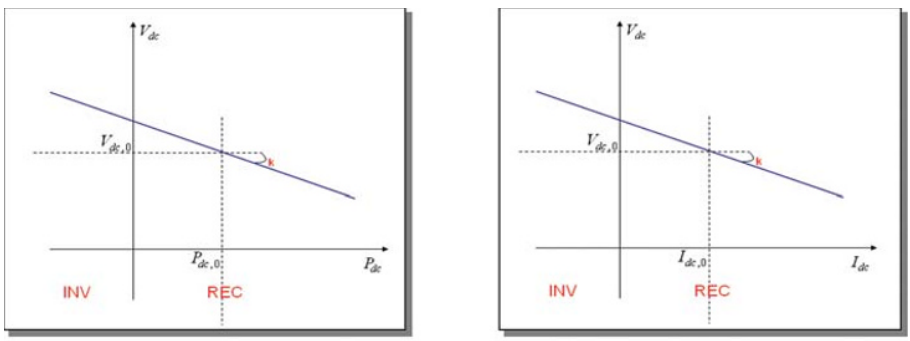

Figure 2.8. *Voltage droop characteristics: a) voltage/power and b) voltage/current*

For a given node I, the voltage droop is described as follows:

$$P_{dc,i} = P_{dc,0,i} - \frac{1}{k_{pi}}\left(V_{dc,i} - V_{dc,0,i}\right) \quad [2.1]$$

or:

$$I_{dc,i} = I_{dc,0,i} - \frac{1}{k_{Ii}}\left(V_{dc,i} - V_{dc,0,i}\right) \quad [2.2]$$

For a monopolar converter, the expression of the DC power injection as a function of the DC voltage and DC current is:

$$P_{dc,i} = V_{dc,i} I_{dc,i} \quad [2.3]$$

From the above expressions, the power and current droop constants could be written as follows:

$$k_{pi} = \frac{V_{dc,i} - V_{dc,0,i}}{P_{dc,i} - P_{dc,0,i}} \quad [2.4]$$

$$k_{Ii} = \frac{V_{dc,i} - V_{dc,0,i}}{I_{dc,i} - I_{dc,0,i}} \quad [2.5]$$

The values of these droop constants are compared within the same operating conditions. We suppose a converter substation with the values of the references of the power and voltage in per unit (p.u.) as follows:

– $P_{dc,0,i} = 0.35\ p.u.\ V_{dc,0,i} = 1\ p.u.$

then equation [2.3] gives

$I_{dc,0,i} = 0.35\ p.u.$

– $P_{dc,i} = 0.75\ p.u.\ V_{dc,i} = 0.97\ p.u.$

then equation [2.3] gives

$I_{dc,i} = 0.335\ p.u.$

The same for the operating point, giving $I_{dc,i} = 0.335\ p.u.$

Using the expressions [2.4] and [2.5] to calculate the droop constants at node *i*, it results in:

$k_{pi} = 0.075\ p.u.$ and $k_{Ii} = 0.07088\ p.u.$

The droop constants do not have the same value but are very close, because under nominal operation, V_{dc} is approximately equal to its nominal value.

However, in the case of a monopolar symmetrically grounded or bipolar converters, the expression of the DC power injection should be duplicated as follows:

$$P_{dc,i} = 2V_{dc,i}I_{dc,i} \quad [2.6]$$

Within the same operating conditions, the values of the reference current as well as the current in the operation point are, respectively:

$$I_{dc,0,i} = 0.175\ p.u. \text{ and } I_{dc,i} = 0.3866\ p.u.$$

And thus, using equations [2.4] and [2.5], the values of the droop constants are:

$$k_p = 0.075\ p.u. \text{ and } k_I = 0.1417\ p.u.$$

It is understandable that the droop constants do not have similar values because of the duplication. Under nominal conditions, V_{dc} is approximately equal to its nominal value, meaning that the way to get almost the same behavior is to have a factor near to two between the voltage/power droop constant and the voltage/current droop constant as:

$$k_I \approx 2k_p$$

Generally, it is worth noting that, to get precise results and not confound the power with the current, one droop characteristic has to be chosen.

A set point given by the DC voltage $V_{dc,0}$ and power $P_{dc,0}$ or current $I_{dc,0}$ for the converters under voltage droop control is introduced. In the implementation, these reference values are obtained from the system under normal operation, with no droop control active [BEE 11]. The smaller the voltage droop constant k, the bigger the converter power contribution. If $k \to 0$, the converter controls the DC voltage (slack) and $V_{dc} = V_{dc,0}$. When $k \to \infty$, the converter works as a P-controller and $P_{dc} = P_{dc,0}$ or $I_{dc} = I_{dc,0}$.

Based on the droop control philosophy, some variations of these characteristics can be obtained by considering voltage and/or power limitations (see Figures 2.9 and 2.10).

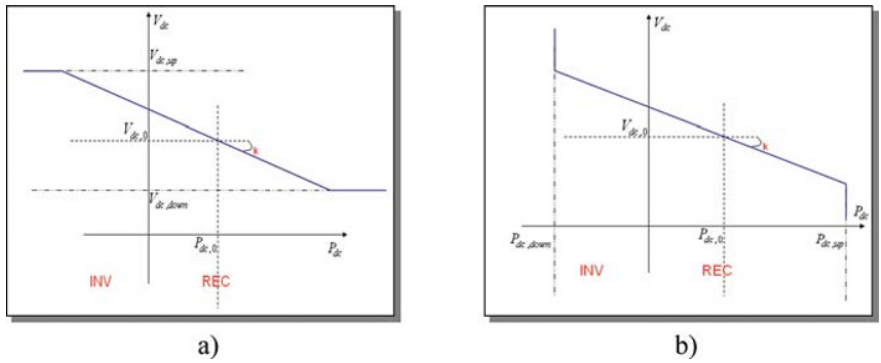

a) b)

Figure 2.9. *Voltage droop characteristics: a) voltage limitation and b) power limitation*

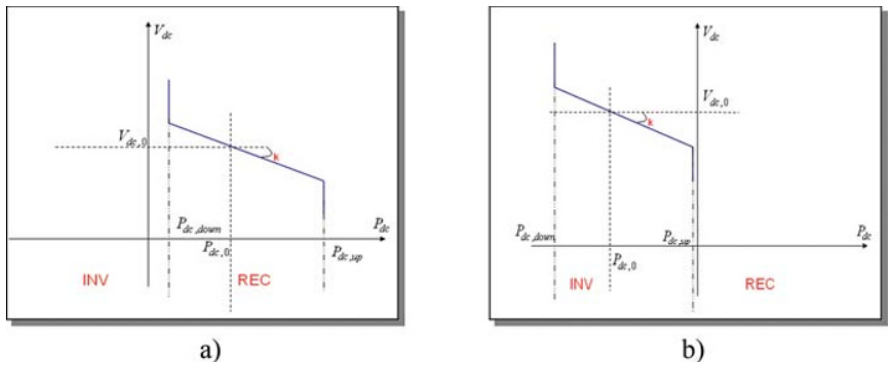

a) b)

Figure 2.10. *Power limitation: a) for a node which is capable of working only as a generator (P > 0) and b) for a node which is capable of working only as a load (P < 0)*

2.3.4. *Dead-band-droop control*

Since the droop presented in the previous section does not distinguish normal and disturbed operations, a dead-band has been integrated as shown in Figure 2.11. Inside the band of normal operation just one converter controls the V_{dc} voltage, while the control action of the others reminds inactive, and in failure condition all converters take their share to

compensate the disturbance via their k-value according to their capabilities and limitations.

Following the characteristic shown in Figure 2.11(a), the converter works as a slack bus in normal operation and assumes the responsibility to regulate the DC voltage of the MTDC network. In a disturbed operation, this converter turns to work under droop control following its characteristic. A converter, that used to work as a P-controller in a normal operation, has to be capable of introducing DC voltage control by changing its power injection according to its droop characteristic, see Figure 2.11(b).

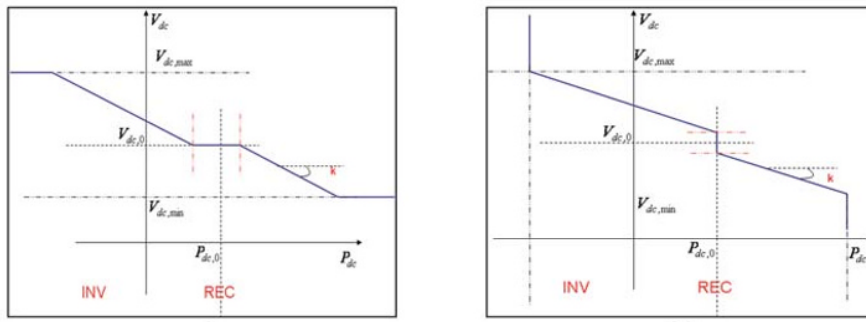

Figure 2.11. *Voltage droop characteristics with dead-band: a) voltage dead-band and b) power dead-band*

2.3.5. *Undead-band-droop-control*

The control activity of the converters within the band is not fully dead in normal operation, but only reduced, since several converters could have non-zero k-value and contribute to the DC voltage (V_{dc}) control even without any perturbation. In MTDC grid configuration, it could be chosen to assign only few of the DC grid converters with higher gains allowing them to carry the main load, while the others have smaller values, as shown in Figure 2.12. For more details, the readers can refer to [VRA 12].

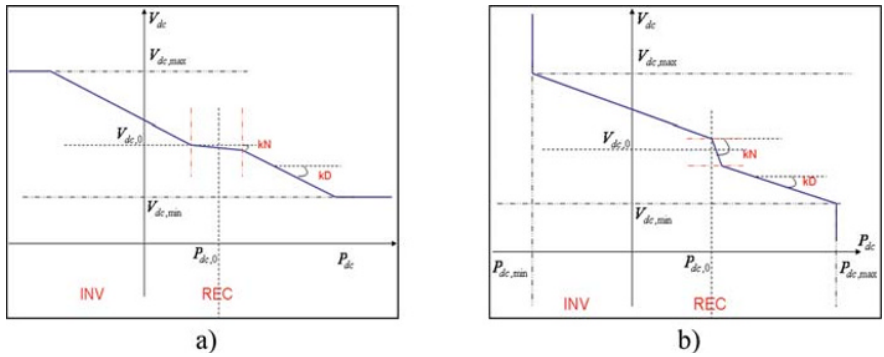

Figure 2.12. *Voltage droop characteristics with undead-band: a) voltage undead-band and b) power undead-band*

2.3.6. *Priority control*

The priority control is a personalized strategy of using DC voltage droop controllers to perform priority power sharing. The terminal with the highest priority controls the DC voltage, until its rated capacity or a maximum power set point is reached. The second converter starts transmitting power only when the first converter has attained its limits.

In practice, when a three-terminal system is considered (one of which could be a country), it gets priority to obtain the power produced by the wind farm (for example), until a particular limit is achieved, at which point the other "country(s)" will take the excess power. In other words, as long as the power delivered to the first prioritized system does not reach the limit, the second prioritized system will not receive any power from the source system (in this example, the wind farm).

2.3.7. *Ratio control*

The DC voltage controlling stations share the generated power according to a certain ratio. Using this control strategy, the system operator could vary the power ratio between the participating terminals by changing the slope of the droop characteristic [VRA 12]. The expression of the ratio (r) between two terminals is:

$$r = \frac{P_{dc,1}}{P_{dc,2}} \approx \frac{I_{dc,1}}{I_{dc,2}} \qquad [2.7]$$

The approximation is due to the fact that DC voltage is considered to be the "same" in both converters; hence, the power share is approximately equal to the DC current ratio. The drawback of this control strategy is that communication is necessary if there are more than two DC voltage controlling stations.

2.3.8. *DC voltage control strategy summary*

The above discussed DC voltage control strategies are summarized. Droop constants for normal operation k_N and disturbed operation k_D are introduced for the proposed control strategies in a three-terminal HVDC grid. The summary on how to set the droop gain of each converter for a given strategy is given in Table 2.1. The third converter has the role of the slack bus for a master/slave control strategy and therefore its droop constant value is 0.

Within the voltage margin control strategy, converter 3 is the slack bus in a normal condition and in a disturbed condition converter 2 becomes a slack bus, while converter 3 is transformed into a power controller. The same droop constant for normal operation and disturbed operation is applied to the three converters for the droop control. Concerning the dead-band droop control strategy, the dead-band is presented for a droop constant set to 0 for the slack bus converter and set to ∞ for a P-controller, in normal operation conditions. In disturbed operation, the droop constants have values different from 0 or ∞. Finally, regarding the undead-band droop control strategy, the droop constants are set to values different from 0 and ∞ even for normal operations. The droop constants are supposed to be equal to calculated values when they are not set to zero or infinity.

Converter 1		Converter 2		Converter 3		Control strategy
k_N	k_D	k_N	k_D	k_N	k_D	
∞	∞	∞	∞	0	0	Master/slave
∞	∞	∞	0	0	∞	Voltage margin
K_3	K_3	K_2	K_2	K_1	K_1	Droop
∞	K_3	∞	K_2	0	K_1	Dead-band-droop
K_{3N}	K_{3D}	K_{3N}	K_{3D}	K_{3N}	K_{3D}	Undead-band-droop

Table 2.1. *Summary of the control strategy gain settings*

2.4. DC grid steady state modeling

In the DC grid, the power flow is imposed by the differences in the voltage magnitude between the different nodes contrarily to the AC system, where the active power flow is linked with the phase shifting between the interconnected busses. The absence of the reactive power makes the power flow calculation easier, since only active power is concerned.

The second specification of the DC grid is that the frequency is absent. Thus, only resistances are introduced to calculate the nodal admittance matrix in steady state regimes. As done in practice, a shunt resistance that represents the losses of the converter is inserted into the admittance matrix.

Generally, each node could control the active power injection or the DC bus voltage. In a P-controller bus, the injected power is kept constant. The V_{dc} controller holds the DC bus voltage constant by adapting its active power injection.

In the adopted convention, the DC power and current are assumed to be positive when they are flowing away from the VSC-HVDC to the DC grid. In this section, our aim is to perform DC grid modeling with the main objective of the calculation of the power flow necessary for control reference settings.

In a multi-terminal HVDC system, the current injected in a node i is calculated as the sum of all currents flowing to the other interconnected $(n-1)$ nodes and the current flowing to the shunt resistance (R_{ii}) as shown in Figure 2.13.

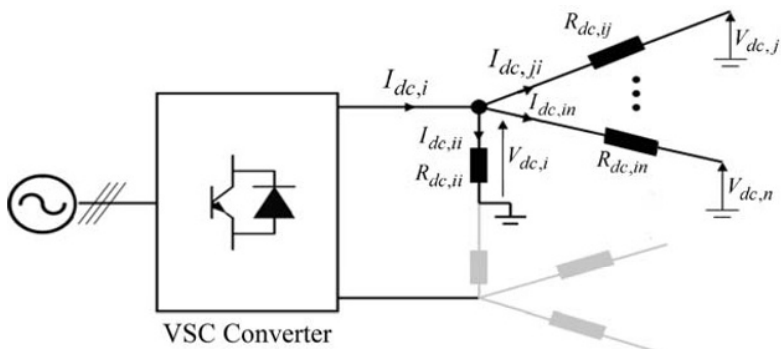

Figure 2.13. *Monopolar symmetrically grounded VSC substation connected to an MTDC network*

Considering the mathematical description, we have:

$$I_{dc,i} = \left(\sum_{\substack{j=1 \\ j \neq i}}^{n} I_{dc,ij} \right) + I_{dc,ii} \quad [2.8]$$

The current flowing from a node i to a node j is calculated as shown in Figure 2.14.

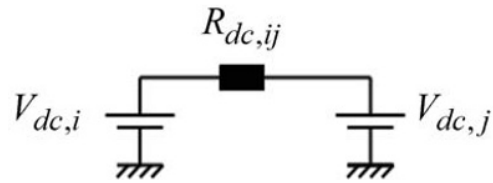

Figure 2.14. *i, j connection*

That is:

$$I_{dc,ij} = \frac{1}{R_{dc,ij}} \left(V_{dc,i} - V_{dc,j} \right) \quad [2.9]$$

And the current flowing to the shunt resistance is described as given in Figure 2.15.

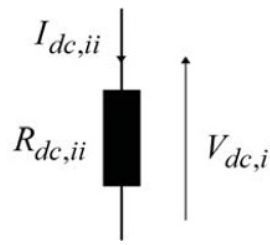

Figure 2.15. *Current flowing to the shunt resistance*

That is:

$$I_{dc,ii} = \frac{V_{dc,i}}{R_{dc,ii}} \quad [2.10]$$

Taking into consideration equations [2.9] and [2.10] into [2.8], the current injected at node i is described using the equation below as:

$$I_{dc,i} = \left(\sum_{\substack{j=1 \\ j \neq i}}^{n} \frac{1}{R_{dc,ij}} \left(V_{dc,i} - V_{dc,j} \right) \right) + \frac{V_{dc,i}}{R_{dc,ii}} \quad [2.11]$$

Rewriting the expression of equation [2.11] in matrix and vector form, we could derive the relationship between all the n injected currents, the n DC voltages and the admittances of the lines as follows:

$$I_{dc} = Y_{dc} V_{dc} \quad [2.12]$$

With, respectively, the DC current and DC voltage vectors:

$$I_{dc} = [I_{dc,1}, \quad I_{dc,2}, \quad \cdots \quad I_{dc,n}]^T$$

$$V_{dc} = [V_{dc,1}, \quad V_{dc,2}, \quad \cdots \quad V_{dc,n}]^T$$

And the DC admittance matrix:

$$Y_{dc} = \left[\begin{pmatrix} Y_{dc,11} & \cdots & Y_{dc,1n} \\ \vdots & \ddots & \vdots \\ Y_{dc,n1} & \cdots & Y_{dc,nn} \end{pmatrix} \right] \quad [2.13]$$

With terms of expression [2.13] given as below:

$$Y_{dc,ij} = Y_{dc,ji} = \frac{1}{R_{dc,ij}}, i \neq j$$

$$Y_{dc,ii} = \sum_{\substack{j=1 \\ j \neq i}}^{n} \frac{1}{R_{dc,ij}} + \frac{1}{R_{dc,ii}} = \sum_{j=1}^{n} \frac{1}{R_{dc,ij}}$$

If there is no link between the two stations i and j, the admittance value is set to zero because the resistance has an infinite value.

The active power in each node is the product of DC voltage and DC current. For a monopolar symmetrically grounded converter and the bipolar converters, the power injection is duplicated as shown below:

$$P_{dc,i} = 2 V_{dc,i} I_{dc,i} \quad [2.14]$$

Replacing equation [2.11] into [2.14], we obtain the following expression of the power injection at node i. That is:

$$P_{dc,i} = 2V_{dc,i}\left(\left(\sum_{\substack{j=1 \\ j\neq i}}^{n} \frac{1}{R_{dc,ij}}\left(V_{dc,i} - V_{dc,j}\right)\right) + \frac{V_{dc,i}}{R_{dc,ii}}\right) \quad [2.15]$$

This expression is used to calculate the power injection into each DC node, when the DC voltage values are known beforehand. Considering the fact that, in a DC grid, the nodes are either P-controllers or V_{dc}-controllers, the known variable is either the DC voltage or the DC power injection. Therefore, a system of nonlinear equations has to be solved to find these variables. This is the role of the power flow calculation. First, let us have a quick overview on the resolution technique.

2.5. Newton–Raphson technique

The NR technique is an efficient procedure for solving equations numerically. It is based on the idea of linear approximation. It is a technique for successively finding better approximations to the roots (or zeroes) of a function.

The NR technique is based on the principle that, if the initial guess of the root of $f(x)$ is at x_i, then by drawing the tangent to the curve at $f(x_i)$, the point x_{i+1} where the tangent crosses the x-axis is an improved estimate of the root, see Figure 2.16.

Using the definition of the slope of a function, at $= x_i$:

$$f'(x_i) = \tan(\theta) = \frac{f(x_i)}{x_i - x_{i+1}}$$

Consequently, we obtain:

$$x_{i+1} = x_i - \frac{f(x_i)}{f'(x_i)} \quad [2.16]$$

Equation [2.16] is called the NR formula for solving nonlinear equations of the form $f(x) = 0$. Starting with an initial first guess x_i, the next guess which should be x_{i+1} could be founded using equation [2.16]. This

process is repeated until a desirable tolerance is founded. To summarize, the NR procedure is organized according to the following steps:

Step 1: choose the initial value of x which is x_i;

Step 2: estimate the value of function $f(x_i)$;

Step 3: estimate the value of function $f'(x_i)$;

Step 4: calculate the deviation $\Delta x_i = \frac{f(x_i)}{f'(x_i)}$;

Step 5: obtain the updated value x_{i+1} of x, with: $x_{i+1} = x_i - \Delta x_i$;

Step 6: check the value of $f(x_{i+1})$ and its difference to zero. If this difference is lower than a fixed tolerance, the NR converges to the value x_{i+1}; if not, the previous steps have to be repeated.

2.6. DC power flow

The power flow calculation aims to reach the steady state operating point of the power system, by solving a system of nonlinear equations. It is one of the most important calculations to analyze the power systems, and could be used to find a starting point for dynamic system-analysis, next steady state operation points or to make an n–1 contingency analysis.

Starting from the mathematical model of the DC grid, the equations could be rewritten in order to be resolved using a chosen resolution method. In this section, the power flow is solved using NR technique which was presented previously.

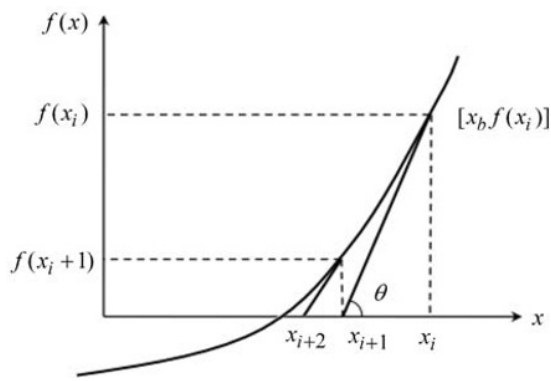

Figure 2.16. *Geometrical illustration of the Newton–Raphson technique*

Depending on the DC grid topology as well as the adopted control strategy, two different methods of problem-positioning will be dealt with. The first method could be used to calculate the power flow of a DC network that contains one node as a slack bus and the rest as P-controllers. The second method offers the possibility to integrate the DC voltage droop control which for many reasons will be referred as "generalized" method.

2.6.1. *The first method: for master/slave control strategy*

This load flow calculating method is valid only for a master/slave control strategy. As shown in the chart presented in Figure 2.17, the inputs of the power flow calculation are the DC voltage in the slack bus, the DC power injection in the P-controller nodes and the nodal admittance matrix, which is formed as described by equation [2.13]. The calculation aims to find the values of the unknown power injection in the slack bus and the DC voltages in the P-controllers (outputs).

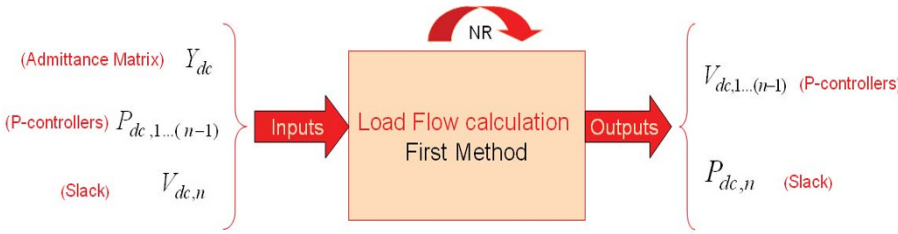

Figure 2.17. *Chart of the power flow calculation: first method*

2.6.1.1. *Mathematical formulation*

Since a DC node could be P-controller or V_{dc}-controller, the nonlinearity of the problem is evident. A reformulation is inevitable to obtain a solution through numerical techniques. Within this first method, the combination of equations [2.12] and [2.14] results in the following system of nonlinear equations. That is:

$$I_{dc}V_{dc} - \left[\frac{P_{dc,i}}{2V_{dc,i}}\right] = 0 \qquad [2.17]$$

And more explicitly:

$$\begin{bmatrix} Y_{dc,11} & \cdots & Y_{dc,1(n-1)} & Y_{dc,1n} \\ \vdots & \ddots & \vdots & \vdots \\ Y_{dc,(n-1)1} & \cdots & Y_{dc,(n-1)(n-1)} & Y_{dc,(n-1)n} \\ Y_{dc,n1} & \cdots & Y_{dc,n(n-1)} & Y_{dc,nn} \end{bmatrix} \begin{bmatrix} \\ V_{dc,1} \\ \vdots \\ V_{dc,(n-1)} \\ V_{dc,n} \end{bmatrix} - \begin{bmatrix} P_{dc,1} \\ \vdots \\ P_{dc,(n-1)} \\ P_{dc,n} \end{bmatrix} ./ \left(2 \begin{bmatrix} V_{dc,1} \\ \vdots \\ V_{dc,(n-1)} \\ V_{dc,n} \end{bmatrix} \right) = 0 \quad [2.18]$$

The unknowns in this system are the DC voltages in all the P-controllers and the power injection of the slack bus. Thus, the vector of the unknown variables could be defined as shown in [BEE 12a]. That is:

$$X = \begin{bmatrix} X_1 \\ X_2 \end{bmatrix} \quad [2.19]$$

With the following vector distribution of the DC voltages in the P-controller nodes and the power injection in slack bus, we have:

$$X_1 = \begin{bmatrix} V_{dc,1} \\ \vdots \\ V_{dc,(n-1)} \end{bmatrix} \quad [2.20]$$

$$X_2 = P_{dc,n} \quad [2.21]$$

And the known terms are the power injections in all the P-controllers defined by the following vector:

$$\begin{bmatrix} P_{dc,1} \\ \vdots \\ P_{dc,(n-1)} \end{bmatrix} \quad [2.22]$$

The DC voltage value of the slack bus is also known and is described by:

$$V_{dc,n}$$

Taking into consideration the expression [2.18], a partition of the DC bus admittance matrix is very useful to clarify the original full system of equations. That is:

$$Y_{dc} = \begin{bmatrix} Y_{11} & Y_{12} \\ Y_{21} & Y_{22} \end{bmatrix} \quad [2.23]$$

With Y_{11} a matrix of dimension $(n-1) \times (n-1)$. Thus:

$$Y_{11} = \begin{bmatrix} Y_{dc,11} & \cdots & Y_{dc,1(n-1)} \\ \vdots & \ddots & \vdots \\ Y_{dc,(n-1)1} & \cdots & Y_{dc,(n-1)(n-1)} \end{bmatrix} \quad [2.24]$$

Y_{12}: a row vector of length (n-1). Thus:

$$Y_{12} = \begin{bmatrix} Y_{dc,1n} \\ \vdots \\ Y_{dc,(n-1)n} \end{bmatrix} \quad [2.25]$$

Y_{21}: a column vector of length (n-1). Thus:

$$Y_{21} = [Y_{dc,n1} \quad \cdots \quad Y_{dc,n(n-1)}] \quad [2.26]$$

Y_{22}: a scalar. Thus:

$$Y_{22=}Y_{dc,nn} \quad [2.27]$$

The combination of the above expressions leads to the following modified system of equations. That is:

$$\begin{cases} Y_{11}X_1 + Y_{12}V_{dc,n} - \frac{P_{dc,j}}{2X_{1j}} = 0 \rightarrow (n-1\ equations) \\ Y_{21}X_1 + Y_{22}V_{dc,n} - \frac{X_2}{2V_{dc,n}} = 0 \rightarrow (1\ equation) \end{cases} \quad [2.28]$$

2.6.1.2. *Jacobean and resolution*

The unknown DC voltages and the slack bus DC power injection are calculated using NR technique, where n nonlinear equations have to be solved. Consider F, the vector containing the equations of system [2.28]. The NR resolution aims to find the vector X when $F = 0$ with a fixed tolerance, which has been set here equal to $1e^{-8}$ in the implementation. As explained before, a format problem rewriting is necessary. The only difference here is that the function is multi-dimensional. Consequently, this leads to the following equation:

$$\left(\frac{\partial F}{\partial X}\right)^{(k)} (\Delta X)^{(k)} = (\Delta F)^{(k)} = F^{(k)} \quad [2.29]$$

$$F = \begin{bmatrix} F_1 \\ \vdots \\ F_{(n-1)} \\ F_n \end{bmatrix} \quad [2.30]$$

(k) is the iteration counter and $(\Delta X)^{(k)} = X^{(k)} - X^{(k+1)}$. With the Jacobean:

$$J = \frac{\partial F}{\partial X} = \begin{bmatrix} \frac{\partial F_1}{\partial X_1} & \cdots & \frac{\partial F_1}{\partial X_n} \\ \vdots & \ddots & \vdots \\ \frac{\partial F_n}{\partial X_1} & \cdots & \frac{\partial F_n}{\partial X_n} \end{bmatrix} \quad [2.31]$$

The terms of the Jacobean for the iteration (k) are:

$$\left(\frac{\partial F_i}{\partial X_j}\right)^{(k)} = Y_{dc,ij} + 0.5\frac{P_{dc,i}}{{X_j}^{(k)^2}} \rightarrow \text{for } 1 \leq i,j \leq n-1 \quad [2.32]$$

$$\left(\frac{\partial F_n}{\partial X_i}\right)^{(k)} = Y_{dc,ni} \rightarrow \text{for } 1 \leq i,j \leq n-1 \quad [2.33]$$

$$\left(\frac{\partial F_i}{\partial X_n}\right)^{(k)} = 0 \rightarrow \text{for } 1 \leq i,j \leq n-1 \quad [2.34]$$

$$\left(\frac{\partial F_n}{\partial X_n}\right)^{(k)} = -\frac{0.5}{V_{dc,n}} \rightarrow \text{for } 1 \leq i,j \leq n-1 \quad [2.35]$$

The initial conditions of unknown variables vector X are set as: $X_0 = \left[1, \ldots, 1, -\sum_{i=1}^{n-1} P_{dc,i}\right]$ (DC voltages are initialized to 1 p.u., while the power injection at the slack bus is set to $-\sum_{i=1}^{n-1} P_{dc,i}$).

Once the power flow is solved, the power distributions in each line between different interconnected nodes (from i to j) are calculated as follows:

$$P_{l,ij} = 2V_{dc,i}Y_{dc,ij}\left(V_{dc,j} - V_{dc,i}\right) \quad [2.36]$$

The power flowing to the shunt resistance at node i is calculated as follows:

$$P_{l,ii} = 2{V_{dc,i}}^2 \frac{1}{R_{ii}} \quad [2.37]$$

The flow chart of the resolution of the power flow using this first method is presented in Figure 2.18.

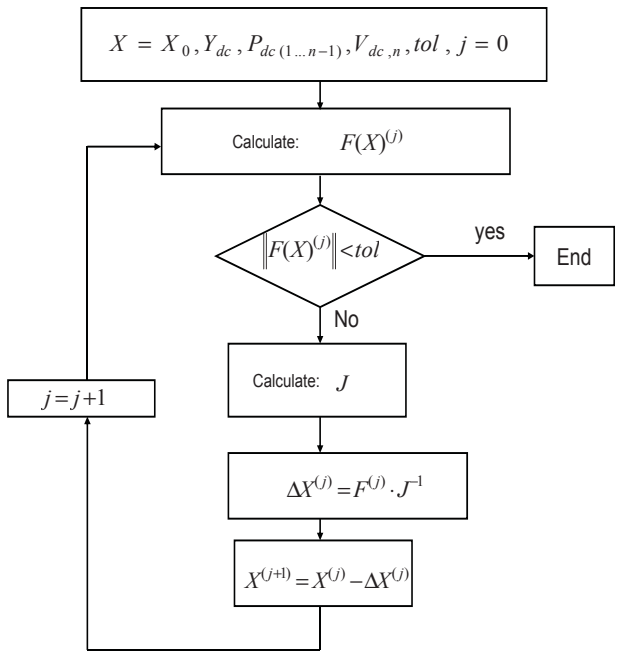

Figure 2.18. *NR flow chart for the first power flow resolution method*

2.6.2. *The second method (for a droop control): generalized approach*

Alternatively to the first proposed approach, the nonlinear DC network equations could be solved using a generalized method with NR. The advantage of this method is the possibility to include converters under distributed voltage control. Two different droop integration ways are possible: the droop following a voltage/power characteristic and a droop following a voltage/current characteristic as shown in Figure 2.8. This resolution method aims to find the DC voltages. After this, the unknown power injections are calculated via equation [2.15]. The process of the power flow calculation using the generalized approach is shown in Figure 2.19.

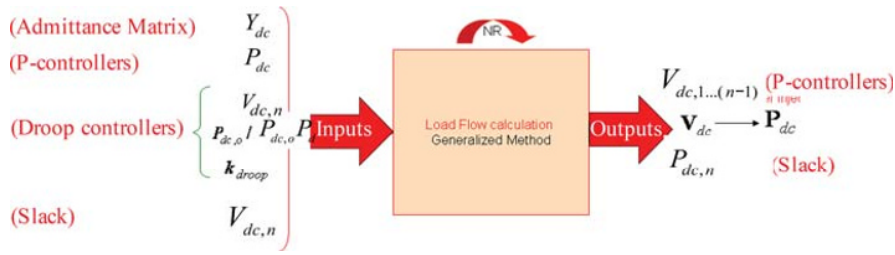

Figure 2.19. *Chart of the power flow calculation with droop characteristics: second method*

2.6.2.1. *Voltage/power droop*

Recall the expression [2.1] describing the voltage/power droop given previously:

$$P_{dc,i} = P_{dc,0,i} - \frac{1}{k_p}\left(V_{dc,i} - V_{dc,0,i}\right)$$

In the above equation, terms $V_{dc,0,i}$ and $P_{dc,0,i}$ are physically possible since they are the results under normal condition of a power flow calculation using a master/slave strategy. To apply the NR technique, the problem should be written in a form to minimize a system of equations which depends only on the DC voltages. This method could be applied to a grid topology with or without a slack bus. In the case of slack bus existence (considering that the DC voltage of this bus is known), all the terms corresponding to this bus are removed from the problem formulation.

This resolution method consists of:

– identifying the value of the power for the power controllers $P_{dc,i}$ busses;

– knowing the power injection in the reference point for the droop controllers $P_{dc,0,i}$ busses;

– building a system of equations, containing the difference between the fixed values and calculated values.

The power flow is solved when this difference is equal or lower than a tolerance, which is also equal to $1e^{-8}$ as before. For the P-controller nodes, the calculation of the power injection derived as given previously by equation [2.15]. That is:

$$P_{dc,i} = 2V_{dc,i}\left(\left(\sum_{\substack{j=1 \\ j\neq i}}^{n} \frac{1}{R_{dc,ij}}\left(V_{dc,i} - V_{dc,j}\right)\right) + \frac{V_{dc,i}}{R_{dc,ii}}\right)$$

For the DC voltage/power droop controllers, the calculation of the power reference could be deduced from equation [2.1] as follows:

$$\boldsymbol{P_{dc,i}} = \boldsymbol{P_{dc,0,i}} - \frac{\mathbf{1}}{\boldsymbol{k_p}}\left(\boldsymbol{V_{dc,i}} - \boldsymbol{V_{dc,0,i}}\right) \qquad [2.38]$$

Replacing [2.15] into [2.38], we have:

$$P_{dc,0,i} = 2V_{dc,i}\left(\sum_{\substack{j=1 \\ j\neq i}}^{n} \frac{1}{R_{dc,i,j}}\left(V_{dc,i} - V_{dc,j}\right) + \frac{V_{dc,i}}{R_{dc,ii}}\right) + \frac{1}{k_p}\left(V_{dc,i} - V_{dc,0,i}\right) \qquad [2.39]$$

Consequently, a modified active power vector taking into account the power controller busses (P-controller) and busses with DC voltage/power droop controller is introduced as follows:

$$P_{dc,mod} = \left[P_{dc,1}, \ldots, P_{dc,k}, P_{dc,0,k+1}, \ldots, P_{dc,0,m}\right]^T \qquad [2.40]$$

The calculation of this modified active power vector is performed as follows:

$$P_{dc,\mathrm{mod},cal} = \begin{cases} P_{dc,i} \ \text{ from equation [2.15] with } i \in [1,k] \\ P_{dc,0,i} \ \text{ from equation [2.39] with } i \in [k+1,m] \end{cases} \quad [2.41]$$

This vector has the dimension of n if there is no slack bus converter in the grid and the dimension of (n-1) in case of the existence of a slack converter which has been removed. This later assumption means the existence of k P-controllers and m-k (DC voltage/power) droop controllers with $m = n$ or $m = n$-1 is depending on the grid topology. In the implementation, it is easier to consider all the nodes as droop controllers and fix the droop constant to 0 if a slack bus is required and to ∞ if a P-controller is required (see Table 2.1). The difference between the modified vector [2.40] and the calculated vector [2.41] is $\Delta P_{dc,mod}$, which should be equal to zero (respecting a tolerance) when solving the equations. All details of calculations can be found in [GHO 12] and [BEN 14].

After convergence, all the DC voltages are known. The power injections of the slack bus and the busses under voltage droop are calculated thereafter using appropriate equations. The flow chart of power flow calculation using this so-called generalized method with voltage/power droop control is presented in Figure 2.20.

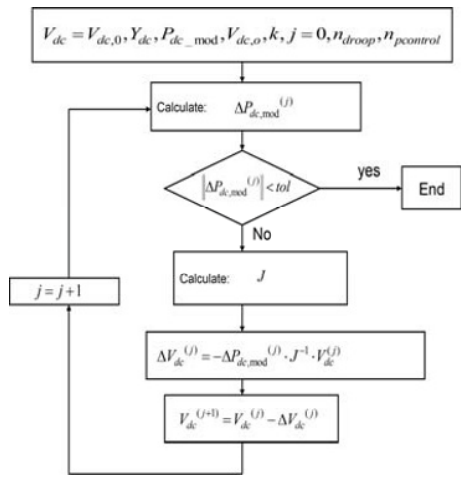

Figure 2.20. *NR flow chart for power flow calculation taking into account voltage/power droop*

2.6.2.2. *Voltage/current droop*

The same resolution principle such as the voltage/power droop is adopted. For more details, the readers can refer to [GHO 12].

2.6.3. *Generalized power flow for multi-terminal DC grids with more than one slack bus*

A new power flow principle and calculation for DC grids is elaborated within the PhD thesis of Miguel Jimenez [JIM 15]. With this new methodology, it is possible to have more than one slack bus (node where voltage is known), in contrast to methods where there is only a node where the voltage is specified. A complete proof is given, which guarantees the unique existence of solutions. This new algorithm could be easily adapted for AC systems. Published paper in this direction is under consideration.

2.7. Steady state control of multi-terminal DC grids

The implementation and simulation are valid on any grid topology. In this section, the calculation of the power flow will be tested using different control strategies in order to confirm the expected behavior of the MTDC grid. Moreover, a power-step disturbance is applied on one node of the DC grid in order to evaluate the responses of the power and DC voltage within the different strategies presented earlier in this chapter. For the sake of clarity, a three-terminal DC network is considered. The development and results obtained for such minimum meshed grid could be easily extended to more complicated DC power network. It has been shown that the methods and solutions presented here are independent from the voltage level.

The base values of the DC power and DC voltage bases are, respectively, $P_{dc_base} = 3MW$ and $V_{dc_base} = 12kV$. The Y_{dc_base} value of the base admittance is calculated using the following expression. That is:

$$Y_{dc_base} = \frac{I_{dc_base}}{V_{dc_base}} = \frac{P_{dc_base}}{2\left(V_{dc_base}\right)^2}$$

The considered three-terminal DC grid is given in Figure 2.21.

It is assumed that all the converters have the same shunt resistance value, $R_{shunt} = 10k\Omega$. In any node i, it is assumed that $R_{shunt} = R_{dc,ii}$. The lineic resistance values and lengths of the multi-terminals cables are given in Table 2.2.

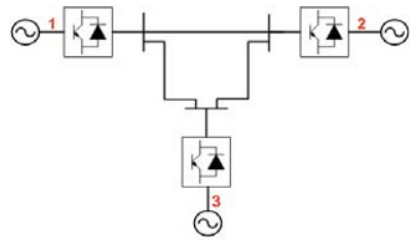

Figure 2.21. *Three-terminal DC grid*

Initial bus	Final bus	R_{dc}[ohm/km]	L[km]
1	2	0,0121	200
1	3	0,0121	100
2	3	0,0121	150

Table 2.2. *Lineic resistance and the length of the cables (links)*

2.7.1. *Normal operation (without fault)*

In this operation mode, no power-step-change is considered. As shown in Figure 2.22, the first two nodes 1 and 2 are considered as P-controllers, while the third node has the slack function. Before solving the power flow, the power injections in the P-controller busses and the DC voltage in the slack bus 3 are fixed in p.u. as shown in Figure 2.22.

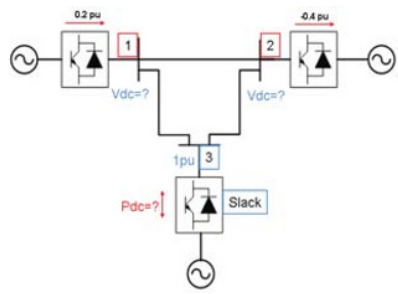

Figure 2.22. *Three-terminal HVDC before the power flow resolution*

Using a master/slave control strategy, the results of the power flow calculation (underlined values) are shown in Table 2.3.

We can remark that for the master/slave control strategy, it is the slack bus that will compensate for the losses.

Node	P_{dc} [p.u.]	V_{dc} [p.u.]
1	0.2	1.000
2	-0.4	0.9977
3	0.2585	1.0000

Table 2.3. *DC power injections and DC voltage values at different nodes*

The transmitted (DC) power between the different nodes is resumed in Table 2.4, while DC power losses in the shunt resistance of the converters are given Table 2.5.

initial bus (i)	final bus (j)	P_{dc}, ij [p.u.]
1	2	0.1802
1	3	0.0006
2	1	-0.1798
2	3	-0.2393
3	1	-0.0006
3	2	0.2399

Table 2.4. *Transmitted DC power between the connected nodes*

Node i	P_{dc}, ii [p.u.]
1	0.0192
2	0.0191
3	0.0192

Table 2.5. *Power losses in the shunt resistance at the different nodes*

These implemented power flow results are shown in Figure 2.23.

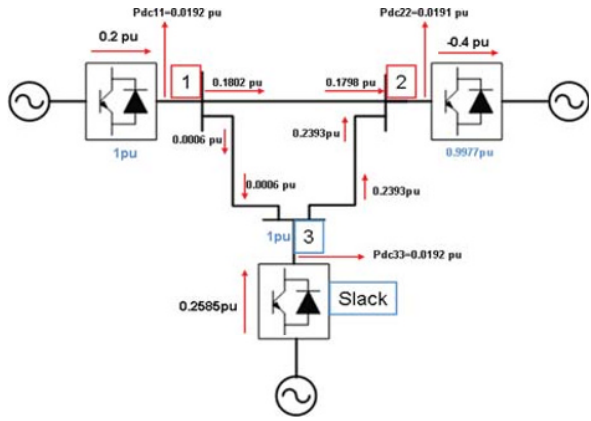

Figure 2.23. *Illustration of the power flow results of a three-terminal HVDC*

2.7.2. *Power-step-change with master/slave strategy of control*

This section treats the case of power-step-change in node 1. The power injection of this node falls from 0.2 to 0 p.u. at time t = 50. In the master/slave control strategy, only the sack bus (bus 3) is responsible for compensating this power variation in the DC system. Figure 2.24 shows the evolution of the power at different nodes, while Figure 2.25 highlights the progress of the corresponding DC voltage in these three nodes. As expected, the slack bus (bus 3) provides the compensation for the losses at bus 1 to restore the power balance.

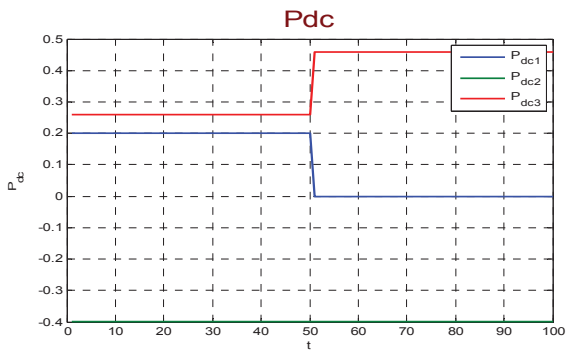

Figure 2.24. *DC grid power response to power disturbance at node 1 with master/slave control strategy. For a color version of the figure see www.iste.co.uk/benchaib/control.zip*

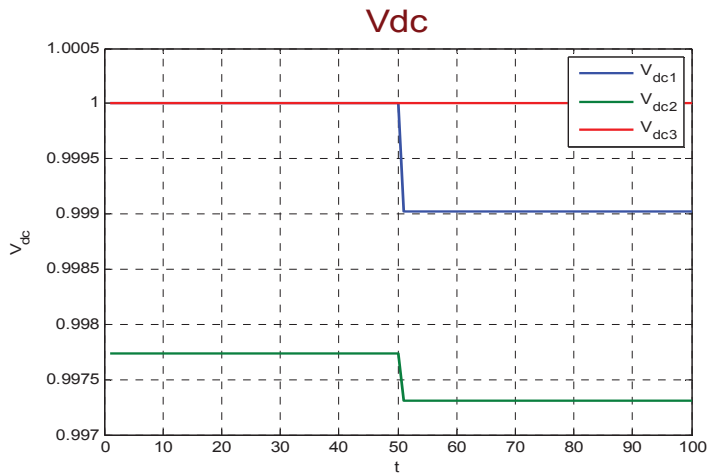

Figure 2.25. *DC grid voltage response to power disturbance at node 1 with master/slave control strategy. For a color version of the figure see www.iste.co.uk/benchaib/control.zip*

However, when power losses occur in an MTDC grid, the DC voltage at each node will decrease until the power balance is satisfied. This is the case for nodes 1 and 2. At node 3, which is the slack bus, the DC voltage is maintained equal the value before the disturbance by injecting the necessary power to satisfy. This is the aim of the master/slave control strategy.

2.7.3. *Voltage margin control*

In this section, the voltage margin control strategy is applied on a three-terminal DC grid. The main property of this strategy, which was discussed earlier in this chapter, consists of the fact that when one station controlling the DC voltage reaches its power limit, the DC voltage control responsibility is transferred to another station with more flexibility at this operating point. If the converter chosen as the initial slack bus is working as a rectifier (DC power injection > 0) and it reaches its upper limit, the DC voltage decreases because the VSC is supposed to generate more power than the value that it is capable of. Contrarily, if the slack converter is working as an inverter (power injection < 0) when it reaches its lower limit, the DC voltage increases because it is supposed to consume more power than the actual value. In the proposed scenario, consider that the injected power in node 1 goes from

0.2 to 0 p.u. At the beginning, node 3 works as a slack bus and controls the DC voltage, while node 2 controls its assigned power injection. When the injected power in node 3 hits the limitation (suppose, here it is limited to 0.4 p.u.), it could not continue to control the DC voltage anymore. In this case, and in accordance with the margin control strategy, the DC voltage control is handed over to station 2, which becomes the new slack bus by keeping its DC voltage at its reference value; consequently, node 2 which is the slack bus at this instant is responsible for the power balance. The described scenario is shown in Figure 2.26.

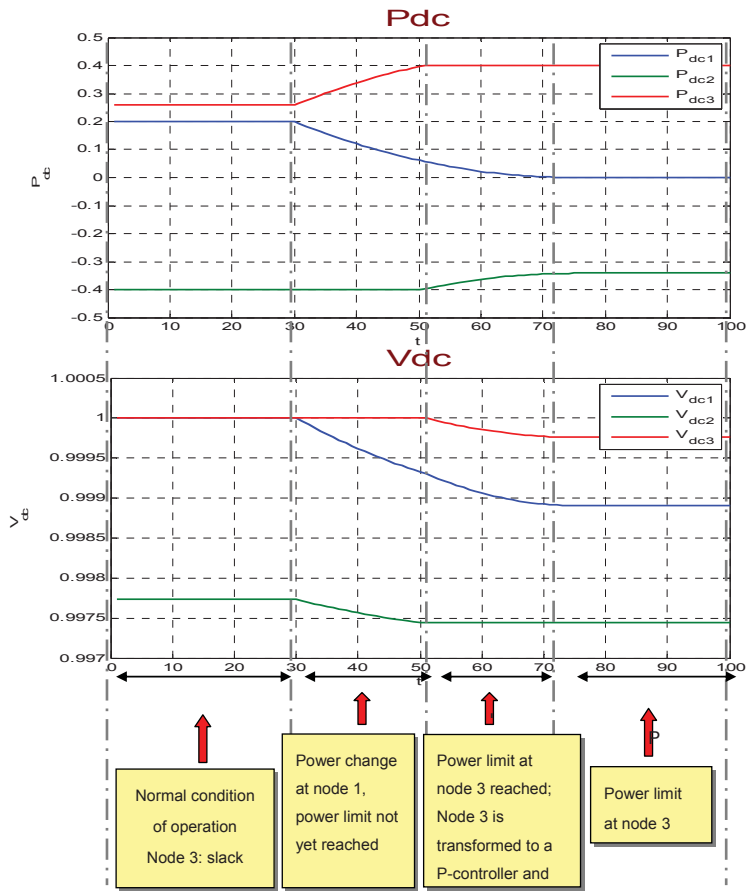

Figure 2.26. *DC grid power voltage responses to power disturbance at node 1 with voltage margin control strategy. For a color version of the figure see www.iste.co.uk/benchaib/control.zip*

2.7.4. *Power-step-change for a voltage/power droop control*

In this test case, the power injection of the node 1 changes and goes from 0.2 to 0 p.u. at t = 50. The DC voltage control is distributed over the two converters of nodes 2 and 3. The droop constants are 0.03 and 0.05, respectively. Figure 2.27 shows the evolution of the DC power injections, while Figure 2.28 highlights the DC grid voltage response to power disturbance using voltage/power droop control strategy. As expected, the power compensation is well distributed over the nodes 2 and 3.

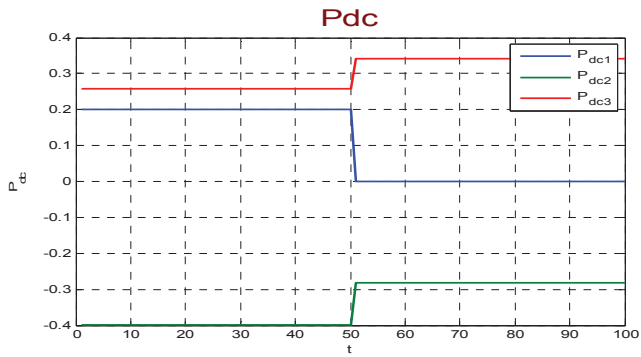

Figure 2.27. *DC grid power response to power disturbance at node 1 with voltage/power droop control strategy. For a color version of the figure see www.iste.co.uk/benchaib/control.zip*

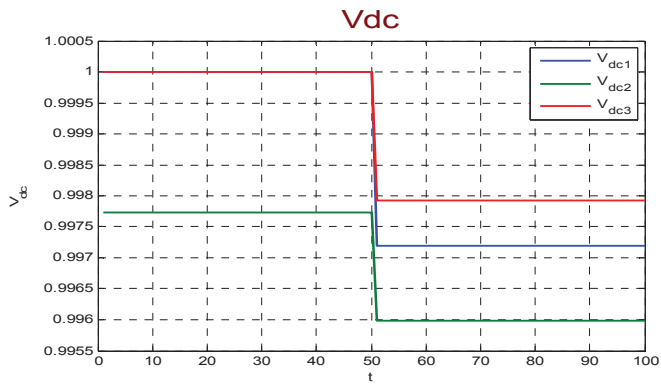

Figure 2.28. *DC grid voltage response to power disturbance at node 1 with voltage/power droop control strategy. For a color version of the figure see www.iste.co.uk/benchaib/control.zip*

2.8. Primary and secondary control strategies

In any electric system, the active power generation and consumption must be balanced. Generation units and even loads in some cases must be maneuvered to maintain power balancing so that the network users are not affected by load changes or generation and transmission outages.

In the AC power network, the secondary control drives the system's frequency and cross-border power exchanges back to the original desired values after 15–30 s (up to 1 mn) if the activated power reserve does not reach the saturation limit. In an MTDC grid, the DC voltage is controlled and should be maintained in an acceptable margin.

The primary control strategy which is a global but distributed control aims to stop the power unbalance by injecting (or less consuming) predefined power quantities. The primary control strategy which mainly performs a disturbance rejection will then force the power system to a new production-consumption balanced situation but at different DC voltage levels. If the new DC voltage values are not close to the nominal ones, a secondary control strategy is performed to satisfy the DC voltage requirements. In this section, primary and then secondary control strategies for the MTDC system are applied on a three-terminal HVDC network. In Figure 2.29, a power balancing process including primary control and secondary control strategies is presented for a specific scenario defined below.

A power flow calculation, with node 3 set as slack bus, is first performed in normal operations. At time 50 s, a disturbance is occurring in node 1 in the form of a power-step-change, where the injected power at this node goes to zero with a given time constant. The power loss will cause a voltage drop at all nodes of the interconnected system. As soon as the voltage drop (resulting from the power disturbance) is detected, the voltage droop control is automatically activated at the healthy nodes in order to compensate for the disturbance. This control process which will last also 50 s (from 50 to 100 s) is known as the "primary" control strategy which is chosen to be based on droop control. At t = 100 s, and in order to reduce the voltage deviation, a power flow is performed to calculate new voltage references taking into account the actual power capabilities of each node. Thereafter, a master/slave control method is applied with node 3 as master bus to bring back the voltage to acceptable margins by fixing the value to 1 p.u. This new

control process is called “secondary” control strategy and is based on the master/slave method. For the sake of responsibility sharing, the secondary control approach could use the so-called voltage margin control. We should note that during the secondary control process (from 100 to 150 s), the power values in all the nodes have an imperceptible deviation as shown in Figure 2.29. At t = 150 s, the power injection at node 1 is back to its initial value (before the disturbance) and consequently a primary strategy based on droop control is reactivated. Contrarily to the power loss shown at first, the DC voltage values increase. Similarly to previous control process, a secondary control is activated at t = 200 s in order to bring DC voltages around nominal values by applying once more a master/slave DC voltage control strategy.

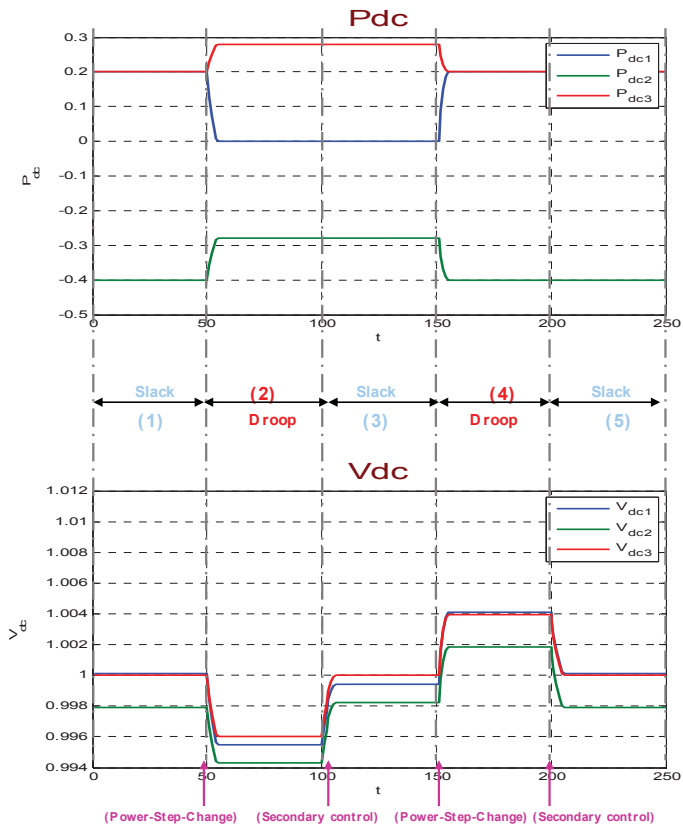

Figure 2.29. *Power balancing of a three-terminal DC grids with primary and secondary control strategies. For a color version of the figure see www.iste.co.uk/benchaib/control.zip*

2.9. Dynamic control of multi-terminal DC grids

A dynamic model for VSC-MTDC systems valid for every DC grid configuration and regardless of the converters' topology was developed in [COL 10], starting with the basic differential equations of the AC and DC circuits to finally add the controller and coupling equations. In this section, the time domain expressions can be obtained to assemble a differential-algebraic equation (DAE) system that allows describing the dynamic behavior of VSC-MTDC systems. In Appendix 1, preliminary results on dynamic behavior of MTDC grid have been derived under the following assumption:

The model is only valid for small deviations from the fundamental frequency, since quasi-stationary phasor representation is used. A full electromagnetic model, valid for a broad frequency range, would require representing the AC and DC filter, valves, etc.

The AC grid voltage is considered as perfectly constant, balanced and stable since the dynamic models of generators, exciters, governors, automatic generation control (AGC), automatic voltage regulator (AVR), power system stabilizer (PSS) among others are not integrated, even though it is acknowledged that the electrical network has its own dynamic performance, which can be influenced by faults, resonances, overload, etc.

The main feature of the proposed work in Appendix 1 is its suitability for studying slow transients in any DC grid configuration regardless of the converters topology. However, the filters, switching components, phase locked loop (PLL), fast-acting protection and firing control are not modeled, which was necessary to confine the range of time constants to a practical wide, appropriated to the phenomena of interest (around the fundamental frequency); otherwise, an enormous modeling effort and a huge computational power would be required. Nevertheless, these elements could be included in further works, as the AC grid generators and their control.

In [SHI 14], physical constraints on MTDC system operation have been considered. The theoretical power transmission capabilities of VSC and the relationship with DC grid voltage have been investigated to clarify the cause of stability problem in MTDC grid. Violation of such power transmission capabilities could be one possible factor of instability. Consequently, by taking appropriate actions in VSC controllers with considered topologies, the risk of instability can be reduced.

2.10. Plug-and-play in interconnected systems: application to MTDC grids

In power grids, electrical engineers have used since the beginning time scales separation to control and operate such systems by setting multi-time scales control layers (local, primary, secondary, tertiary controls, etc.). By considering physical systems together with their associated local controller and upper control layers, time scales are intrinsic in power systems [WIN 80]. To deal with such time scales, control engineers have used backstepping techniques [ROO 01] and singular perturbation theory. The most prominent feature of singularly perturbed systems is that the derivatives of their states are multiplied by a small positive parameter which is used to quantify the time scale decomposition. Based on singular perturbation theory, lower order subsystems in different time scales can be derived to approximate the behavior of the original system [KOK 99]. In addition to the control design, it is mandatory to prove the global stability of the system in order to make sure that there will be no disturbances causing the system collapse. When dealing with high order and complex systems and due to mathematical computation and calculation complexity, it is not easy to prove such stability. It is maybe not the best way to perform the desired control. New control design methodology should be developed in order to deal with complex system of systems. It is needed to work at the junction of the systems in order to propose some kind of separation principle for interconnected systems. In this configuration, the singularly perturbed structure will be a consequence and not a starting point for the control design. The work which has been initiated in [CHE 14] needs to be pursued in order to propose the adequate conditions for plug-and-play properties. The formal conditions could then be added to the grid code connection for power network.

2.11. Control of the actuators connected to the power system

The considered actuators are all non-passive systems that are connected to the power network. That is electrical machines ([GIL 13] and [DEB 13]), photo-voltaic (PV) systems, FACTS, storage systems or sometimes only power electronics converters that are connected to a power network. The control of the considered actuators will have a great influence on the stability of the whole system; see [ETX 02] and [DJO 14]. A coordinated and distributed control satisfying plug-and-play properties as well as stability conditions needs to be proposed taking into account emerging converter technologies.

2.12. Concluding remarks

This chapter has been organized into three main parts:

– The first part has reviewed the principles, tools and control strategies present in the literature and necessary for the control of MTDC grid.

– The second part of this chapter has concerned some recent results on the control of the DC grid. At first, DC power flow calculation is proposed. Depending on the DC grid topology as well as the adopted control strategy, two different methods of problem-positioning have been dealt with. The first method is used to calculate the power flow of a DC network that contains one node as a slack bus with the other busses as P-controllers. The second method offers the possibility to integrate the DC voltage droop control which has been referred as "generalized" method. Thereafter, the implementation and simulation of different control strategies in spite of power disturbance for the MTDC grid have been highlighted. Thereafter, primary and secondary control strategies based on droop and master/slave controls have been shown in section 2.8. More calculation details and simulation results have been presented and discussed in [CAR 12] and [GHO 12].

– The third part of the proposed chapter concerns the present and future research activities in the area of multi-time scales based on control of MTDC grid. Initiation study of dynamic control of MTDC grid has also been considered. Control and simulation of MTDC grid with dynamic aspects have been tackled in the work given in Appendix 1. There is still a lot of research to conduct in this area. Next, plug-and-play properties of networked systems have been discussed. First results on dynamic restrictions have been obtained for VSC converter when connecting DC and AC side [CHE 14]. As before, it is a novel area of research in which some formalism needs to be developed. The latter could provide global stability with its heavy mathematical development and will enable plug-and-play properties which will complete the grid code connection of DC power network in terms of controllers time constants restrictions.

– Finally, control of actuators for power network has been briefly discussed.

3

From Small Signal to Exact Linearization of Swing Equations

3.1. Introduction

In power systems, an operator may be responsible for a small region with its corresponding control area, or a large region with multiple control areas. Considering the size of region, the operator will have to deal with priorities and constraints as imposed by its regional responsibilities. To monitor real-time grid conditions, operators have relied on supervisory control and data acquisition (SCADA) measurements together with state estimations. However, the monitoring is limited to the measured power network within a SCADA system territory. Wide-area monitoring systems (WAMS), which go beyond these limitations to much larger part of the interconnected power networks, will provide real-time grid monitoring capabilities as the primary objective. They will provide grid operators with a comprehensive manner to facilitate decision making and to ensure grid reliability. Wide area grid responsibilities are where GIS and other geo-special visualization technologies can be effectively applied [MAN 12].

In Figure 3.1, as described in [GRI 12], the main components in WAMS are described as follows:

– *PMU*: phasor measurement units (PMUs) dispersed across a wide geographical region to provide subsecond, time-tagged measurements of voltages and currents;

Advance Control of AC/DC Power Network: *System of Systems Approach Based on Spatio-temporal Scales*, First Edition. Abdelkrim Benchaib.
© ISTE Ltd 2015. Published by ISTE Ltd and John Wiley & Sons, Inc.

– *PDC*: phasor data concentrator (PDC) gathers data from several PMUs and aligns the data by time tag to create a time-synchronized dataset and stream this dataset in real-time to the applications;

– communication links and monitoring center: where the operators are provided with information of the current dynamic grid conditions in a comprehensive way for prompting confident decision making.

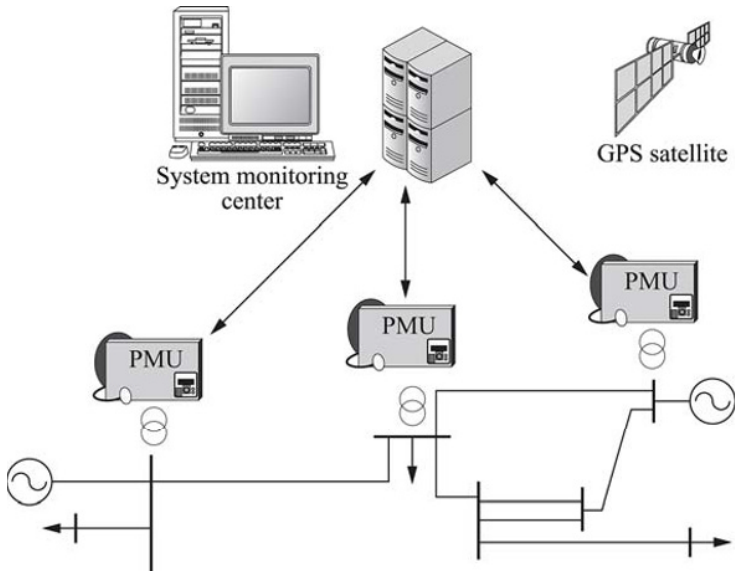

Figure 3.1. *Wide area monitoring system (WAMS) [MAN 12]*

The PMU-based system could provide the following analysis and advantages:

– *Angle monitoring and alarming*

Combined synchro-phasor angle measurements can indicate grid stress. There are two ways to combine synchro-phasor measurements to monitor grid stress:

- the angle differences between multiple pairs of busses are simply obtained and these data can be mined to detect undue stress or unusual events;

- computing the angle across an area is straightforward, but there are additional requirements of synchro-phasor measurements at all the busses along the border of the area and a DC load flow model of the area. The area angle obeys circuit laws and can give more specific information about events inside the area [GRI 12];

– *Small-signal stability (dynamic stability) and oscillations monitoring*

As long as there is power transmission, there exists no way to get rid of oscillations. Normally, if the system is stable, the power imbalances are settled in an oscillatory way and are usually well damped. However, things are looked in a different way when oscillations are growing in amplitude or an interaction occurs between oscillations. The growing oscillations can result from power-system stress, unusual operating conditions or failed controllers (PSS, excitation, etc.). The system can either transient into the oscillation because of an outage/failure or slowly build into the oscillation because of an increased system stress or forced oscillation. Growing power oscillations can cause line openings and generator trippings, and in the worst case, lead to cascading power blackouts, and the interactions between oscillations can lead to major equipment damage. So, it is very important to detect sustained or growing oscillations and to take mitigating actions [GRI 12].

In reality, the power-system is a nonlinear system. Fortunately, the system behaves relatively linear when working at a steady-state operating point [KOS 99].

In addition to the WAMS tools based on remote measurements from multiple locations, a new wide area control systems (WACS) concept is under deployment. This new opportunity will help operators handling local disturbances and external perturbations much quicker than traditional SCADA system. In coordination with controllable actuators such as FACTS, HVDC stations, storage and generators, it will be possible to mitigate power oscillations and instabilities in power networks. WACS will take great part in the control and protection strategies in the power grid of the future. Thanks to controllable devices and in order to stop fault propagation, these strategies can also be applied at local levels if the power network is considered as an interconnection of clusters with a limited number of nodes.

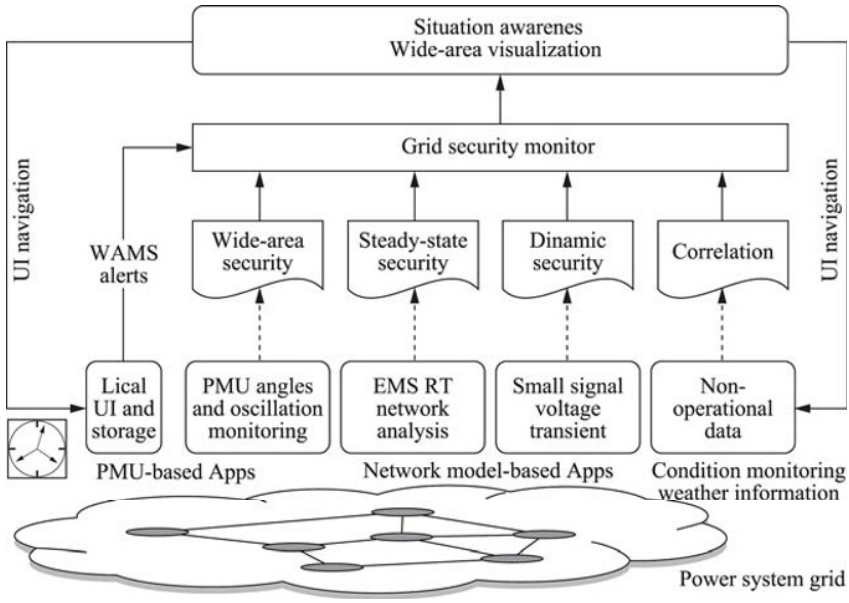

Figure 3.2. *PMU-based WAMS and network-model-based EMS hybrid solution [MAN 12]*

As detailed in [MAN 12], Figure 3.2 illustrates PMU-based WAMS and network-model-based EMS hybrid solutions. In the following, our aim is to propose some methodologies and solutions mainly for grid dynamic security of AC systems and hybrid AC/DC grids.

Unusual operation conditions or outages/failures can give rise to growing oscillations in power networks. As aforementioned, growing oscillations, which in the worst case lead to cascading failures and blackouts, can cause lines openings and generators trippings. Interaction between oscillations could lead to major equipment damages. Therefore, it is important to detect such sustained and growing oscillations and take damping action before it gets out of control with unwanted consequences in power network.

A power network is a nonlinear system which has a relatively linear behavior when disturbances do not force it far from steady-state operations. If the perturbation is too big, linear approximations can highlight limitations in the stability studies and may lead to wrong decisions. In the standard classification of power system response, there are two types: transient (sometimes termed a ring-down) and ambient. Ambient case refers to the

system exited by low-amplitude random variations (such as random load changes), whereas transient response (which has larger amplitude) refers to a sudden switching action, or a sudden step or pulse inputs. Figure 3.3 shows real power flowing on a major transmission line during the Western North American power system breakup of 1996.

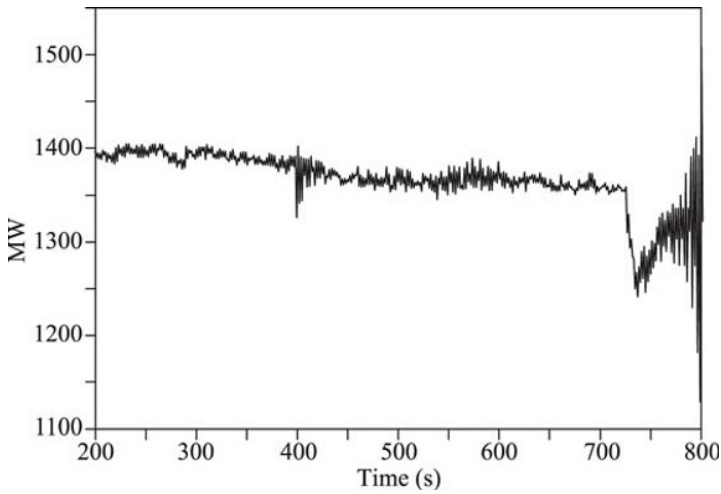

Figure 3.3. *Real power flowing on a major transmission line during the Western North American power system breakup of 1996*

Prior to the transient at the 400 s point, the system is in an ambient condition. After the ringdown at the 400 s, the system returns to an ambient condition. The next event in the system causes an unstable oscillation.

Power system stability is an important issue in the electrical network, recognized since the 1920s, having caused major blackouts around the world. In [KUN 94], power system stability is defined as the ability of an electric power system, for a given initial operating condition, to regain a state of operating equilibrium after being subjected to a physical disturbance, with most system variables bounded so that practically the entire system remains intact. This definition applies to interconnected power systems, a group of generators or a particular generator.

Both the initial operating conditions and the nature of perturbation will influence the stability of a system subjected to a given small or large disturbance. It is the disturbance's degree classification which will drive the system stability studies and consequently the size of the disturbance influences the method of calculation and prediction of stability.

A perturbation is considered to be small (such as insufficient damping of oscillations) if the system is able to adjust without interruption. A large disturbance refers to a power system in severe transient such as short-circuit on transmission lines, loss of generation, or loss of a large load; which often leads to structural changes in order to isolate the faulted element.

In stability studies, mathematical models play a key role in such analysis. If the disturbance is not small enough, the linearized model (small signal model) may lead to erroneous results and several linearized models may be needed. Also, it is not obvious to quantify the operation domain where such linearized models are valid. If an exact linear model is developed, it could fundamentally change the stability analysis of power systems. The following results have been mainly presented in [ROI 13, LI 14] and references therein.

This chapter is organized as follows. In section 3.2, a recapitulation of stability analysis tools as used for power system studies is shown. A detailed modeling of AC power network dynamics with swing equations is given in section 3.3. Nonlinear models and the standard small signal (linearized) swing equation are compared by simulation to multi-machine Simpower models in section 3.4. Thereafter, a revisited swing equation model is proposed in section 3.5. Next, an exact linearized model is given in section 3.6 to cover the whole space, especially when the occurring disturbance is big enough to force the system far away from its trajectory of equilibrium.

3.2. Recalling stability analysis tools

The power system dynamic behavior is expressed in a state space representation by a set of n first order nonlinear models. Nonlinear systems may have at least one equilibrium point and the system's stability is categorized depending on the region around it (see [ROI 13] and references therein) yielding:

– local stability or "stability in the small", when a system subjected to small perturbation, stays within an infinitesimal region around the equilibrium;

– finite stability, when a system returns to the equilibrium point from any point within a region R of finite dimensions surrounding it;

– global stability or "stability in the large", if the region R includes the entire finite space.

3.2.1. *Small signal analysis – first method of Lyapunov*

The *first Lyapunov method* helps to determine stability in the immediate vicinity of the equilibrium point by the linearized system around it, and then calculate the roots of the characteristic equation by the eigenvalues of the state matrix:

– if the eigenvalues have negative real parts, the nonlinear system is asymptotically stable;

– if at least one or more eigenvalues have positive real part, the original system is unstable;

– if the eigenvalues have real parts equals to zero, the nonlinear system can be either asymptotically stable or unstable.

The eigenvalues of a linearized system reveal if the system is stable or unstable around an equilibrium point for small perturbations. This is the first stability theory.

3.2.2. *Transient stability*

If a large disturbance occurs, the transient stability theory is implemented in order to determinate the critical clearing time before the loss of synchronism of rotating machines. This usually appears when mechanical and electrical torques are unequal. As shown in Figure 3.4, the stability is influenced by the relationship between the rotor angle and the accelerating power.

Assuming a short-circuit fault introduced on the transmission line, $P_{e-prefault}$ is the power delivered under normal operations (no disturbance);

$P_{e-duringfault}$ is the power delivered during short-circuit and $P_{e-postfault}$ is the power distributed after clearing the perturbation.

If a perturbation occurs at t_0, the operating points shifts from a to b, while the rotor angle does not change instantly due to inertia. Since P_m is bigger than P_e, the rotor accelerates until reaching the operating point c and stores energy (kinetic). At t_{c1}, the fault is cleared, thus the operating point moves to d. Currently, P_e is greater than P_m which entails the rotor's deceleration. However, when the rotor speed is higher than this reference, it keeps increasing until the kinetic energy gained during the acceleration is converted into potential energy. The operating point swifts from d to e, where the areas A_1 and A_2 are equivalent. At this instant, the rotor angle reached its maximal value δ_m, whereas P_e is still higher than P_m. The rotor angles decreases until the operation point is in position d. Consequently, the generator returns to a stable state leading to a stability region definition around this stable point.

However, if the clearing time will be longer (Figure 3.4 on the left), the kinetic energy stored during the fault is not entirely consumed (A_1 and A_2 are not equal). Besides, the speed is greater than its nominal value ω_0 and keeps increasing. Thereafter, the rotor speed and angle will continue to augment until loss of synchronism.

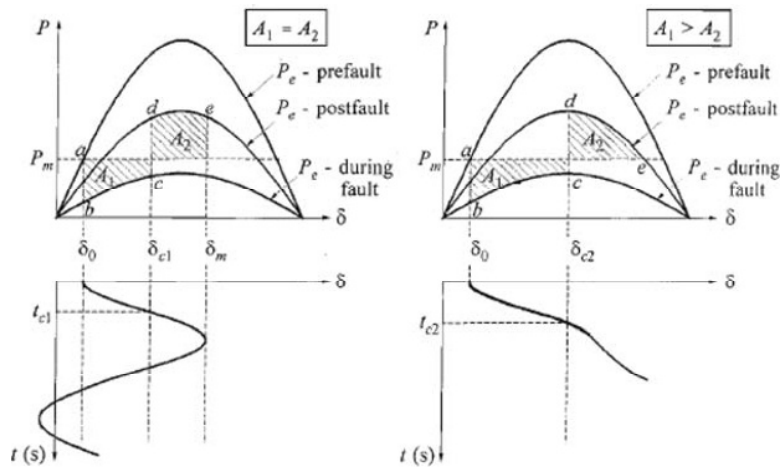

Figure 3.4. *Response to a fault cleared in t_{c1} seconds, stable case (left), in t_{c2} seconds unstable case (right)*

3.2.2.1. *Equal area concept*

The relationship between areas A_1 and A_2 can be shown as follows. Let us consider the well-known swing equation of generators:

$$\frac{d^2\delta}{d^2t} = \frac{\omega_0}{2H}(P_m - P_e) \quad [3.1]$$

δ is the rotor angle, H is the inertia constant, ω_0 is the reference angular velocity, P_m is the mechanical power entering at the machine and P_e is the output electrical power. The instant t_0 is the time when the fault appears. The fault disappears at time t_1. This perturbation will modify the power flow and consequently the rotor angle δ. As stated above, two areas A_1 (the acceleration zone) and A_2 (the deceleration zone) are to be considered. If the stored kinetic energy is given back during zone A_2, the rotor will retrieve its stability. If not, the rotor will decelerate until the loss of synchronism. Therefore, there exists a close relationship between the two areas A_1 and A_2 and the transient stability. Multiply the above equation by $2d\delta/dt$ in each side, that is:

$$\frac{d}{dt}\left[\frac{d\delta}{dt}\right]^2 = \frac{\omega_0(P_m - P_e)}{H}\frac{d\delta}{dt} \quad [3.2]$$

Integrating both sides, we have:

$$\left[\frac{d\delta}{dt}\right]_{\boldsymbol{\delta_0}}^{\boldsymbol{\delta_2}} + cte = \int_{\boldsymbol{\delta_0}}^{\boldsymbol{\delta_2}} \frac{\omega_0(P_m - P_e)}{H} d\delta \quad [3.3]$$

When $t = 0 \rightarrow \delta = \delta_0 \rightarrow cte = 0$, after the fault elimination, δ will stop varying and the generator will retrieve the synchronism speed. Consequently, we have:

$$\int_{\delta_0}^{\delta_2}(P_m - P_e)d\delta = 0 \Rightarrow \int_{\delta_0}^{\delta_1}(P_m - P_e)d\delta + \int_{\delta_1}^{\delta_2}(P_m - P_e)d\delta = 0 \Rightarrow A_1 = A_2 \quad [3.4]$$

Therefore, the recovery limits of the transient stability can be mathematically formalized by the equality of the areas A_1 and A_2. This condition is called the equal area criterion. Consequently, the transient stability can be improved by decreasing the acceleration zone or increasing the deceleration zone. The latter can be obtained by increasing the electric power or decreasing the mechanical

power. The control of these two zones is closely linked with the regulation of the internal angle δ. When the fault is located, the clearing time is of great importance in order to guarantee the stability of the system. The main objective is to find the maximum clearing time which can be obtained from the criterion above in order to prevent instability of the system.

The state of the system after the fault-clearing can be assimilating to the value of the energy function at this time. The direct method, also named as *second Lyapunov theory*, solves the stability problem by comparing the clearing fault energy V_{cl} to the critical energy V_{cr}. If V_{cr} is greater than V_{cl}, the system is stable. The difference $(V_{cr} - V_{cl})$ is the transient energy margin with V_{cl}, the amount of transient energy injected into the system by the fault while the critical energy measures the energy absorbing capacity of the post-fault system.

3.2.3. *Global stability*

Global stability determines how far from the equilibrium point can be from the trajectory and still converge to it. The theory assessment involves the following steps:

– assimilate the origin as an equilibrium point of the nonlinear system, $\dot{x} = f(x)$;

– find a Lyapunov function $V(x)$;

– suppose that the time derivative of the Lyapunov function exists. Calculate $V'(x)$ which must be negative (sometimes, it is necessary to maximize this function);

– consider the system stability analysis.

The third approach enables us to solve the stability issue for an entire region around an equilibrium point.

3.2.4. *Summary of stability approaches*

The different approaches presented are summarized in the Table 3.1.

Methods	*Description*
Small Signal Analysis – First method of Lyapunov	Determines the stability in the immediate vicinity of the equilibrium point by the Lyapunov's first method.
Transient Analysis – Equal area criterion	Estimates the stability in a region closer to the equilibrium point, through the equal area criterion: – determines the critical energy V_{cr}. – calculates the clearing fault energy V_{cl}. – compares the transient energy margin of $(V_{cr} - V_{cl})$.
Global Analysis – Second (or direct) Lyapunov method	Analyzes the stability in the entire finite space around the system, considering the nonlinear model if it is the case.

Table 3.1. *Summary of stability approaches*

REMARK.– If an exact linearization of the power system model is derived, it could change the stability analysis and studies. This will be presented later in the book.

3.3. Modeling of AC power network – swing equation

Energy functions are useful tools for such transient or synchronous stability analysis. The study of energy functions arises from the fundamental swing dynamics defining the electromechanical notion of synchronous machines in any n-machine power systems, given by Newton's laws of angular motion. Let us recall the mathematical development of the swing equation derivation. Consider first the following definitions:

– θ is the rotor angle in radian;

– θ_s is the system angle in radian;

– δ is the rotor angle deviation with a reference frame in radian.

We have:

$$\theta = \theta_s + \delta \quad [3.5]$$

Define thereafter:

– Ω is the nominal speed of electrical system in radian/second (rd/s). Make the assumption of equivalent machine with one pair of poles;

– ω is the rotor speed in radian/second (rd/s);

– $\Delta\omega = \omega - \Omega$ is the rotor speed deviation with a reference frame in radian/second (rd/s).

The corresponding derivatives of time are:

$$\dot{\theta} = \omega$$

$$\dot{\theta_s} = \Omega \quad [3.6]$$

$$\dot{\delta} = \Delta\omega$$

Considering the time derivative of equation [3.5], we obtain:

$$\omega = \Omega + \dot{\delta} \quad [3.7]$$

Thereafter:

$$\ddot{\theta} = \dot{\omega} = \ddot{\delta} \quad [3.8]$$

3.3.1. *Nonlinear swing equation*

From the Newton mechanical law which indicates (F = force)

$$\sum_i F_i = 0$$

The equilibrium of the machine torques is obtained by the following expression:

$$J\dot{\omega} + f\omega = \tau_a = \tau'_m - \tau_e \quad [3.9]$$

where J is the combined inertia of the turbine, shaft and rotor, f is the total damping, τ_a is the accelerating torque, τ'_m is the prime mover torque and τ_e is the electrical counter torque.

Using equations [3.6] and [3.8],

$$\dot{\theta} = \omega \; \dot{\theta} = \omega$$

equation [3.9] can be rewritten as:

$$J\ddot{\theta} + f\dot{\theta} = \tau_a = \tau'_m - \tau_e \quad [3.10]$$

Multiplying by ω, we have:

$$J\ddot{\theta}\dot{\theta} + f\dot{\theta}\dot{\theta} = \tau'_m\dot{\theta} - \tau_e\dot{\theta} \quad [3.11]$$

Adding term $-f\dot{\theta}\,\Omega$ at both sides of the equation above leads to:

$$J\ddot{\theta}\dot{\theta} + f\dot{\theta}\dot{\theta} - f\dot{\theta}\,\Omega = \tau'_m\dot{\theta} - f\dot{\theta}\,\Omega - \tau_e\dot{\theta} \quad [3.12]$$

where

$$Pm = \tau'_m\dot{\theta} - f\dot{\theta}\,\Omega = (\tau'_m - f\Omega)\dot{\theta} = \tau_m\dot{\theta} \quad [3.13]$$

is the mechanical power, with τ_m the mechanical torque, and

$$Pe = \tau_e\dot{\theta} \quad [3.14]$$

is the electrical power. Replacing both equations [3.13] and [3.14] into [3.12], we obtain:

$$J\ddot{\theta}\dot{\theta} + f\dot{\theta}\dot{\theta} - f\dot{\theta}\,\Omega + Pe = Pm \quad [3.15]$$

Multiply the first term of equation above by 1 in the form $\frac{2\Omega^2}{2\Omega^2}$

$$\frac{2\Omega^2}{2\Omega^2}J\ddot{\theta}\dot{\theta} + f\dot{\theta}\dot{\theta} - f\dot{\theta}\,\Omega + Pe = Pm \qquad [3.16]$$

where $W_{KE} = \frac{J\Omega^2}{2}$ represents the initial kinetic energy at nominal frequency. We can rewrite the above equation as:

$$\frac{2}{\Omega^2}W_{KE}\ddot{\theta}\dot{\theta} + f\dot{\theta}\dot{\theta} - f\dot{\theta}\,\Omega + Pe = Pm \qquad [3.17]$$

Dividing equation above by $S_{base}^{3\emptyset}$ yields:

$$\frac{2}{\Omega^2}\frac{W_{KE}}{S_{base}^{3\emptyset}}\ddot{\theta}\dot{\theta} + \frac{f}{S_{base}^{3\emptyset}}\dot{\theta}\dot{\theta} - \frac{f}{S_{base}^{3\emptyset}}\dot{\theta}\,\Omega + Pe_{pu} = Pm_{pu} \qquad [3.18]$$

By considering the following definitions:

$H = \frac{W_{KE}}{S_{base}^{3\emptyset}}$ is the inertia time constant

$D = \frac{f}{S_{base}^{3\emptyset}}$ as the damping constant

equation [3.18] leads to:

$$\frac{2}{\Omega^2}H\ddot{\theta}\dot{\theta} + D\dot{\theta}\dot{\theta} - D\dot{\theta}\,\Omega + Pe_{pu} = Pm_{pu} \qquad [3.19]$$

Setting $M = \frac{2H}{\Omega^2}$ known as the inertia moment constant, the nonlinear swing equation is finally obtained as:

$$\ddot{\theta} = -\frac{D}{M}\dot{\theta} + \frac{1}{M\dot{\theta}}(Pm_{pu} + D\dot{\theta}\,\Omega - Pe_{pu}) \qquad [3.20]$$

3.3.2. *Linearized swing equation*

Consider again equation [3.10]:

$$J\ddot{\theta} + f\dot{\theta} = \tau_a = \tau'_m - \tau_e$$

Taking into account equations [3.7] and [3.8], the rotor angles deviation is obtained by:

$$J\ddot{\delta} + f(\Omega + \dot{\delta}) = \tau'_m - \tau_e \quad [3.21]$$

or

$$J\ddot{\delta} + f\dot{\delta} + f\Omega = \tau'_m - \tau_e \quad [3.22]$$

Multiply both sides by rotor speed $\dot{\theta}$ and replace the mechanical power Pm and electrical power Pe as obtained above, so we have:

$$J\ddot{\delta}\dot{\theta} + f\dot{\delta}\dot{\theta} = Pm - Pe \quad [3.23]$$

where:

$$Pm = \tau'_m\dot{\theta} - f\dot{\theta}\,\Omega = (\tau'_m - f\Omega)\dot{\theta} = \tau_m\dot{\theta}$$

is the mechanical power, with τ_m the mechanical torque, and

$$Pe = \tau_e\dot{\theta}$$

is the electrical power as shown for the nonlinear case.

As we did above, multiply the first term by 1 in the form $\frac{2\Omega^2}{2\Omega^2}$ and replace the initial kinetic energy by $W_{KE} = \frac{J\Omega^2}{2}$, such that equation [3.23] becomes:

$$\frac{2}{\Omega^2}W_{KE}\ddot{\delta}\dot{\theta} + f\dot{\delta}\dot{\theta} = Pm - Pe \quad [3.24]$$

Dividing the two sides in equation above by the energy base S_{base} and replace the inertia time constant $H = \frac{W_{KE}}{S^{3\emptyset}_{base}}$ and damping constant $D = \frac{f}{S^{3\emptyset}_{base}}$, we have:

$$\frac{2}{\Omega^2}H\ddot{\delta}\dot{\theta} + D\dot{\delta}\dot{\theta} = Pm_{pu} - Pe_{pu} \quad [3.25]$$

It is realistic to assume that the nominal speed is much bigger than the speed deviation, $\Omega \gg \dot{\delta}$, thus: $\dot{\theta} \cong \Omega$. Replacing it in the equation above, we obtain:

$$\frac{2}{\Omega}H\ddot{\delta} + D\dot{\delta}\Omega = Pm_{pu} - Pe_{pu} \quad [3.26]$$

Taking into account the inertia moment $M = \frac{2H}{\Omega^2}$, we obtain the standard linear swing equation:

$$\ddot{\delta} = -\frac{D}{M}\dot{\delta} + \frac{1}{M\Omega}(Pm_{pu} - Pe_{pu}) \quad [3.27]$$

Equation [3.27] in an approximation (linearized) of the nonlinear swing equation obtained in equation [3.20].

3.3.3. *Development of the electrical power term*

The real power in a multi-terminal system with n machines is given by the following equation

$$Pei = Re[E_i \cdot I_i{}^*] = Re\left[E_i \sum_{j=1}^{n} Y_{ij}{}^* E_j^*\right] i = 1,2,\ldots n \quad [3.28]$$

with

$$E_i = |E_i|\angle\theta_i,\ Y_{ij} = G_{ij} + jB_{ij} = E_i = |Y_{ij}|\angle\alpha_{ij}$$

where α_{ij} is the impedance angle of the admittance between machines, and $G_{ij} = |Y_{ij}|cos\alpha_{ij}, B_{ij} = |Y_{ij}|sin\alpha_{ij}$.

Consequently, equation [3.28] can be rewritten as:

$$Pei = \mathrm{Re}\left[E_i E_i^* Y_{ii}{}^* + E_i \sum_{\substack{j=1 \\ j\neq i}}^{n} Y_{ij}{}^* E_j^*\right] = \mathrm{Re}\left[\begin{array}{l} |E_i|^2(G_{ii} - jB_{ii}) \\ +\sum_{\substack{j=1 \\ j\neq i}}^{n} |E_i||E_j||Y_{ij}|\angle\theta_i - \theta_j - \alpha_{ij} \end{array}\right]$$

$$= \mathrm{Re}\left[\begin{array}{l} |E_i|^2(G_{ii} - jB_{ii}) + \sum_{\substack{j=1 \\ j\neq i}}^{n} |E_i||E_j||Y_{ij}|[\cos\cos(\theta_i - \theta_j - \alpha_{ij}) \\ +jsin(\theta_i - \theta_j - \alpha_{ij})] \end{array}\right]$$

$$= 3\,[|E_i|^2 G_{ii} + \sum_{\substack{j=1 \\ j\neq i}}^{n} |E_i||E_j||Y_{ij}|\cos\cos((\theta_i - \theta_j) - \alpha_{ij})]$$

$$= 3\{|E_i|^2 G_{ii} + \sum_{\substack{j=1 \\ j\neq i}}^{n} |E_i||E_j||Y_{ij}|[\cos[\cos\alpha_{ij}\cos\cos(\theta_i - \theta_j)$$
$$+ \sin\alpha_{ij}\sin(\theta_i - \theta_j)]\}$$

Finally, we obtain:

$$Pei = 3\{|E_i|^2 G_{ii} + \sum_{\substack{j=1 \\ j\neq i}}^{n} [|E_i||E_j|G_{ij}\cos|E_i||E_j|G_{ij}\cos(\theta_i - \theta_j) \quad [3.29]$$
$$+ |E_i||E_j|B_{ij}\sin(\theta_i - \theta_j)]\}$$

where G_{ii} is the self-conductance of the generator. As it is applied for most modeling calculations, suppose that the losses are neglected. That is, $Z_{ij} \cong jX_{ij}$, thus $G_{ij} \cong 0$, $Y_{ij} \cong B_{ij}$. We obtain:

$$Pei = 3 \cdot [|E_i|^2 G_{ii} + \sum_{\substack{j=1 \\ j\neq i}}^{n} |E_i||E_j||B_{ij}|\, sin(\theta_i - \theta_j)] \quad [3.30]$$

Dividing by $S_{base}^{3\emptyset}$, the per unit (p.u.) active power is then:

$$Pei_{pu} = |E_{ipu}|^2 G_{iipu} + \sum_{\substack{j=1 \\ j\neq i}}^{n} |E_{ipu}||E_{jpu}||B_{ijpu}|\, sin(\theta_i - \theta_j) \quad [3.31]$$

Consequently, the final form of swing equation taking into accounts the active power and neglecting the losses ($Y_{ij} \cong B_{ij}$) is given by:

– in nonlinear form, that is:

$$\ddot{\theta}_i = -\frac{D_i}{M_i}\dot{\theta}_i + \frac{1}{M_i\dot{\theta}_i}\left(\begin{array}{l} Pmi_{pu} + D_i\dot{\theta}_i\,\Omega - |E_{ipu}|^2 G_{iipu} \\ -\sum_{\substack{j=1 \\ j\neq i}}^{n} |E_{ipu}||E_{jpu}||Y_{ijpu}|\sin\sin(\theta_i - \theta_j) \end{array}\right)$$

$$i = 1,2,\ldots n \quad [3.32]$$

– *in linear form, we have*:

$$\ddot{\delta}_i = -\frac{D_i}{M_i}\dot{\delta}_i + \frac{1}{M_i\Omega}\left(\begin{array}{l} Pmi_{pu} - \left|E_{ipu}\right|^2 G_{iipu} \\ -\sum_{\substack{j=1 \\ j\neq i}}^{n} \left|E_{ipu}\right|\left|E_{jpu}\right|\left|Y_{ijpu}\right| \sin\sin\left(\delta_i - \delta_j\right) \end{array}\right)$$

$$i = 1,2,\ldots n \qquad [3.33]$$

where $\theta_i - \theta_j = \delta_i - \delta_j$ when working at the same reference nominal speed, with $D_i = \frac{f_i}{Si_{base}^{3\emptyset}}$ and $M_i = \frac{2H_i}{\Omega^2}$ in both cases.

3.4. Simulation of AC swing equation

In this section, simulation results will be performed to compare the coherency of the behavior between the Simpower model, which represents the "real machine", and the obtained mathematical swing equation nonlinear and linearized models. Here the machine behavior indicates frequency, electrical power and angle differences.

– *Simulation Conditions:* consider a system of three generators with a same power base (3 MVA 20 kV·RMS), and 3 transformers (D20 kV/ Y230 kV), inter-connected by three transmission lines with three different loads in each area. At first, a model of Simpower system of Simulink is established and simulated in the condition without regulators (no excitation regulator, no governor). We then take the same value of excitation voltages and mechanical powers of each machine to our swing equation models for both nonlinear and linear cases.

– *Simpower model:* the modeled system with Simpower system toolbox is shown in Figure 3.5.

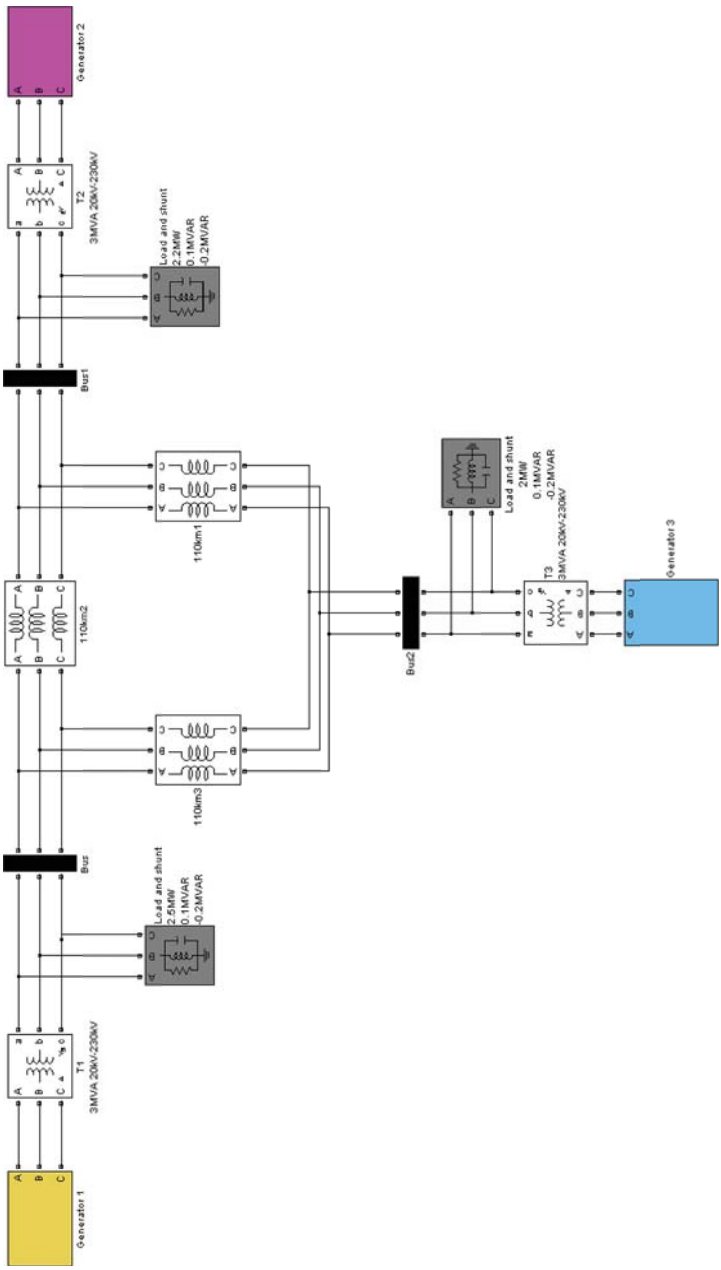

Figure 3.5. *Three-interconnected generators model with Simpower system. For a color version of the figure see www.iste.co.uk/benchaib/control.zip*

The three generators are represented in three colors: Generator 1 *(yellow)*, Generator 2 *(pink)* and Generator 3 *(blue)*. The principle system parameter in p.u. related to the swing equation model is detailed below in Table 3.2 with proper specified power and voltage base, all system impedance are referred to *Kundur's 4 machines 2 areas system* (see Appendix 3 for parameters).

– *Generators*:

	Type	$Base(3\emptyset, 2\emptyset \cdot RMS)$	$X_d^{'}\ (p.u.)$	$Z_{stator}\ (p.u.)$	*Nominal power* $(3\emptyset)$
Generator 1, 2	*P&V generator*	$3MVA, 20\ kV$	0.3	$0.0025 + j2.5$	$2.2\ MW$
Generator 3	*Swing generator*	$3\ MVA, 20\ kV$	0.3	$0.0025 + j2.5$	$2.2\ MW$

Table 3.2. *Generator parameters*

– *Transformers*:

	Type	$Base(3\emptyset, 2\emptyset \cdot RMS)$	$R\ (p.u.)$	$X\ (p.u.)$
Winding 1	*D*	$3\ MVA, 20\ kV$	1×10^{-6}	0
Winding 2	*Y*	$3\ MVA, 230\ kV$	1×10^{-6}	0.15

Table 3.3. *Transformer parameters*

– *Transmission lines*:

	length	$Base(3\emptyset, 2\emptyset \cdot RMS)$	$X\ (p.u)$
line	$110\ km$	$3\ MVA, 230\ kV$	-2.5×10^{-3}

Table 3.4. *Transmission line parameters*

– *Loads*:

	Active power	*Inductive reactive power*	*Capacitive reactive power*
Load 1	$2.5\ MW$	$0.1\ MVAR$	$-0.2\ MVAR$
Load 2	$2.2\ MW$	$0.1\ MVAR$	$-0.2\ MVAR$
Load 3	$2\ MW$	$0.1\ MVAR$	$-0.2\ MVAR$

Table 3.5. *Load parameters*

– *Swing equation model*: the swing equation models (nonlinear and linear models) are established by Simulink block and Matlab function code. It is the Matlab function where the type of the considered model of the swing equation will be programmed (see Figure 3.6).

In the Matlab/Simulink, the rotor angles are obtained after that the accelerations variables are integrated twice by Simulink integrator block, with an initial value that represents the different initial speeds and angles (also referred to as the Simpower model). The linearized swing equation model is also programmed in the same manner as the nonlinear model, where the rotor angle deviations are also set with initial values coming from the Simpower system. The nonlinear swing equation model for three interconnected machines is given by the following system of equations:

$$\begin{cases} \ddot{\theta}_1 = -\dfrac{D_1}{M_1}\dot{\theta}_1 + \dfrac{1}{M_1\dot{\theta}_1} \\ \quad \left(Pm1_{pu} + D_1\dot{\theta}_1\Omega - |E_{1pu}|^2 G_{11pu} - |E_{1pu}||E_{2pu}||Y_{12pu}|\sin(\theta_1-\theta_2) - |E_{1pu}||E_{3pu}||Y_{13pu}|\sin(\theta_1-\theta_3) - Pn1_{pu} \right) \\ \ddot{\theta}_2 = -\dfrac{D_2}{M_2}\dot{\theta}_2 + \dfrac{1}{M_2\dot{\theta}_2} \\ \quad \left(Pm2_{pu} + D_2\dot{\theta}_2\Omega - |E_{2pu}|^2 G_{22pu} - |E_{2pu}||E_{1pu}||Y_{21pu}|\sin(\theta_2-\theta_1) - |E_{2pu}||E_{3pu}||Y_{23pu}|\sin(\theta_2-\theta_3) - Pn2_{pu} \right) \\ \ddot{\theta}_3 = -\dfrac{D_3}{M_3}\dot{\theta}_3 + \dfrac{1}{M_3\dot{\theta}_3} \\ \quad \left(Pm3_{pu} + D_3\dot{\theta}_3\Omega - |E_{3pu}|^2 G_{33pu} - |E_{3pu}||E_{1pu}||Y_{31pu}|\sin(\theta_3-\theta_1) - |E_{3pu}||E_{2pu}||Y_{32pu}|\sin(\theta_3-\theta_2) - Pn3_{pu} \right) \end{cases} \quad [3.34]$$

where $D_i = \dfrac{f_i}{Si^{3\emptyset}_{base}}$ and $M_i = \dfrac{2H_i}{\Omega^2}$.

See Appendix 2 for the swing equation programming code.

3.4.1. *Post-fault simulation case (transient response)*

In this section, we will compare the responses of the three models (Simpower, nonlinear and linearized) following a disturbance rejection. The disturbance consists of mechanical power drop in generator 1 (G1) for 4 s.

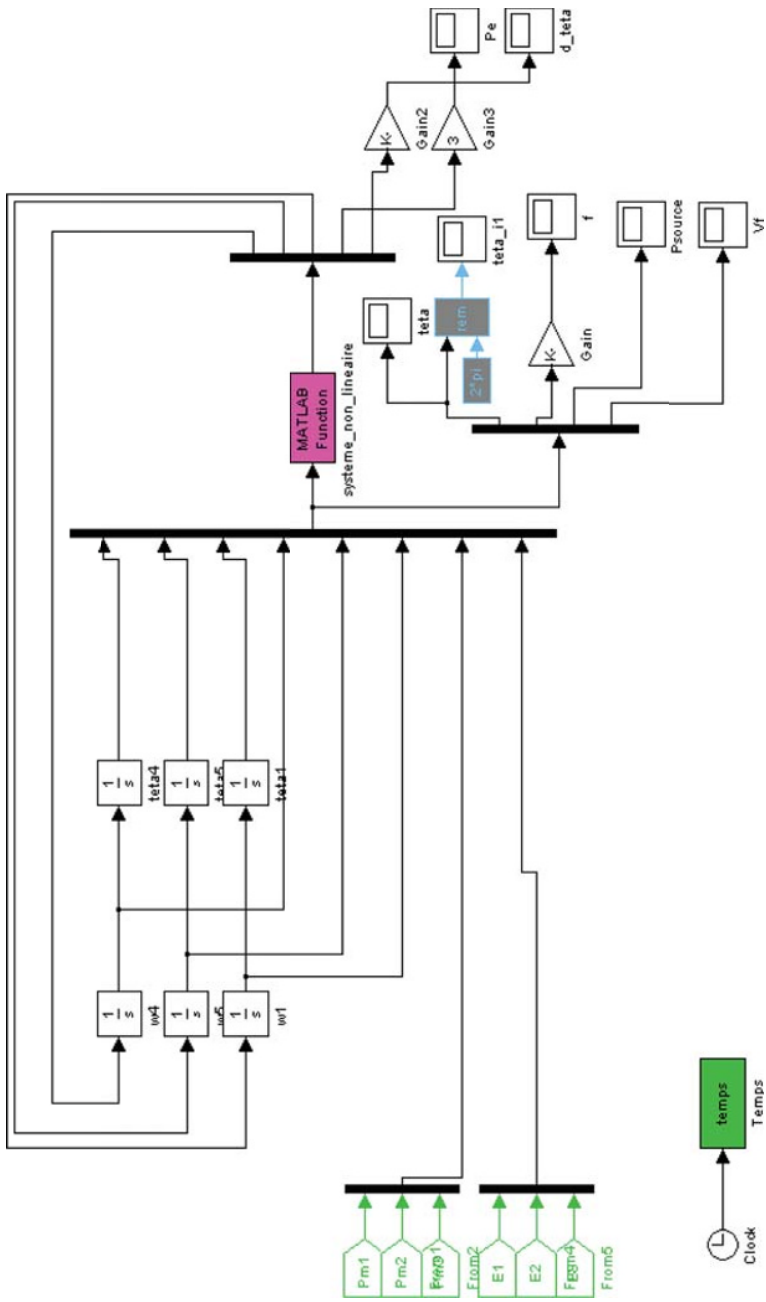

Figure 3.6. *Interconnected generators model (swing equation) with Matlab/Simulink*

3.4.1.1. *Frequency response*

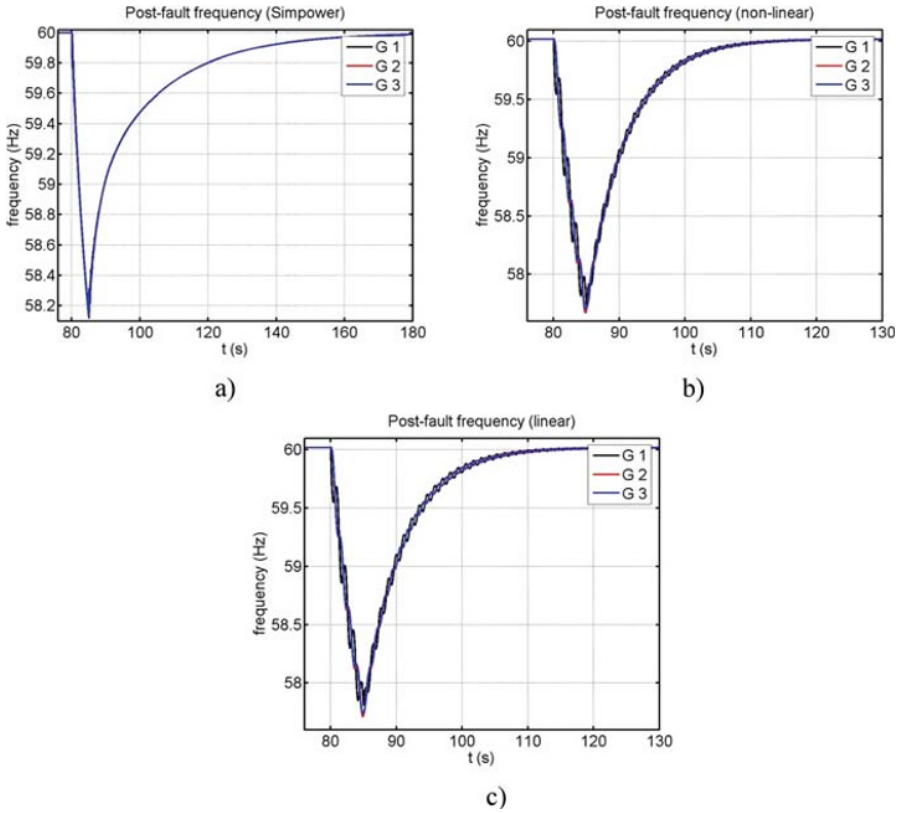

Figure 3.7. *Post-fault frequency responses of a) Simpower system, b) nonlinear swing equation model and c) linearized swing equation model. For a color version of the figure, see www.iste.co.uk/benchaib/control.zip*

Figure 3.7 shows the frequency responses for the three considered models. All curves have the same behavior except for the maximum amplitude where it is -2.4 Hz for the linearized model and less for the two others. All models recover after fault clearance. However, the recovery time for Simpower system is much longer that the two others.

– *Electrical power*:

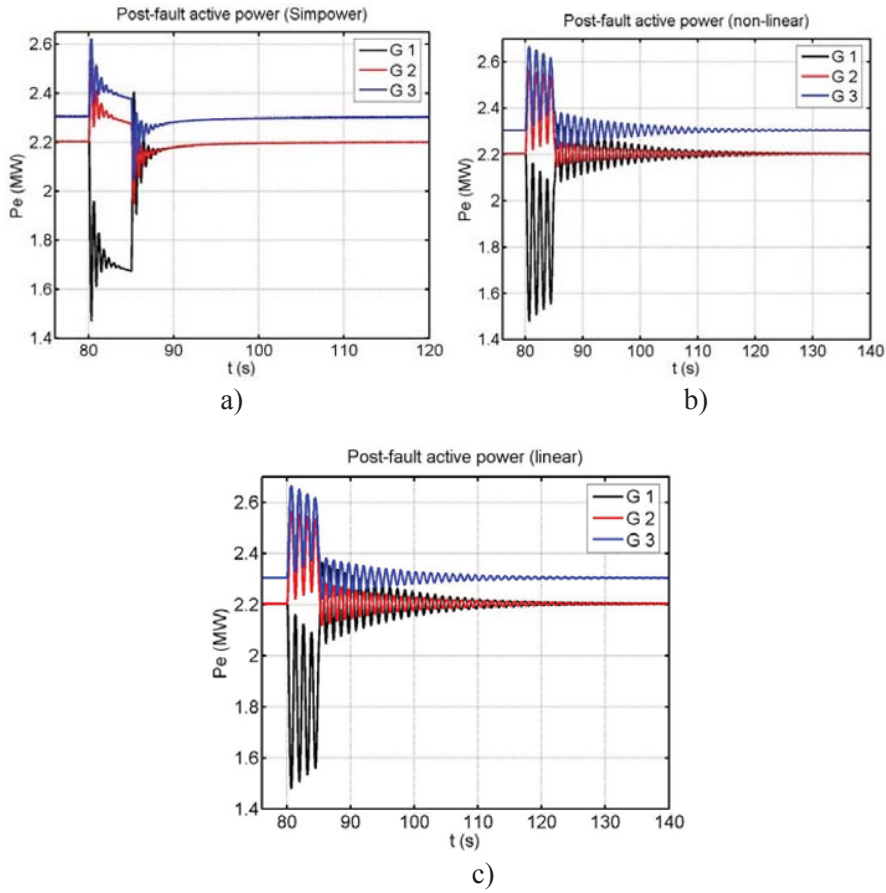

Figure 3.8. *Post-fault electrical power of a) Simpower system, b) nonlinear swing equation model and c) linearized swing equation model. For a color version of the figure, see www.iste.co.uk/benchaib/control.zip*

During the fault, the electrical power of G1 falls, meanwhile G2 and G3 increase their power to compensate. After disturbance, the powers in all machines recover the nominal power outputs as pre-fault status, with G1 swings stronger and longer to recover. The transient behavior of electrical power in the two mathematical models (nonlinear and linearized) is exactly the same. Except for the responses in the Simpower model which is more damped, the transient behaviors of the three models are quite similar.

– *Angle differences*:

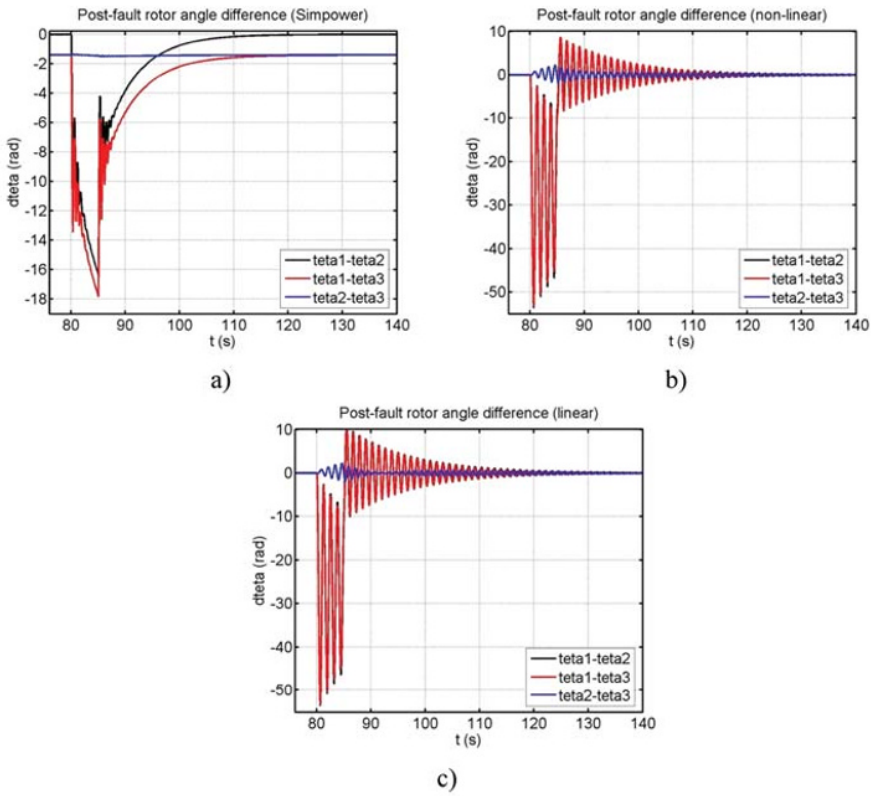

Figure 3.9. *Post-fault angle differences of a) Simpower system, b) nonlinear swing equation model and c) linearized swing equation model. For a color version of the figure, see www.iste.co.uk/benchaib/control.zip*

During fault, it is noticed that all angle differences relate to G1 (green and red) fall in both the two mathematical models in the same manner, which is due to the drop of mechanical power in G1 resulting in changes in its frequency and thus its rotor speed. While the difference of G2 and G3 (blue) stays at the same value with just some oscillations. After the fault, all angle differences recover to their steady-state value. The transient behavior of angle differences in the two mathematical models remains the same. The Simpower model is more damped, with red and blue curves not having the same steady value compared to the other two models.

3.5. Revisited swing equation for multi-machines power system modeling

The name "swing equation" is originated from swings in rotor angle δ during disturbances. As described in [KUN 94], the "swing equation" express the dynamics of the rotor of a synchronous generator, which is the effect of unbalance between the electromagnetic torque and the mechanical torque of individual machine. This is one of the major elements for power system stability studies. For analysis of power system dynamics, the model is developed as a combination of the synchronous machine equations and the network frequency.

The modeling standard approach for swing equation is based on the Newton law of force balance. Let us consider here the power balance for interconnected subsystems (or generators). In the following, three-node synchronized multi-machine systems composed of one motor and two generators will be considered, as shown in Figure 3.10.

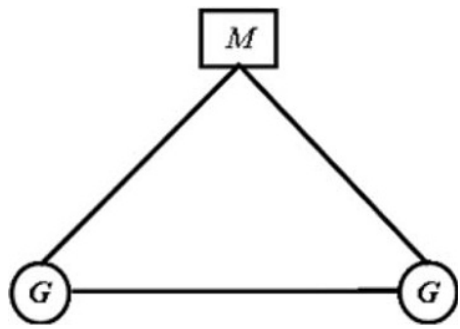

Figure 3.10. *Three-node interconnected AC power network*

The power balance at each node is given by the following expression:

$$P_{source_i} = P_{trans_i} + P_{acc_i} + P_{diss_i} \qquad [3.35]$$

where:

– $P_{trans_i} = \sum_j P_{ij}^{max} \sin(\theta_j - \theta_i)$ is the transmitted active power.

– $P_{acc_i} = \frac{1}{2} J_i \frac{d}{dt} (\dot{\theta}_i)^2$ is the accumulated kinetic energy.

– $P_{diss_i} = K_{D_i}(\dot{\theta}_i)^2$ is the dissipated power at the considered node.

K_{D_i} is a constant, J_i is the moment of inertia and $\dot{\theta}_i$ represents the rotor angular velocity of the machine i. Equation [3.35] can be rewritten as:

$$P_{source_i} = \sum_j P_{ij}^{max} \sin(\theta_j - \theta_i) + \frac{1}{2} J_i \frac{d}{dt}(\dot{\theta}_i)^2 + K_{D_i}(\dot{\theta}_i)^2 \qquad [3.36]$$

Thereafter, a nonlinear model may be expressed as follows:

$$\ddot{\theta}_i = -\frac{K_{D_i}}{J_i}\dot{\theta}_i + \frac{1}{\dot{\theta}_i}\frac{1}{J_i}\left[P_{source_i} + \sum_j P_{ij}^{max} \sin(\theta_j - \theta_i)\right] \qquad [3.37]$$

Compared to equation [3.32], this nonlinear system model is somehow simplified by not taking into account the electric power term development without the loss of pertinence. The above equation can be generalized to multi-machine systems and, in our case, it is for the 3-node power network. That is:

$$\begin{cases} \ddot{\theta}_1 = -\frac{K_{D_1}}{J_1}\dot{\theta}_1 + \frac{1}{\dot{\theta}_1}\frac{1}{J_1}\left[P_{source_1} + P_{12}^{max} \sin(\theta_2 - \theta_1) + P_{13}^{max} \sin(\theta_3 - \theta_1)\right] \\ \ddot{\theta}_2 = -\frac{K_{D_2}}{J_2}\dot{\theta}_2 + \frac{1}{\dot{\theta}_2}\frac{1}{J_2}\left[P_{source_2} + P_{12}^{max} \sin(\theta_1 - \theta_2) + P_{23}^{max} \sin(\theta_3 - \theta_2)\right] \\ \ddot{\theta}_3 = -\frac{K_{D_3}}{J_3}\dot{\theta}_3 + \frac{1}{\dot{\theta}_3}\frac{1}{J_3}\left[P_{source_3} + P_{13}^{max} \sin(\theta_1 - \theta_3) + P_{23}^{max} \sin(\theta_2 - \theta_3)\right] \end{cases} \qquad [3.38]$$

For n-nodes power network, we have:

$$\begin{cases} \ddot{\theta}_1 = -\frac{K_{D_1}}{J_1}\dot{\theta}_1 + \frac{1}{\dot{\theta}_1}\frac{1}{J_1}\left[P_{source_1} + \sum_j P_{1j}^{max} \sin(\theta_j - \theta_1)\right] \\ \vdots \qquad\qquad \vdots \\ \ddot{\theta}_n = -\frac{K_{D_n}}{J_n}\dot{\theta}_n + \frac{1}{\dot{\theta}_n}\frac{1}{J_n}\left[P_{source_n} + \sum_j P_{nj}^{max} \sin(\theta_j - \theta_n)\right] \end{cases} \qquad [3.39]$$

All stability studies could be performed on the proposed model given by equation [3.39].

3.6. Exact linearization of swing equation

Consider the nonlinear model given by equation:

$$\ddot{\theta}_i = -\frac{K_{D_i}}{J_i}\dot{\theta}_i + \frac{1}{\dot{\theta}_i}\frac{1}{J_i}\left[P_{source_i} + \sum_j P_{ij}^{max} \sin(\theta_j - \theta_i)\right] \qquad [3.40]$$

The approach, usually used to study stability, is used to linearize the model around an operating point which is called the small signal stability method. Our aim is to propose a technique able to give feedback on stability issues for the whole working space. Such results can be obtained from a so-called "exact linearization" of the model. Instead of considering the frequency of the system, let us consider the square value of the frequency which could be interpreted as the energy related to any control purpose. Set now the following variable Z_{AC}:

$$Z_{AC,i} = \left(\dot{\theta}_i\right)^2 \qquad [3.41]$$

Using equation [3.40], the derivative time of equation [3.41] can be rewritten as:

$$\dot{Z}_{AC,i} = -2\frac{K_{D_i}}{J_i} Z_{AC,i} + \frac{2}{J_i}\left[P_{s_i} + \sum_j P_{ij}^{max} \sin\left(\theta_j - \theta_i\right)\right] \qquad [3.42]$$

It can be noted that the nonlinear swing equation as presented by equation [3.40] is transformed into a linear form (equation [3.41]) without loss of information. This obtained swing linear equation represents the nonlinear equation in the whole state space. In the automatic control domain, it could be called an exact linearized equation. If the term $\sum_j P_{ij}^{max} \sin\left(\theta_j - \theta_i\right)$ is considered as an input to the system which is a realistic assumption considering that power flow is controlled by the control center at different time scale, the above relation constitutes an exact representation of the system, valid on all the operating points. It is possible to go back to the original nonlinear model by a simple change of variable. In the same configuration as before, the obtained model will be tested for three-node multi-machine systems with a disturbance of power occurring at 2 s for 0.15 s. The simulation model is given by the following system of equations:

$$\begin{cases} \dot{Z}_{AC,1} = -2\frac{K_{D_1}}{J_1} Z_{AC,1} + \frac{2}{J_1}\left[P_{s_1} + P_{12}^{max} \sin(\theta_2 - \theta_1) + P_{13}^{max} \sin(\theta_3 - \theta_1)\right] \\ \dot{Z}_{AC,2} = -2\frac{K_{D_2}}{J_2} Z_{AC,2} + \frac{2}{J_2}\left[P_{s_2} + P_{12}^{max} \sin(\theta_1 - \theta_2) + P_{23}^{max} \sin(\theta_3 - \theta_2)\right] \\ \dot{Z}_{AC,3} = -2\frac{K_{D_3}}{J_3} Z_{AC,3} + \frac{2}{J_3}\left[P_{s_3} + P_{13}^{max} \sin(\theta_1 - \theta_3) + P_{23}^{max} \sin(\theta_2 - \theta_3)\right] \end{cases} \qquad [3.43]$$

For a better understanding, a frequency (pulsation) comparison is made between the nonlinear model and the exact linearized model. As shown in Figure 3.11, both models are giving the same outputs for steady state and

with disturbance. The obtained linearized model with a $Z_{AC,i}$ variable can be used for stability issues in the whole state space.

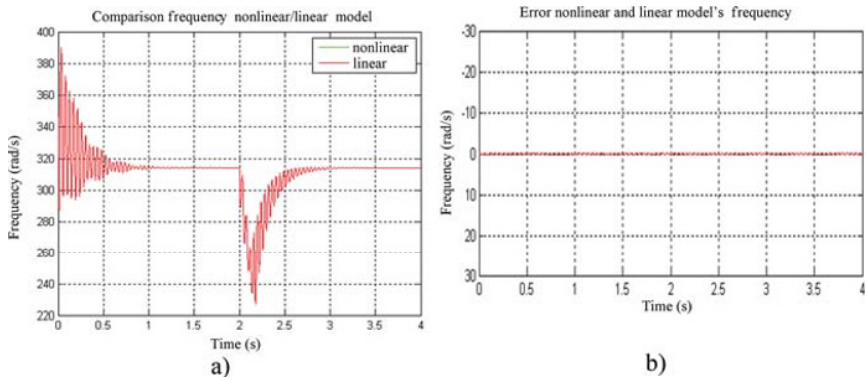

Figure 3.11. *Simulation results for a nonlinear model and linearized model*

Moreover, the obtained linearized model can be rewritten as follows:

$$\dot{Z_{AC,i}} = -\alpha_i Z_{AC,i} + \beta_i\left[P_{s_i} + \sum_j P_{ij}^{max} \sin\left(\theta_j - \theta_i\right)\right] \quad [3.44]$$

where,

$$\alpha_i = 2\frac{K_{D_i}}{J_i} Z_{AC,i} \text{ and } \beta_i = \frac{2}{J_i} \quad [3.45]$$

In order to obtain a good precision of the proposed model given by equation [3.44], an identification of parameters $\propto_i$ and β_i has to be performed. The identification techniques are to be developed together with specialists as this could constitute a new area of research for power systems.

3.7. Concluding remarks

In this chapter, we recalled stability analysis tools as used for power system studies. Thereafter, a detailed modeling of AC power network dynamics with swing equations was given in which nonlinear and small signal swing equations were derived. Following the proposed modeling, simulation comparison between nonlinear model and the standard small signal (linearized) swing equation was undertaken for multi-machine systems. Moreover, a revisited swing equation modeling was proposed.

Next, an exact linearized model has been proposed in order to cover the whole state space. Compared with the standard tools for power system stability analysis, this last result could represent a big advance in the power system modeling. Direct application of the proposed exact linearized swing equation could be the stability analysis of power system when the occurring disturbance is big enough to force the system far away from its trajectory of equilibrium.

4

Space Scale Properties for AC/DC Power Network Control and Operations: New Aggregation Methods in Power Systems

4.1. Introduction

As shown in Chapter 3, considered models are of key importance in the stability studies of power systems. Even if stability analysis tools are well developed, the users' interpretation can lead to wrong decisions when the considered model is not accurate enough. However, detailed models are not practical and often too heavy to compute at system-level considerations. It is sometimes more convenient to consider averaged or aggregated models for such purposes. Averaging models could be done for both time and space considerations. For some actuators, such as power electronics-based converts, the average model is obtained when some time constants are neglected. It is not necessary to consider components switching when dealing with active and reactive power exchange with the grid. It is what we can identify as "time/frequency" average model. However, multi-machine systems could be averaged by considering geographic/space distribution in which time/frequency is also considered. In the following, a new averaging/aggregating technique will be proposed for multi-machine power systems modeling. This chapter will show some recent results and discuss research directions which could be pursued based on the given results. In section 4.2, the inter-area oscillation damping technique is proposed. Thereafter, the free of space-scale model based on averaging technique for an alternating current (AC) system is proposed in section 4.3. Then, a modeling of direct current (DC) technology-based power grids in line with swing

Advance Control of AC/DC Power Network: *System of Systems Approach Based on Spatio-temporal Scales*, First Edition. Abdelkrim Benchaib.
© ISTE Ltd 2015. Published by ISTE Ltd and John Wiley & Sons, Inc.

equations use philosophy is proposed in section 4.4. Section 4.5, which mainly highlights results are from the literature, briefly discusses how voltage source converters (VSCs) are controlled to mimic synchronous generators. The proposed philosophy could have its importance when dealing with hybrid AC/DC grids. Finally, some concluding remarks end the chapter.

4.2. Inter-area oscillation damping: locally intelligent substation

In the power network of the future where it is requested to react as fast as possible, the control system will be distributed at substation level. The aim is to limit the oscillations in order to dampen the disturbance with no action from the control center nor from enabling the system protection limits or damaging involved elements [SNY 98]. In fact, we will focus our interest on the system behavior between two stable operating points, by keeping the frequency as constant as possible and by rejecting perturbations. Therefore, and as long as the control bandwidth is concerned, we will determine a control law integrated with the voltage position in order to respond to this criterion, with the main objective to dampen the effect on power flow oscillations. The measured angles have the following form:

$$\theta_i = \theta_{iN} + \Delta\theta_i \qquad [4.1]$$

The voltage angle can be written as sum of a nominal value given by the network operator θ_{iN} and a variation around this angle $\Delta\theta_i$ which each station can use as new degree of freedom to locally dampen oscillation. Of course, $\Delta\theta_i$ will be set to zero in steady state and when oscillations are inhibited. A feedback control law, based on the linear model, will be found as an exact representation of the system dynamic behavior. Consider the new reference variable Z_i:

$$Z_i = Z_{iN} + \Delta Z_i \qquad [4.2]$$

$$\dot{Z}_i = \dot{Z}_{iN} + \Delta\dot{Z}_i \qquad [4.3]$$

$$P_{s_i} = P_{s_iN} + \Delta P_{s_i} \qquad [4.4]$$

where,

$$P_{s_i} = \frac{2P_{source_i}}{J_i} \qquad [4.5]$$

The linear model may be expressed as:

$$\dot{Z}_{iN} + \Delta\dot{Z}_i = -2\frac{K_{D_i}}{J_i}\left(Z_{iN} + \Delta Z_i\right) + P_{s_{iN}} + \Delta P_{s_i} + \frac{2}{J_i}\left[\sum_j P_{ij}^{\max} \sin\sin\left(\theta_{jN} + \Delta\theta_j + -\theta_{iN} - \Delta\theta_i\right)\right] \quad [4.6]$$

Using the trigonometric expression $\sin(a+b) = \sin(a)\cos(b) + \sin(b)\cos(a)$ with

$$\Delta\theta_j - \Delta\theta_i = \Delta\theta_{ji} \quad [4.7]$$

and supposing $\Delta\theta_{ij}$ is small, the trigonometric approximations give the following relations:

$$\sin\left(\Delta\theta_{ij}\right) = \Delta\theta_{ij},\ \cos\left(\Delta\theta_{ij}\right) = 1\ ,\ P_{ij}^{max}\cos\left(\theta_{jN} - \theta_{iN}\right) = P_{ij} \quad [4.8]$$

Finally, the equation expressing the swing becomes:

$$\dot{Z}_{iN} + \Delta\dot{Z}_i = -2\frac{K_{D_i}}{J_i}\left(Z_{iN} + \Delta Z_i\right) + P_{s_{iN}} + \Delta P_{s_i} + \frac{2}{J_i}\left[\sum_j P_{ij}^{\max}\left(-\sin\sin\left(\theta_{iN} - \theta_{jN}\right) - \Delta\theta_{ij}\cos\cos\left(\theta_{iN} - \theta_{jN}\right)\right)\right] \quad [4.9]$$

The linear swing equation may be divided into two subsystems, one nominal system corresponding to the reference values previously calculated by the power flow and provided by the control center which does not evolve, and the second one called the correction system, rectifying the trajectory for oscillation damping purpose. Of course, the correction system dynamics will depend on the actuators capabilities at each substation. Consider only the correction system given by:

$$\begin{cases} \Delta\dot{Z}_\iota = -2\frac{K_{D_1}}{J_1}\Delta Z_1 + \Delta P_{s_1} + \frac{2}{J_1}(-\Delta\theta_{12}P_{12} - \Delta\theta_{13}P_{13}) \\ \Delta\dot{Z}_2 = -2\frac{K_{D_2}}{J_2}\Delta Z_2 + \Delta P_{s_2} + \frac{2}{J_2}(\Delta\theta_{12}P_{12} - \Delta\theta_{23}P_{23}) \\ \Delta\dot{Z}_3 = -2\frac{K_{D_3}}{J_3}\Delta Z_3 + \Delta P_{s_3} + \frac{2}{J_3}(\Delta\theta_{23}P_{23} + \Delta\theta_{13}P_{13}) \end{cases} \quad [4.10]$$

In the matrix form, we have:

$$\begin{bmatrix} \dot{\Delta Z}_i \\ \dot{\Delta Z}_2 \\ \dot{\Delta Z}_3 \end{bmatrix} = -2 \begin{bmatrix} \frac{K_{D_1}}{J_1} & 0 & 0 \\ 0 & \frac{K_{D_2}}{J_2} & 0 \\ 0 & 0 & \frac{K_{D_3}}{J_3} \end{bmatrix} \begin{bmatrix} \Delta Z_1 \\ \Delta Z_2 \\ \Delta Z_3 \end{bmatrix} + 2 \begin{bmatrix} \frac{-P_{12}}{J_1} & 0 & \frac{-P_{13}}{J_1} \\ \frac{P_{12}}{J_2} & \frac{-P_{23}}{J_2} & 0 \\ 0 & \frac{P_{23}}{J_3} & \frac{P_{13}}{J_3} \end{bmatrix} \begin{bmatrix} \Delta\theta_{12} \\ \Delta\theta_{23} \\ \Delta\theta_{13} \end{bmatrix} + \begin{bmatrix} \Delta P_{s_1} \\ \Delta P_{s_2} \\ \Delta P_{s_3} \end{bmatrix} \quad [4.11]$$

Even so, $\begin{bmatrix} \frac{-P_{12}}{J_1} & 0 & \frac{-P_{13}}{J_1} \\ \frac{P_{12}}{J_2} & \frac{-P_{23}}{J_2} & 0 \\ 0 & \frac{P_{23}}{J_3} & \frac{P_{13}}{J_3} \end{bmatrix}$ is a singular matrix, thus we cannot perform the control law. A standard solution is to fix a bus of reference, in our case bus 1, in which the reference angle equals to the measured angle and the variation angle is canceled. That is $\Delta\theta_1 = 0$.

Consequently, the angles become:

$$\Delta\theta_{12} = \Delta\theta_1 - \Delta\theta_2 = -\Delta\theta_2$$

$$\Delta\theta_{13} = \Delta\theta_1 - \Delta\theta_3 = -\Delta\theta_3$$

and,

$$0 = P_{s_1} + \frac{2}{J_1}(\Delta\theta_2 P_{12} + \Delta\theta_3 P_{13}) \quad [4.12]$$

Substituting into the correction system, we obtain:

$$\begin{cases} \dot{\Delta Z_2} = -2\frac{K_{D_2}}{J_2}\Delta Z_2 + \Delta P_{s_2} + \frac{2}{J_2}(-\Delta\theta_2(P_{12} + P_{23}) + \Delta\theta_3 P_{23}) \\ \dot{\Delta Z_3} = -2\frac{K_{D_3}}{J_3}\Delta Z_3 + \Delta P_{s_3} + \frac{2}{J_3}\left(\Delta\theta_2 P_{23} - \Delta\theta_3(P_{13} + P_{23})\right) \end{cases} \quad [4.13]$$

The matrix equivalent form of the correction system:

$$\begin{bmatrix} \dot{\Delta Z_2} \\ \dot{\Delta Z_3} \end{bmatrix} = -2 \begin{bmatrix} \frac{K_{D_2}}{J_2} & 0 \\ 0 & \frac{K_{D_3}}{J_3} \end{bmatrix} \begin{bmatrix} \Delta Z_2 \\ \Delta Z_3 \end{bmatrix} - 2 \begin{bmatrix} \frac{P_{12}+P_{23}}{J_2} & \frac{-P_{23}}{J_2} \\ \frac{-P_{23}}{J_3} & \frac{P_{13}+P_{23}}{J_3} \end{bmatrix} \begin{bmatrix} \Delta\theta_2 \\ \Delta\theta_3 \end{bmatrix} + \begin{bmatrix} \Delta P_{s_2} \\ \Delta P_{s_3} \end{bmatrix} \quad [4.14]$$

Hence, the proposed feedback control law is:

$$\begin{bmatrix}\Delta\theta_2\\ \Delta\theta_3\end{bmatrix} = \begin{bmatrix}\frac{P_{12}+P_{23}}{J_2} & \frac{-P_{23}}{J_2}\\ \frac{-P_{23}}{J_3} & \frac{P_{13}+P_{23}}{J_3}\end{bmatrix}\begin{bmatrix}K_{1p} & 0\\ 0 & K_{2p}\end{bmatrix}\begin{bmatrix}\Delta Z_2\\ \Delta Z_3\end{bmatrix} \quad [4.15]$$

where K_{1p} and K_{2p} are the tuning gains.

The obtained values in equation [4.15] will be automatically added to control/command signals provided by the control center, between two steady state operation points or when correction to damp the power oscillation is needed.

Consider the power network of Figure 3.10, with disturbance of 1 MW drop occurring in generator 1 at time 2 s. Generator 2 responds immediately (after 0.15 s) to restore the power balance by injecting the missing 1 MW. Simulation results are given in Figure 4.1, highlighting the effectiveness of the proposed control by damping the oscillations initiated by the disturbance. Figure 4.1(b) shows the associated control inputs $\Delta\theta_2$ and $\Delta\theta_3$ which act only when oscillation damping is needed and tend to zero in steady state making sure not to interfere with the voltage position set by the operator.

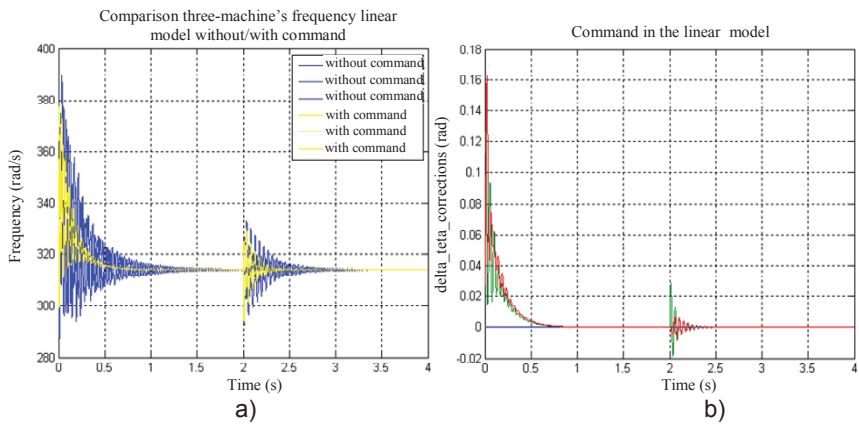

Figure 4.1. *Simulation results of the linear model without/with command. For a color version of the figure see www.iste.co.uk/benchaib/control.zip*

4.3. Free of space-scale model for AC systems: model reduction

One of the particularities of the AC networks is to enable long-distance power transmission. Nevertheless, it is complicated to perform the simulation of such high-order system. To obtain a realistic simulation in time and precision, a judicious model reduction needs to be performed. The aim of this section is to develop an average model representing the N interconnected machines.

4.3.1. *Average model for N stations multi-terminal systems: aggregated power system*

Aggregation of multi-machine power systems based on the center of inertia principle has been proposed in the literature. This technique could present limitations since it considers only the mechanical part of the machines. For networked systems, there always exists a variable that gives an indication on the global behavior and reflects the influence of disturbances. For AC power systems, this variable, which is called the global one, is the frequency (50 or 60 HZ).

PROPOSITION.– The subsystems (or nodes) of a considered system are said to be interconnected if the variations of the global variable at each node are equal to the same value. In the case of AC power systems, the variables concerned are the time derivatives of the angular speed at each machine. That is:

$$\ddot{\theta}_1 = \ddot{\theta}_2 = \cdots = cte = \ddot{\theta}_{average} \qquad [4.16]$$

$\ddot{\theta}_{\text{average}}$ is equal to zero if the system reaches its stable operating points.

This statement (or proposition) will hold for every interconnected system as long as the corresponding global variable is known. For some considered networked systems, finding such a global variable is a research subject in itself.

As frequency is considered to be the global variable in the AC system, we will try to take advantage of such global notions in order to reduce the original model. Apply the proposition above to the linearized swing equation obtained previously:

$$\ddot{Z}_1 = \ddot{Z}_2 = \cdots = cte = \ddot{Z}_{average} \quad [4.17]$$

and suppose that:

$$\sum_{i=1}^{N} Z_i = NZ_{average} \quad [4.18]$$

From equation [4.17], we can obtain:

$$\sum_{i=1}^{N} \dot{Z}_i = N\dot{Z}_{average} \quad [4.19]$$

Considering the linearized model obtained in equation [3.42], we obtain:

$$\sum^{i=1N} \dot{Z}_i = \sum^{i=1N} \left(-2\frac{K_{D_i}}{J_i} Z_i \right) + \sum^{i=1N} \left(\frac{2}{J_i} \left[P_{source_i} + \sum_j P_{ij}^{\max} \sin\sin\left(\theta_j - \theta_i\right) \right] \right) \quad [4.20]$$

Substituting [4.18] and [4.19] into [4.20], we have:

$$\dot{Z}_{moyen} = \sum^{i=1N} \left(-2\frac{K_{D_i}}{J_i} \right) Z_{moyen} + \frac{1}{N} \sum^{i=1N} \left(\frac{2}{J_i} \left[P_{source_i} + \sum_j P_{ij}^{\max} \sin\sin\left(\theta_j - \theta_i\right) \right] \right) \quad [4.21]$$

Suppose $P_{s_i} = \frac{2P_{source_i}}{J_i}$ and $P_{ij}^{max} = \frac{2P_{ij}^{max}}{J_i}$

Thereafter, a global equation for N interconnected nodes representing the AC power system can be expressed as follows:

$$\dot{Z}_{moyen} = \sum^{i=1N} \left(-2\frac{K_{D_i}}{J_i} \right) Z_{moyen} + \frac{1}{N} \sum^{i=1N} P_{s_i} + \frac{1}{N} \sum^{i=1N} \sum^{j=1N-1} P_{ij}^{\max} \sin\sin\left(\theta_j - \theta_i\right) \quad [4.22]$$

The above equation can be identified as the Kuramoto equation to which all the theory developed in this area could be applied. It is also another direction of research that could be treated.

For the simulations, consider the three-nodes power system parameters as given in Table 4.1. The power balance perturbation occurs at 2 s and is cleared 150 ms later.

		Power motor (MW)	Power generator 1 (MW)	Power generator 2 (MW)
Time	t = 0 s to t = 2 s	-3	2	1
	t = 2.0001 s to t = 2.15 s	-4	2	1
	t = 2.150001 s to t = 6 s	-3	2	1
Constants	K_{D_i}	5	5	5
	J_i	1	1	1
	$\frac{K_{D_i}}{J_i}$	5	5	5

Table 4.1. *Simulation data for three interconnected machines*

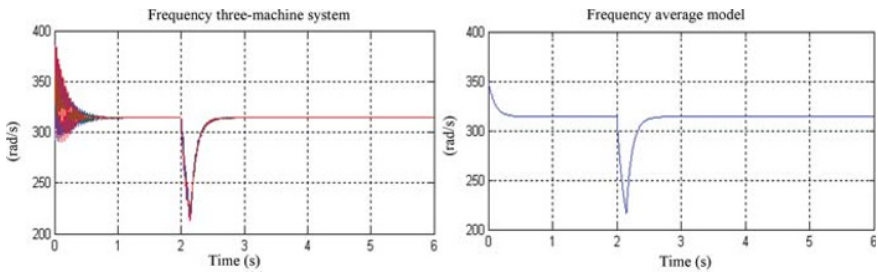

Figure 4.2. *Simulation results for the three-machine system and average model. For a color version of the figure see www.iste.co.uk/benchaib/control.zip*

As shown in Figure 4.2, the average model is quite representative of the multi-machine systems behavior. In the proposed simulation, it has been considered that all parameters are known, which is difficult to obtain in real world. Here again, identification techniques will be of great help.

4.3.2. *Free of space scale model for inter-regions application*

A power network may be separated into many regions synchronized together and with each region having a different operator. Our aim is to

propose a simulation model or tool able to reproduce the interaction between these two areas without considering all the machines inside them. Such interactions are of great interest if one of these areas is subjected to perturbations. Consider two areas region 1 (r_1) and region 2 (r_2) as shown in Figure 4.3. If the power demand of region 1 collapses, it will affect the power network r_2.

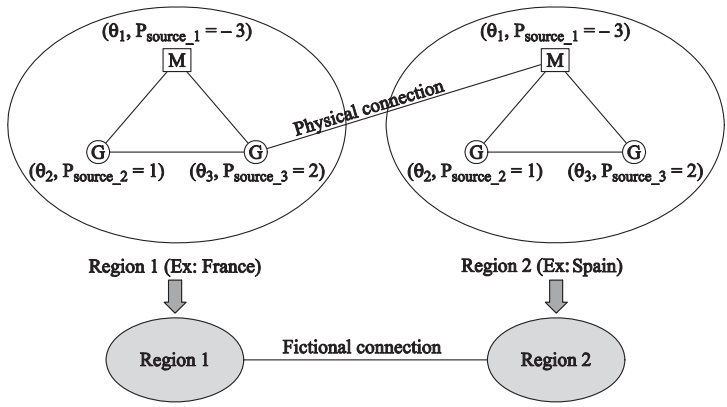

Figure 4.3. *Interconnection of two power systems – regions r_1 and r_2*

According to expression of equation [4.22] and respecting the power exchange, the equations of *the average model* for each area can be written in the following form:

$$\dot{Z}_{r_1} = \sum^{i=1N^{r_1}} \left(-2\frac{K_{D_i}{}^{r_1}}{J_i^{r_1}} \right) Z_{average}^{r_1} + \frac{1}{N^{r_1}} \sum^{i=1N^{r_1}} P_{s_i}{}^{r_1} + \frac{1}{N^{r_1}} \sum^{i=1N^{r_1}} \left(\sum^{j=1N^{r_1}-1} P_{ij}^{\max,r_1} \sin\sin\left(\theta_j^{r_1} - \theta_i^{r_1}\right) \right) + P_{ex}{}^{r_1_r_2} \sin\sin\left(\theta_{average}^{r_2} - \theta_{average}^{r_1}\right) \quad [4.23]$$

$$\dot{Z}_{r_2} = \sum^{i=1N^{r_2}} \left(-2\frac{K_{D_i}{}^{r_2}}{J_i^{r_2}} \right) Z_{average}^{r_2} + \frac{1}{N^{r_2}} \sum^{i=1N^{r_2}} P_{s_i}{}^{r_2} + \frac{1}{N^{r_2}} \sum^{i=1N^{r_2}} \left(\sum^{j=1N^{r_2}-1} P_{ij}^{\max,r_2} \sin\sin\left(\theta_j^{r_2} - \theta_i^{r_2}\right) \right) + P_{ex}{}^{r_1_r_2} \sin\sin\left(\theta_{average}^{r_1} - \theta_{average}^{r_2}\right) \quad [4.24]$$

$P_{ex}^{r_1_r_2}$ is the power exchanged between the two regions. However, using the linear swing equation (exact linearized model), we can define the behavior of each machine in each area by the systems of equation below:

– *Region 1*

$$\dot{Z}_1 = -2\frac{K_{D_1}}{J_1}Z_1 + \frac{2}{J_1}\begin{bmatrix} P_{source,1} + P_{1,2}^{\max}\sin\sin(\theta_2 - \theta_1) \\ +P_{1,3}^{\max}\sin\sin(\theta_3 - \theta_1) + P_{r_1_r_2}\sin\sin\left(\theta_3^{r_2} - \theta_1^{r_1}\right) \end{bmatrix}$$

$$\dot{Z}_2 = -2\frac{K_{D_2}}{J_2}Z_2 + \frac{2}{J_2}\begin{bmatrix} P_{source,2} + P_{1,2}^{\max}\sin\sin(\theta_1 - \theta_2) \\ +P_{2,3}^{\max}\sin\sin(\theta_3 - \theta_2) \end{bmatrix}$$

$$\dot{Z}_3 = -2\frac{K_{D_3}}{J_3}Z_3 + \frac{2}{J_3}\begin{bmatrix} P_{source,3} + P_{1,3}^{\max}\sin\sin(\theta_1 - \theta_3) \\ +P_{2,3}^{\max}\sin\sin(\theta_2 - \theta_3) \end{bmatrix}$$

– *Region 2*

$$\dot{Z}_1 = -2\frac{K_{D_1}}{J_1}Z_1 + \frac{2}{J_1}\begin{bmatrix} P_{source,1} + P_{1,2}^{\max}\sin\sin(\theta_2 - \theta_1) \\ +P_{1,3}^{\max}\sin\sin(\theta_3 - \theta_1) \end{bmatrix}$$

$$\dot{Z}_2 = -2\frac{K_{D_2}}{J_2}Z_2 + \frac{2}{J_2}\begin{bmatrix} P_{source,2} + P_{1,2}^{\max}\sin\sin(\theta_1 - \theta_2) \\ +P_{2,3}^{\max}\sin\sin(\theta_3 - \theta_2) \end{bmatrix}$$

$$\dot{Z}_3 = -2\frac{K_{D_3}}{J_3}Z_3 + \frac{2}{J_3}\begin{bmatrix} P_{source,3} + P_{1,3}^{\max}\sin\sin(\theta_1 - \theta_3) \\ +P_{2,3}^{\max}\sin\sin(\theta_2 - \theta_3) + P_{r_1_r_2}\sin\sin\left(\theta_1^{r_1} - \theta_3^{r_2}\right) \end{bmatrix}$$

As considered in the system of equations above, we can notice that node 1 of area 1 (r1) is connected to node 3 in region 2 (r2). The simulation scenario is given in Table 4.2. Both generators in the two regions are kept with the same power. At the time of 2 s, the motor in region 1 increases its consumption from 3 to 4 MW. Meanwhile, the motor in region 2 decreases its consumption from 3 to 2 MW. The power exchange between the two regions is shown in Figure 4.4 for the nonlinear that is considered here as the reference model and in Figure 4.5 for the average model.

	Time(s)	P_{source_i} (MW)	
Motor	[0 2 2.0001 2.15 2.150001 6]	Region 1 : [-3 -3 -4 -4 -4 -4]	Region 2 : [-3 -3 -2 -2 -2 -2]
Generator 2	[0 2 2.0001 2.1 2.10001 6]	[1 1 1 1 1 1]	
Generator 3	[0 2 2.0001 2.1 2.10001 6]	[2 2 2 2 2 2]	

Table 4.2. *Simulation scenario for inter-region connection*

The frequency of regions 1 and 2 for both nonlinear and average model is given in Figures 4.6 and 4.7. We notice that these curves are quite similar and the method could constitute a useful tool for fast acting power oscillations at local substations.

Figure 4.8 shows the time derivative of the frequency for the two regions. We can remark that just after the disturbance, these two quantities stay in opposition for almost 1 s before vanishing.

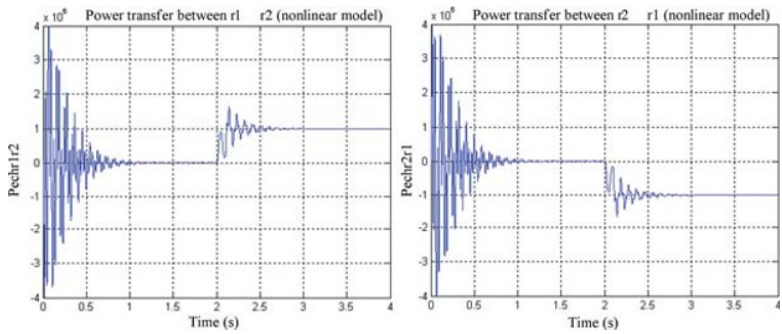

Figure 4.4. *Power transfer between regions 1 and 2 (nonlinear model)*

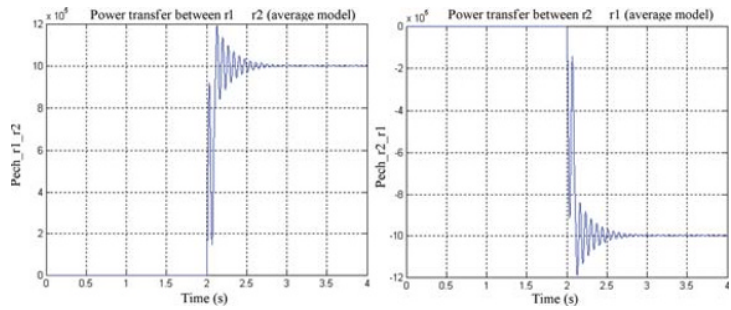

Figure 4.5. *Power transfer between regions 1 and 2 (average model)*

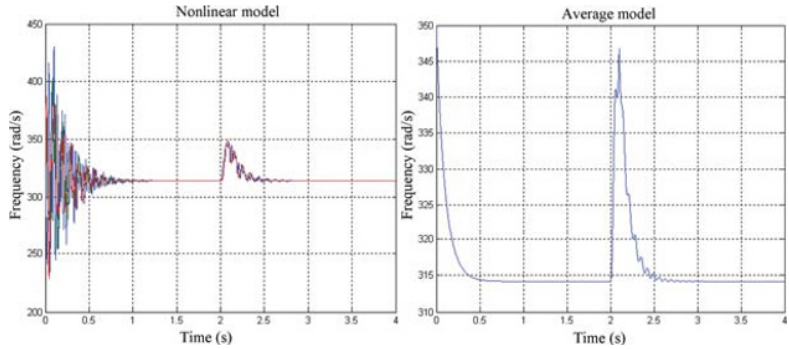

Figure 4.6. *Frequency (rd/s) in region 1: nonlinear model a), average model b). For a color version of the figure see www.iste.co.uk/benchaib/control.zip*

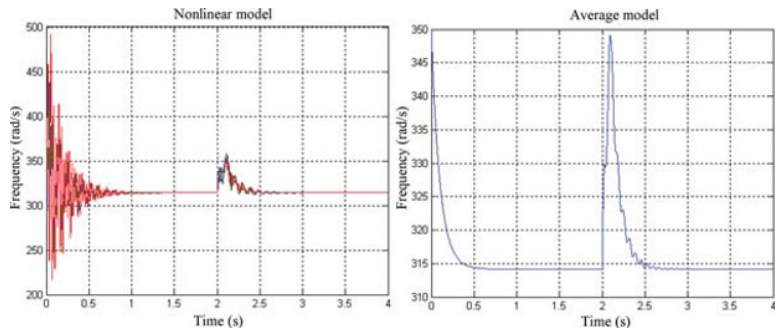

Figure 4.7. *Frequency (rd/s) in region 2: nonlinear model a), average model b). For a color version of the figure see www.iste.co.uk/benchaib/control.zip*

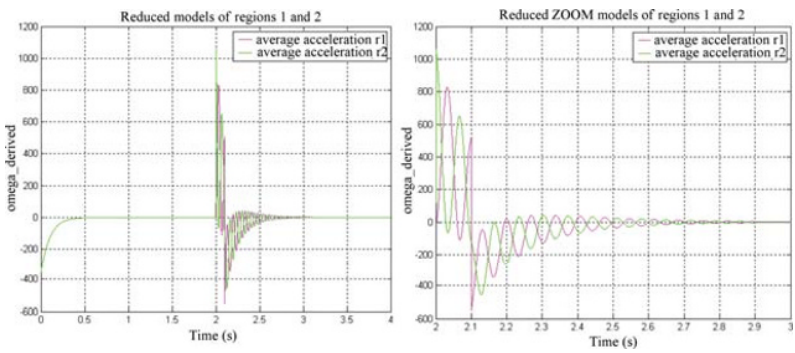

Figure 4.8. *Time derivative of the frequency in regions 1 and 2. For a color version of the figure see www.iste.co.uk/benchaib/control.zip*

This phenomenon is quite similar to what has been shown by research in the Kumamoto concept which states that each region works at its own frequency and the coupling between regions tends to synchronize both regions. If the coupling is weak, we talk about disconnectedness. All tools that have been developed in synchronization of N oscillators can be applied for the obtained average model which could also be treated as "free scale" model. Today, this remains an unresolved problem in power networks.

4.4. Modeling of DC power networks

The high voltage direct current (HVDC) technology is used to transmit electricity over long distances by overhead transmission lines or submarine cables. It is also used to interconnect separate power systems, where conventional AC connections cannot be used. To increase renewable energy (RE) penetration and, more specifically, energy related to wind, multi-terminal HVDC grids are needed. Our aim is to be able to perform the modeling of such systems for local and global purposes. Different types of models will be needed to deal with the control of such systems

4.4.1. *Mathematical approach of two-terminal DC grid modeling*

With reference to [RAU 14], consider a two-terminal DC grid given in Figure 4.9.

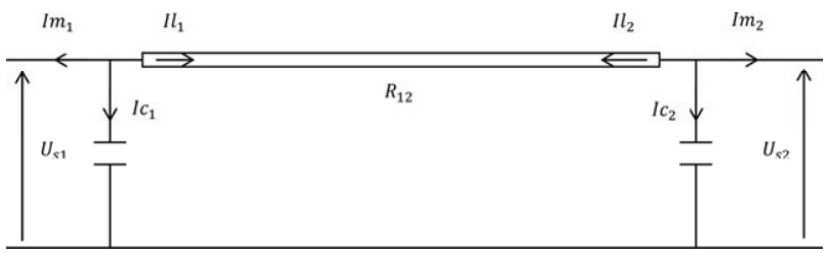

Figure 4.9. *Two-terminal DC grid*

where:

– Imi is the current into the converters;

– Il is the current in the cables between the stations;

– Ic is the current in the capacitors;

– Us is the voltage of the capacitors;

– R is the cable resistance.

Voltage equation for station 1 is given as follows:

$$C_1 \frac{dU_{s1}}{dt} = I_{c1} = -I_{m1} - I_{l1} \quad [4.25]$$

where

$$I_{l1} = \frac{U_{s1} - U_{s2}}{R_{12}} \quad [4.26]$$

In light of [RAU 14], consider the variation of variable around the operation points and define:

$$Im = Im0 + \Delta im$$

$$Il = Il0 + \Delta il$$

$$Us = Us0 + \Delta us$$

where Im0, Il0 and Us0 are the operating points at a steady state (due to the slight difference of voltage potentials in each station (Us0), to transport electrical power from one station to another one), Δim, Δil and Δus are the deviations under a disturbance or a change of operations.

At operating point, we have the relation:

$$C_1 \frac{dUs0_1}{dt} = Ic0_1 = -Im0_1 - Il0_1 \quad [4.27]$$

where:

$$Il0_1 = \frac{Us0_1 - Us0_2}{R_{12}} \quad [4.28]$$

Subtracting equation [4.27] from [4.25] and regrouping with [4.26] and [4.28], we obtain:

$$C_1 \frac{d\Delta us_1}{dt} = -\Delta im_1 - \frac{\Delta us_1 - \Delta us_2}{R_{12}} \quad [4.29]$$

Similarly, voltage deviation equation for terminal 2 is obtained, that is:

$$C_2 \frac{d\Delta us_2}{dt} = -\Delta im_2 - \frac{\Delta us_2 - \Delta us_1}{R_{12}} \quad [4.30]$$

It is evident that the voltage changes in the stations are mainly due to the current flowing through from/to the considered nodes.

4.4.2. *Multi-terminal DC (MTDC) grid modeling: generalized MTDC model*

Consider a three-terminal DC system given in Figure 4.10.

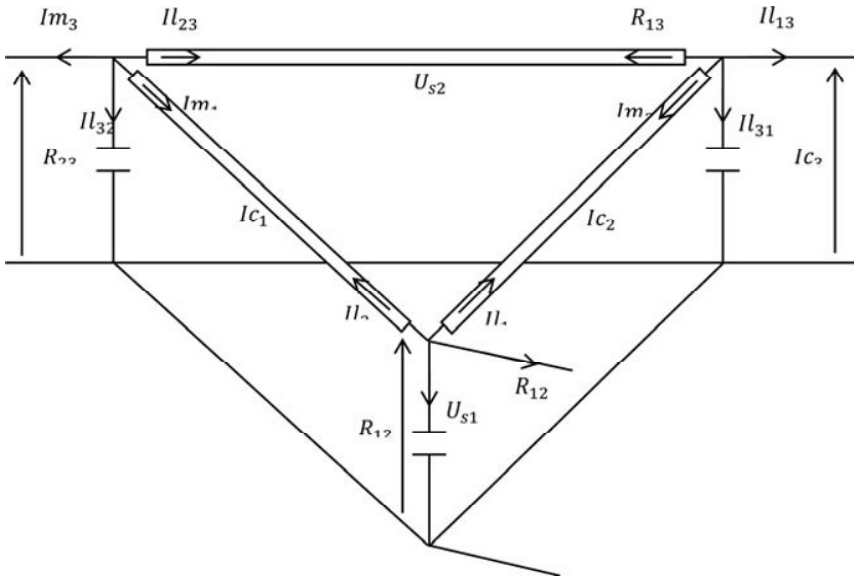

Figure 4.10. *Three-terminal DC grid*

In the base of the current flowing through the nodes, we have:

$$\begin{cases} C_1 \frac{dU_{s1}}{dt} = -I_{m1} - I_{l12} - I_{l13} \\ C_2 \frac{dU_{s2}}{dt} = -I_{m2} - I_{l21} - I_{l23} \\ C_3 \frac{dU_{s3}}{dt} = -I_{m3} - I_{l31} - I_{l32} \end{cases} \quad [4.31]$$

The voltage deviation is also given by:

$$\begin{cases} C_1 \frac{d\Delta us_1}{dt} = -\Delta im_1 - \frac{\Delta us_1 - \Delta us_2}{R_{12}} - \frac{\Delta us_1 - \Delta us_3}{R_{13}} \\ C_2 \frac{d\Delta us_2}{dt} = -\Delta im_2 - \frac{\Delta us_2 - \Delta us_1}{R_{12}} - \frac{\Delta us_2 - \Delta us_3}{R_{23}} \\ C_3 \frac{d\Delta us_3}{dt} = -\Delta im_3 - \frac{\Delta us_3 - \Delta us_1}{R_{13}} - \frac{\Delta us_3 - \Delta us_2}{R_{23}} \end{cases} \quad [4.32]$$

Considering equation [4.32], the voltage deviation of the ith station of an MTDC grid with *n* nodes is then:

$$C_i \frac{d\Delta us_i}{dt} = -\Delta im_i - \sum_{j=1, j\neq i}^{n} \frac{\Delta us_i - \Delta us_j}{R_{ij}} \quad [4.33]$$

Unlike in [RAU 14], where the currents flow between the stations (Il) was neglected, and thus supposing all the voltage changes post faults (Δus) in the stations are the same, in the equation above it is supposed that in transient the voltage deviation at each station could be different.

4.4.3. *Toward DC swing equation*

Even if the dynamics involved in a DC grid are much faster than for AC systems, which is mainly due to the inertia for each technology, our aim is to be able to perform the modeling of MTDC grid with a global variable such as the frequency in AC power system. Such global variables could be good indicators on the health of a DC grid and maybe also help in protection strategies. Again, it is an unresolved problem where a lot of work still needs to be done.

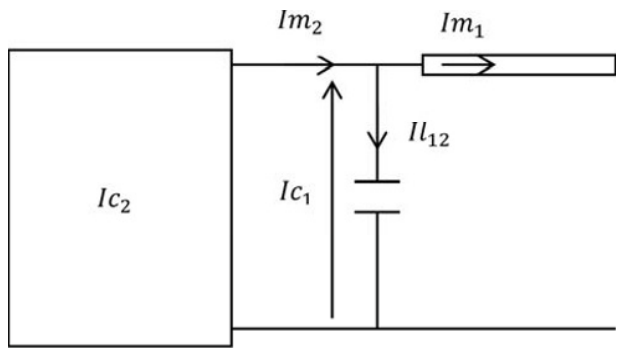

Figure 4.11. *DC station*

Recall the model we previously developed, taking one side of a DC transmission station:

$$C\frac{dU}{dt} = I_c = I_m - I_l$$

Multiplying by voltage U on both sides, we have:

$$CU\frac{dU}{dt} = UI_m - UI_l \quad [4.34]$$

Note that:

$P_m = UI_m$ and $P_e = UI_l$

P_m is the power entering the capacitor node and P_e is the power transmitted to the other nodes.

Multiply equation [4.34] by $\frac{2U_0^2}{2U_0^2}$ to obtain:

$$\frac{2U_0^2}{2U_0^2}CU\frac{dU}{dt} = P_m - P_e \quad [4.35]$$

Consider $H_c = \frac{\frac{1}{2}CU_0^2}{P_{base}}$ as the time constant (in second) of the capacitor, where $\frac{1}{2}CU_0^2$ is its kinetic energy stored at nominal voltage value. As for rotor of electrical machines, assume that this time constant describes a form of rotating energy. Consider then the parameter H_c as the "inertia" (time constant) of the DC system. H_c is usually in ms, where the time constant for AC swing equations is about 3–10 s.

Isolating the H_c term in equation [4.35], we obtain:

$$\frac{2H_c}{U_0^2}U\frac{dU}{dt} = \frac{P_m - P_e}{P_{base}}$$

Thereafter, the equivalent DC swing equation could have the following form:

$$\frac{dU}{dt} = \frac{U_0^2}{2H_cU}(P_{mpu} - P_{epu}) \quad [4.36]$$

4.4.4. *Development of the electric power term P_e*

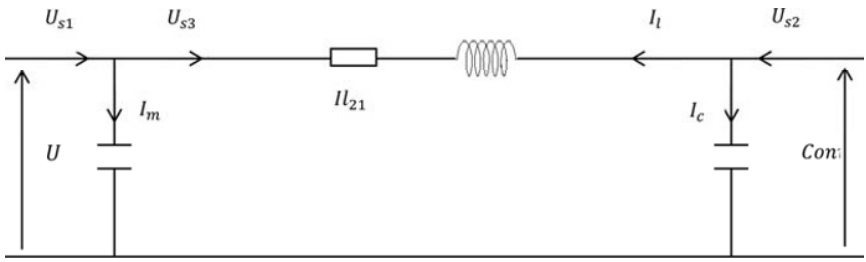

Figure 4.12. *Two-terminal DC grid for electric power term calculation*

In steady state, the power transmitted from one station to another can be described as:

$$P_e = U_i Il_{ij} = U_i \frac{U_i - U_j}{R_{ij}} \quad [4.37]$$

where U_j is the voltage at each station j connected to station i, and R_{ij} is the cable resistance between stations i and j.

However, due to the nature of cable, the inductive effect as well as the capacitive influence cannot be ignored. Considering the cable inductance, we have:

$$U_i - U_j = R_{ij} Il_{ij} + L_{ij} \frac{dIl_{ij}}{dt} \quad [4.38]$$

with $Il_{ij} = -Il_{ji}$.

For multi-terminals DC grid, the transmitted power can be calculated as:

$$P_e = U_i Il_{ij} = U_i \sum_j \frac{U_i - U_j}{R_{ij}} \quad [4.39]$$

4.4.5. *AC and DC "swing equations" equivalence*

In order to establish a parallel between the AC and DC side, some important quantities are summarized in Table 4.3.

We may notice few similarities; as an equivalent structure of each term (powers transmitted, accumulated and dissipated), the damping constant K_{D_i} (or D) could be assimilated to the cable resistance R_{ij} and the constant of inertia J_i could be represented by the DC capacitance C_i.

	Power transmitted	Power accumulated	Power dissipated	Inertia time constant
AC side	$\sum_{\substack{j=1 \\ j\neq i}}^{N_i} P_{ij} = \sum_{\substack{j=1 \\ j\neq i}}^{N_i} P_{ij}^{max} \sin(\theta_j - \theta_i)$	$\frac{1}{2} J_i \frac{d}{dt} (\dot{\theta}_i)^2$	$D\dot{\theta}_i^{\,2}$	$H = \frac{\frac{1}{2} J_i \dot{\theta}_i^{\,2}}{S_{base}^{3\phi}}$
DC side	$\sum_{\substack{j=1 \\ j\neq i}}^{N_i} P_{ij} = \sum_{\substack{j=1 \\ j\neq i}}^{N_i} \frac{1}{R_{ij}} (U_i - U_j) U_i$	$\frac{1}{2} C_i \frac{d}{dt} (U_i)^2$	$\sum_{\substack{j=1 \\ j\neq i}}^{N_i} R_{ij} i l_{ij}^{\,2}$	$H_c = \frac{\frac{1}{2} C_i U_i^{\,2}}{P_{base}}$

Table 4.3. *Similarities between AC and DC systems*

4.5. AC/DC converter control to mimic synchronous generators

High REs penetration, and more specifically the photo-voltaic (PV) type, constitutes the biggest challenge for power utilities to ensure grid stability. The association of these different RE technologies with their associated diversity will fundamentally change the behavior of power systems at regional, national and continental levels. In order to have a coherent and unified direction when considering these RE technologies, the authors in [ZHO 11] propose to control the power electronics (VSC) connected networks by "mimicking" the behavior of synchronous generators including inertia.

The first part of the control enforces the AC/DC converter to mimic a synchronous generator with its associated inertia which has a stabilizing effect (to naturally dampen frequency oscillations when primary control is not yet activated). The second part will make the converter participating to the power system stabilization in coherence with other generators (frequency drooping and regulation of active (real) power, voltage drooping and regulation of reactive power).

Of course, it is supposed that the power (energy) is coming from somewhere else (for example, storage system). The synchronverter is controlled via the electronic scheme of Figure 4.14. It is the signal *e* which will drive the switch of the power part in Figure 4.13 via PWM function.

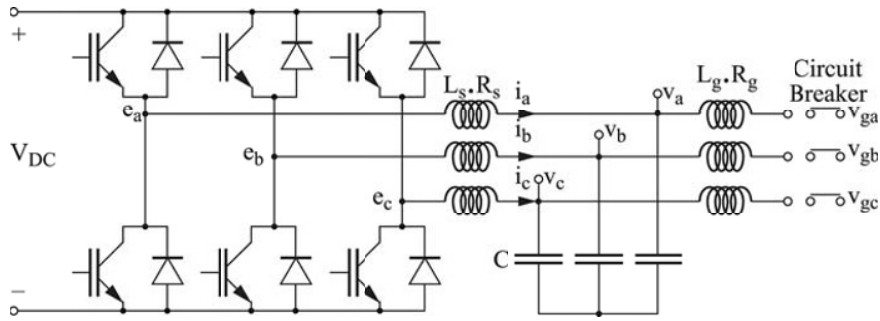

Figure 4.13. *Power part of a synchronverter – a three-phase inverter, including LC filter [ZHO 11]*

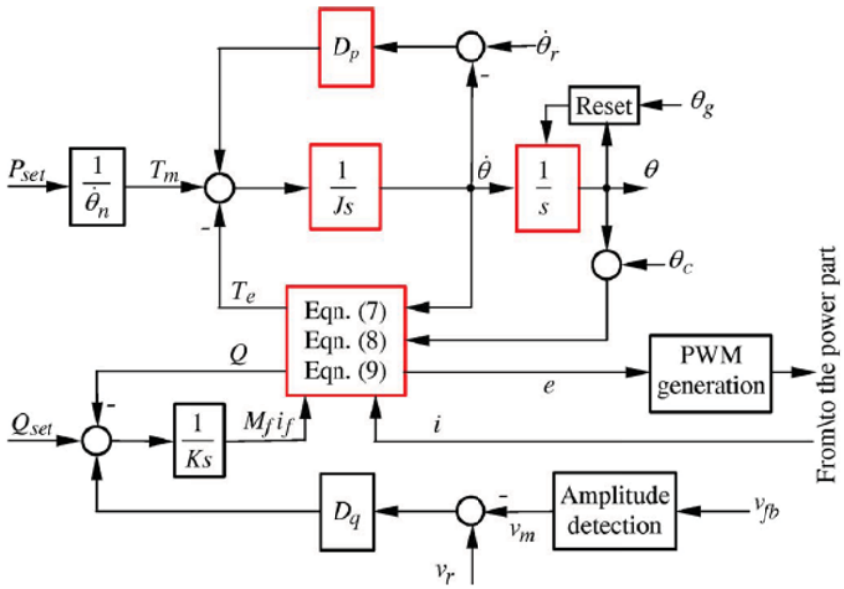

Figure 4.14. *Electronic (control) part of a synchronverter [ZHO 11]*

The proposed concept will certainly contribute in the control, operation and fault recovery of power system. It could constitute a natural continuity between traditional synchronous generators and power electronics-based converters. Therefore, the following features can be highlighted:

– analysis and improvement of stability in power system;

– control of the inertia and link with multi-terminals DC system in hybrid power grid;

– model reduction and equivalent model;

– protection "selectivity" as for synchronous generator in transient stability.

4.6. Concluding remarks

In this chapter, a space dimension of the power network has been overviewed. Taking advantage of the new "exact" linear model obtained in Chapter 3, an inter-area oscillations damping controller has been proposed. Thereafter, a free of space-scale model for an AC system has been proposed. This latter, which was possible to obtain by using averaging techniques, has an interesting use in model reduction and interconnection system analysis. If we want to obtain more accurate models, parameters identification as well as state observation tools must be investigated and developed for power systems (see [TRI 09, OUV 10, KAN 12]). Next, a modeling of DC technology toward what has been developed for AC systems, and especially in a global (or system) approach, has been proposed. The results in this area are still at the beginning and there is a lot of work to perform if we would like to reach the same standards as in AC systems. Finally, and in order to have a complete picture for AC and DC power systems connection via converters, an interesting approach is proposed in the literature for VSCs which are controlled to mimic synchronous generators. This new concept could give the opportunity to vary and control the inertia, damping constants and impedance of this virtual generator. It is an important research direction toward developing hybrid AC/DC power systems.

Conclusion

For over a century, the generation, transmission, distribution and utilization of electric energy has been based principally on alternating current (AC), since Westinghouse's proposal overcame Edison's in the debate of the best technology for power transmission, at the beginning of the era of electricity. Throughout the years, AC power has become more complex and difficult to control since it involves many domains, aspects and actors which are given in the following non-exhaustive list:

– power electronics;

– cables and electric devices;

– production, load and storage;

– communication;

– signal processing;

– automatic control;

– computer science;

– human in the loop;

– policy and regulatory, etc.

AC engineers did a fantastic job to handle the requirements needed to make AC power networks one of the best human inventions. However, the increasing world population, technology advances and environmental issues have driven changes in the energy sector outlook, which have impacted

Advance Control of AC/DC Power Network: *System of Systems Approach Based on Spatio-temporal Scales*, First Edition. Abdelkrim Benchaib.
© ISTE Ltd 2015. Published by ISTE Ltd and John Wiley & Sons, Inc.

national energy policies across the world, associated with the exploitation of renewable energy sources (RESs), giving rise to electricity sector reforms (deregulation).

For now, transmission system operators (TSOs) ensure grid stability with grid codes. Wind power operators, for example, must comply with codes for anti-islanding, power factor control and no-trip low voltage ride-through. However, tighter codes constrain the large-scale grid integration of RES, and calls for more constraints will only further compound matters. More efficient means of transmitting energy must be used. One solution gathering momentum in the R&D community is the high voltage direct current (HVDC) "supergrid".

The concept of multi-terminal DC (MTDC) grids, where DC cables connect more than two AC/DC converter stations, is nowadays spreading driven by different criteria, all necessary for large-capacity RES grid integration, such as larger flexibility of grid operation, the possibility of reversible power flows, increased redundancy and reduction of maximum power loss in case of a grid disturbance.

As shown throughout this book, system of systems was informally developed by AC grid engineers. Today, we are formalizing the concept in DC grids. It is an active example of thinking globally and acting locally. This brings to mind the theory of complex systems. In a school of fish, for example, each fish keeps a certain distance and follows the fish in front (see Figure C.1). The result is that each fish acts like the whole school, while the whole school acts like an individual fish. Systems of systems are naturally occurring forms of organization. They will underpin the 2030 transmission grid in which control will be distributed among the nodes [ALS 14].

To enable plug-and-play behavior in an MTDC system, primary, secondary and even tertiary control functions are used. They operate on different timescales and at different system levels to ensure grid stability. It should be pointed out that in our approach, the control algorithm is considered as a full system. Primary control represents the variation of the power/current injection set-points caused by disturbances in the system. This is different from the local controller of the AC/DC converter, the role of which is to track any set-points. In the "system of systems" approach, a

solution with different timescales has been adopted. The formal plug-and-play property could be formally proposed by working at the junction between systems and control layers (still more work to be performed). Then, it could be possible to get rid of heavy and complex mathematical proofs in order to show the stability of the system. Formal plug-and-play properties could somehow constitute equivalence to the "separation principle" that is used in automatic control for linear systems.

Figure C.1. *School of fish*

However, the spatial dimensions of the considered system could be an additional difficulty for control and stability. There is still much work to do in terms of first understanding the physical phenomena and then modeling (perhaps model reduction) the system. We also need to consider tools and techniques such as communication, measurements, signal processing, observations and estimations, identification, etc.

After reviewing the state of the art, some results have been shown to propose research directions that could be pursued. This work, in formalizing a system of systems approach for DC grids, could be usefully applied to several other fields. My mind goes to the European financial system in which the single currency represents the global variable, “it’s a whole philosophy”.

APPENDICES

Appendix 1

Time Scale Tools: Control Tools Solution for MTDC Complex System with Plug-and-Play Requirements

The work proposed in the following paper[1] proposes a global control strategy for voltage systems control multi-terminal direct current (VSC-MTDC) grid connected to AC network, taking into account not only the DC grid intrinsic dynamics but also interconnected systems and subsystems time variations. This work has been published in the Alstom Think-Grid magazine.

1 http://www.think-grid.org/sites/default/files/MTDC_control_Alstom_Grid.pdf.

Advance Control of AC/DC Power Network: *System of Systems Approach Based on Spatio-temporal Scales*, First Edition. Abdelkrim Benchaib.
© ISTE Ltd 2015. Published by ISTE Ltd and John Wiley & Sons, Inc.

Appendix 2

Swing Equation Programming Code

Inputs

Referred to the swing equations, four groups of inputs are taking into account:

– Nonlinear case: rotor angle *(teta)* in *radian*, rotor speed *(omega)* in *radian/sec*, mechanical power in p.u*(pmpu)* and excitation voltage in p.u.*(E)* of each generator.

– Linear case: rotor angle deviation *(d_teta)* in *radian*, rotor speed deviation *(d_omega)* in *radian/sec*, mechanical power in p.u*(pmpu)* and excitation voltage in p.u.*(E)* of each generator.

The first two groups of inputs can be solved, integrated and feedback from the output of the equation, the last two groups are the same constants with the parameters solved by Powergui in Simpower model.

Outputs

Three groups of outputs are generated, the second time derivative of rotor angles, the electrical power term (Pe) in MW and the difference of rotor angles (d_teta) in deg.

Swing equation parameters

Other than mechanical power and excitation voltage, we are about to determine several constants to adapt to the power balance of the equation due to the parameters settled in Simpower model:

Advance Control of AC/DC Power Network: *System of Systems Approach Based on Spatio-temporal Scales*, First Edition. Abdelkrim Benchaib.
© ISTE Ltd 2015. Published by ISTE Ltd and John Wiley & Sons, Inc.

– $H = \frac{W_{KE}}{S_{base}^{3\emptyset}}$: basic value set in the generator block, in our case, *H=3(s)* for all generators.

– f: stands for friction factor representing the friction torque at nominal speed divided by its speed deviation. Suppose that the machine operates at quasi-nominal speed, we obtain $f = \frac{S_{base}^{3\emptyset}}{\Omega^2} = 21.11\ (N \cdot m \cdot s)$. The obtained value corresponds to the friction factor set in the synchronous machine block, which is "0" (the friction factor is exactly $D = \frac{f}{S_{base}^{3\emptyset}} = 7.04 \times 10^{-6}\ (p.u.)$).

– $Y_{ijp.u.}$: for simplification, the line impedances are symmetric in our system, which implies: $Y_{ij} = \frac{1}{X_{ij}} = \frac{1}{X_{transformer}+X_{transmissionline}+X_q'}$ in p.u. with a same reference current base, which comes from *3MVA 20kV·RMS* in our case.

With the per unit values as:

$$X_{transmissionline\ p.u.}^{new} = X_{transmissionline\ p.u.}^{old} \frac{S_{basenew}}{S_{baseold}} \left(\frac{V_{baseold}}{V_{basenew}} \right)^2 = -0.3306 \text{ p.u.}$$

$$X_{transformer\ p.u.}^{new} = X_{transformer\ p.u.}^{old} \frac{S_{basenew}}{S_{baseold}} \left(\frac{V_{baseold}}{V_{basenew}} \right)^2 = 19.8375 \text{ p.u.}$$

resulting in $Y_{12} = Y_{23} = Y_{13} = \frac{1}{X_{transformer} + X_{transmissionline} + X_q^{'}} = -0.0505 \text{ j p.u.}$

– G_{iipu}: the self-conductance implies the admittance of the synchronous machines themselves, in our case:

$$G_{ii\ pu} = Re\left(\frac{1}{Z_{stator\ p.u.}} \right) = 0.0004\ p.u.$$

With all the parameters settled down, we are able to program our equation in M file.

– Pn_{ipu}: in our case, with three loads in the system, we have to define the nominal active power output for generator 1 and generator 2, and a power for generator 3, which is a swing bus, to compensate the lack of needed power. Referred to Tables 3.2 and 3.5, we have:

$$Pn_{1\ p.u.} = Pn_{2\ p.u.} = \frac{2.2MW}{S_{base}^{3\emptyset}} = 0.733\ \ p.u. Pn_{3\ p.u.} = \frac{P_{L\ total} - 2.2MW - 2.2MW}{S_{base}^{3\emptyset}} = 0.767\ p.u.$$

Simulation results

The initial condition of angles in the Simpower model and nonlinear blocks are set to: $(-48.2194°, -48.2094°, -46.8062°)$. The deviations of rotor angle referenced to δ_1 here are set to: $\delta(0°, -0.01°, -1.4132°)$.

We set here an initial differential rotor speed in generator 3 as well, with $dw_3 = 0.004\%$.

Appendix 3

Kundur's 4-Machines-2-Areas System

The power flow at these specified initial conditions is computed using the PowerGUI solver. Thereafter, the values of mechanical power and excitation voltage in p.u. reference to the base as calculated by PowerGUI are available. These two values (in p.u.) will be useful for the coherency comparison of the obtained swing equations for both nonlinear and linear cases.

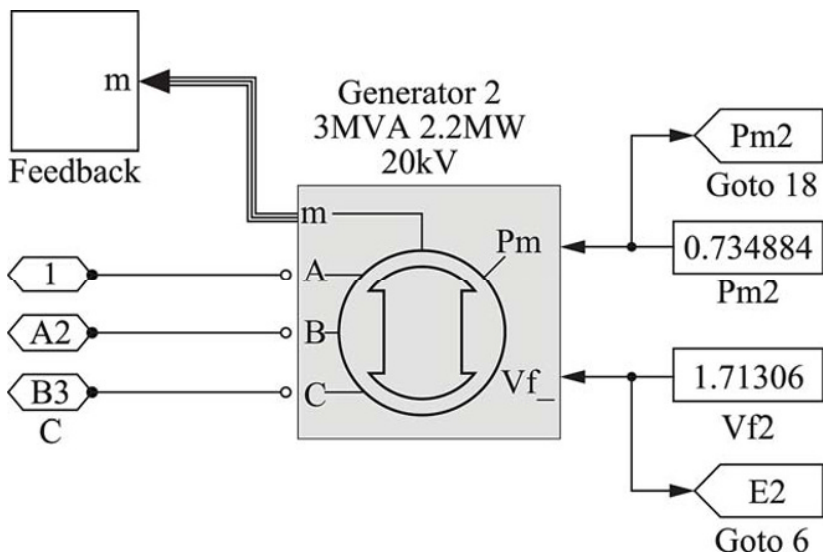

Figure A3.1. *Simulation of generator (2) with Simpower system*

Advance Control of AC/DC Power Network: *System of Systems Approach Based on Spatio-temporal Scales*, First Edition. Abdelkrim Benchaib.
© ISTE Ltd 2015. Published by ISTE Ltd and John Wiley & Sons, Inc.

```
Machine :    Sub system/Generator 3/Generator 3 3MVA 2.2MW 20kV
Nominal :    3 MVA 20 kv rms
Bus Type :   Swing generator
Uan phase :  -6.80°
Uab :        2000 Vrms [1 pu] 23.20°
Ubc :        2000 Vrms [1 pu] -96.80°
Uca :        2000 Vrms [1 pu] 143.20°
Ia :         66.598 Arms [0.769 pu] -10.85°
Ib :         66.598 Arms [0.769 pu] -130.85°
Ic :         66.598 Arms [0.769 pu] 109.15°
P :          2.3013e+006 W [0.7671 pu]
Q :          1.6312e+005 Vars [0.05437 pu]
Pmec :       2.3057e+006 W [0.7686 pu]
Torque :     6116.1 N.m [0.7686 pu]
Vf :         1.7645 pu

Machine :    Sub system/Generator 1/Generator 1 3MVA 2.2MW 20kV
Nominal :    3 MVA 20 kv rms
Bus Type :   P&V generator
Uan phase :  -7.10°
Uab :        2000 Vrms [1 pu] 22.90°
Ubc :        2000 Vrms [1 pu] -97.11°
Uca :        2000 Vrms [1 pu] 142.90°
Ia :         63.66 Arms [0.7351 pu] -11.06°
Ib :         63.66 Arms [0.7351 pu] -131.06°
Ic :         63.66 Arms [0.7351 pu] 108.94°
P :          2.2e+006 W [0.7333 pu]
Q :          1.5202e+005 Vars [0.05067 pu]
Pmec :       2.2041e+006 W [0.7347 pu]
Torque :     5846.4 N.m [0.7347 pu]
Vf :         1.7131 pu

Machine :    Sub system/Generator 2/Generator 2 3MVA 2.2MW 20kV
Nominal :    3 MVA 20 kv rms
Bus Type :   P&V generator
Uan phase :  -7.10°
Uab :        2000 Vrms [1 pu] 22.90°
Ubc :        2000 Vrms [1 pu] -97.10°
Uca :        2000 Vrms [1 pu] 142.90°
Ia :         63.66 Arms [0.7351 pu] -11.05°
Ib :         63.66 Arms [0.7351 pu] -131.05°
Ic :         63.66 Arms [0.7351 pu] 108.95°
P :          2.2e+006 W [0.7333 pu]
Q :          1.5182e+005 Vars [0.0506 pu]
Pmec :       2.2041e+006 W [0.7347 pu]
Torque :     5846.4 N.m [0.7347 pu]
Vf :         1.7131 pu
```

Figure A3.2. *Power flow computation with PowerGUI*

Bibliography

[ALS 14] ALSTOM GRID, "DC system of systems", *Alstom Grid Think-Grid Magazine*, available at http://www.think-grid.org/dc-system-systems, 2014.

[BAC 14] BACHA S., MUNTEANU I., BRATCU A., *Power Electronic Conveter Modeling and Control*, Springer, London, 2014.

[BAH 07] BAHRMAN M., JOHNSON B., "The ABCs of HVDC transmission technologies", *IEEE Power & Energy Magazine*, pp. 32–44, 2007.

[BAJ 08a] BAJRACHARYA C., Control of VSC-HVDC for wind power, Norwegian University of Science and Technology, 2008.

[BAJ 08b] BAJRACHARYA C., MOLINAS M., SUUL J. *et al.*, "Understanding of tuning techniques of converters controllers for VSC-HVDC", *Nordic Workshop on Power and Industrial Electronics*, June 2008.

[BAR 10] BARKER C., WHITEHOUSE R., "Autonomous converter control in a multiterminal HVDC system", *Proc. IET ACDC '10*, London, UK, 20–21 October, 2010.

[BEE 10a] BEERTEN J., COLE S., BELMANS R., "A sequential AC/DC power flow algorithm for networks containing multi-terminal VSC HVDC systems", *Proc. IEEE PESGM'10*, 2010.

[BEE 10b] BEERTEN J., VAN HERTEM D., BELMANS R., "VSC MTDC systems with a distributed DC", *IET ACDC '10*, London, U.K., October 20–21, 2010.

[BEE 11] BEERTEN J., COLE S., BELMANS R., "Implementation aspects of a sequential AC/DC power flow computation algorithm for multi-terminal VSC HVDC systems", *Proc. IEEE PowerTech '11*, Trondheim, Norway, 19–23 June, 2011.

Advance Control of AC/DC Power Network: *System of Systems Approach Based on Spatio-temporal Scales*, First Edition. Abdelkrim Benchaib.

© ISTE Ltd 2015. Published by ISTE Ltd and John Wiley & Sons, Inc.

[BEE 12] BEERTEN J., COLE S., BELMANS R., "Generalized steady-state VSC MTDC model for sequential AC/DC power flow algorithms", *IEEE Transactions on Power Systems*, 2012.

[BEN 04] BENCHAIB A., POULLAIN S., THOMAS J., "Robust DC bus voltage control based Backstepping and Lyapunov methods using Kalman filter and adaptive control for long distance VSC transmission scheme", *ISA (Instrumental Systems & Automation Society) Symposium*, 2004.

[BEN 14] BENCHAIB A., Multi-inputs Multi-outputs DC network modelling and Control, Alstom, Deliverable D1.1.3 (alpha) – Winpower Project – ANR-10-SEGI-016, 2014.

[BON 06] BON-G GU G., KWANGHEE N., "A DC-link capacitor minimization method through direct capacitor current control applications", *IEEE Transactions on Industry,* vol. 42, pp. 573–581, 2006.

[CAR 12] CARDOZO ARTEAGA C.C., Modelling and control of VSC based multiterminal HVDC systems, Master Thesis, Massy, Alstom Grid, 2012.

[CHA 13] CHAUDHURI N., CHAUDHURI B., "Adaptive droop control for effective power sharing in multi-terminal DC (MTDC) grids", *IEEE Transactions on Power Systems*, vol. 28, pp. 21–29, 2013.

[CHE 14] CHEN Y., DAMM G., BENCHAIB A. *et al*., "Control induced explicit time-scale separation to attain DC voltage stability for a VSC-HVDC terminal", *19th World Congress of the International Federation of Automatic Control (IFAC)*, Cape Town, South Africa, August 24-29, 2014.

[COL 10] COLE S., Steady-state and dynamic modelling of VSC HVDC systems for power systems simulation, Katholieke Universiteit Leuven, Leuven, 2010.

[DEB 13] DEBBOU M., ACHOUR T., GILLET J. *et al.*, "From simulation to real-time control for DFIM drive" *IEEE 11th International Workshop of Electronics, Control, Measurement*, 2013.

[DJO 14] DJOUDI A., CHEKIREB H., BERKOUK E. *et al*., "Stability analysis of DFIG stator powers control based on sliding mode approach", *Ninth International Conference on Ecological Vehicles and Renewable Energies (EVER)*, 2014.

[DOB 12] DOBSON I., Complex systems and blackouts, available at http://www.ece.wisc.edu/~dobson/PAPERS/publications.html#COMPLEX, 2012.

[ELO 06] ELOY-GARCIA J., POULLAIN S., BENCHAIB A., "Discrete-time dead-beat control of a VSC transmission scheme including voltage and current limitations for wind farm connection", *EPE-PEMC (12th International Power Electronics and Motion ControlConference)*, 2006.

[ETX 02] ETXEBERRIA-OTADUI I., MANZO V., BACHA S. *et al*., "Generalized average modelling of FACTS for real time simulation in ARENE", *IECON*, 2002.

[FLO 09] FLOURENTZOU N., AGELIDIS V., DEMETRIADES G., "VSC-based HVDC power transmission systems: an overview", *IEEE Transactions on Power Electronics*, vol. 24, pp. 592–602, 2009.

[GHO 12] GHOURABI I., DC power flow for multi-terminal VSCHVDC with a distributed DC Voltage Control, Master Thesis, Alstom grid, 2012.

[GIL 13] GILLET J., DAVID M., MESSINE F., "Optimization of the control of a doubly fed induction machine", *IEEE 11th International Workshop of Electronics, Control, Measurement, Signals and their application to Mechatronics (ECMSM)*, 2013.

[GRI 12] GRIGSBY L., *Power System Stability and Control*, 3rd ed., CRC Press, Florida, 2012.

[HAD 13] HADID B., ETIEN E., OUVRARD R. *et al*., "Soft sensor design for power measurement and diagnosis in electrical furnace: a parametric estimation approach", *Industrial Electronics Society, IECON – 39th Annual Conference of the IEEE (IECON)*, 2013.

[HAI 08] HAILESELAISSIE T., Control of multi-terminal VSC-HVDC systems, Norwegian University of Science and Technology, 2008.

[HAM 00] HAMMONS T., WOODFORD D., LOUGHTAN J. *et al*., "Role of HVDC transmissions in future energy development", *IEEE Power Engineering Review*, pp. 10–25, 2000.

[JIM 15] JIMENEZ M., Systèmes de commande de réseaux électriques multi-terminaux à courant continu – High Voltage Direct Current, PhD thesis, February 2015.

[KAN 12] KANOUN H., GABANO J., POINOT T., "Ultracapacitor identification using continuous lpv fractional modelling", In SYSID', *16th IFAC Symposium on System Identification*, Brussels, Belgium, 2012.

[KOK 99] KOKOTOVIC P.V., KHALIL H.K., O'REILLY J., "Singular perturbation methods in control: analysis and design", *SIAM Classics in Applied Mathematics*, USA, vol. 25, 1999.

[KOS 99] KOSTEREV D., TAYLOR C., MITTELSTADT W., "Model validation for the August 10, 1996", *IEEE Transactions on Power Systems*, vol. 14, no. 3, pp. 967–979, August 1999.

[KUN 94] KUNDUR P., *Power System Stability and Control*, McGraw-Hill, New York, 1994.

[LI 14] LI J., On modelling and control of MTDC grid connected to AC systems, Master Thesis, France, Alstom Grid, 2014.

[MAN 12] MANU PARASHAR J.C., "Wide-area monitoring and situational awareness", in GRIGSBY L., *Power System Stability and Control*, CRC Press, April 2012.

[MEA 07] MEAH K., ULA S., "Comparative Evaluation of HVDC and HVAC Transmission systems", *IEEE 2007 PES General Meeting*, Tampa, Florida, USA, 20–24 June 2007.

[MIL 13] MILASI R., LYNCH A., LI Y., "Adaptive control of a voltage source converter for power factor correction", *IEEE Transactions on Power Electronics*, vol. 28, pp. 4767–4779, 2013.

[NAK 99] NAKAJIMA T., IROKAWA S., "A control System for HVDC transmission by voltage sourced converters", *IEEE Power Engineering Society Summer Meeting*, vol. 2, pp. 1113–1119, 1999.

[OUV 10] OUVRARD R., TOHME E., POINOT T. *et al.*, "Model based on the reinitialised partial moments for initialising output-error identification methods", *IET Control Theory and Applications*, vol. 4, no. 9, pp. 1725–1738, 2010.

[RAU 14] RAULT P., Dynamic modeling and control of multi-terminal HVDC grids, PhD thesis, Ecole centrale de Lille, 2014.

[ROI 13] ROINE L., Using time and space scales for multi-terminal DC grid control and operation in system of systems approach, Master Thesis, Alstom Grid, France, 2013.

[ROO 01] ROOSTA A., GEORGES D., HADJ-SAID N., "Nonlinear control for power systems based on a backstepping method", *Proceedings of the 40th IEEE Conference on Decision and Control*, vol. 4, 2001.

[SHI 14] SHINODA K., Dynamic stability analysis of a multi-terminals HVDC network under faults and impacts onto primary controllers of voltage source power electronic converters, Master Thesis, Super Grid Institute, July 2014.

[SNY 98] SNYDER A., HADJ-SAID N., GEORGES D. *et al.*, "Inter-area oscillation damping with power system stabilizers and synchronized phasor measurements", *POWERCON*, 1998.

[SOO 10] SOOD V., PATEL H., "Comparison between direct and vector control strategy for VSC-HVDC system in EMTP-RV", *IEEE*, *Power Electronics*, *Drives and Energy Systems (PEDES) & 2010 Power India*, pp. 1–6, 2010.

[TEO 11] TEODORESCU R., LISERRE M., RODRIGUEZ P., *Grid Converters for Photovoltaic and Wind Power Systems*, John Wiley & Sons, 2011.

[THO 01] THOMAS J.-L., POULLAIN S., BENCHAIB A., "Analysis of a robust DC-bus voltage control system for VSC transmission scheme", *in Seventh International Conference on AC-DC Power Transmission, IEEE conference*, 2001.

[TRI 09] TRIGEASSOU J., POINOT T., BACHIR S., "Parameter estimation for knowledge and diagnosis of electrical machines", in HUSSON R., *Control Methods for Electrical Machines*, ISTE Ltd., London and John Wiley & Sons, New York, 2010.

[VRA 12] VRANA T., ZENI L., FOSSO O., "Active power control with undead-band voltage & frequency droop for HVDC converters in large meshed DC grids", *European Wind Energy Conference (EWEA)*, Denmark, 2012.

[WIN 80] WINKELMAN J., CHOW J., ALLEMONG J. *et al*., "Multi-time-scale analysis of a power system", *Automatica*, vol. 16, no. 1, pp. 35–43, 1980.

[ZHO 11] ZHONG Q.C., WEISS G., "Synchronverters: inverters that mimic synchronous generators", *IEEE Transactions on Industrial Electronics*, 2011.

Index

A, C, D, H

AC side model, 4, 6–8
control strategies, 18, 20, 21, 31, 45, 52, 53, 56
DC grid modeling, 32, 99–101
Hybrid AC/DC grid, 60, 88

L, M, N, P

linearization, 13, 57
Lyapunov, 8, 63, 66, 67
master/slave strategy, 3, 13, 20–22, 31, 37, 42, 47–52, 56
model aggregation, 87
multi-terminal DC grid (MTDC), 101, 102
Newton–Raphson, 18, 35, 36
power losses, 47, 49
primary and secondary controls, 18, 52, 53, 56

S, T, V

shunt resistance, 5, 32, 33, 41, 46, 47
stability analysis tools, 62–67, 85, 87
swing equation, 57, 87, 89, 92, 96, 102–104
system of systems, 18, 55, 110, 112
time scales tools, 17
VSC system, 2
VSC-MTDC model, 3–8

Advance Control of AC/DC Power Network: *System of Systems Approach Based on Spatio-temporal Scales*, First Edition. Abdelkrim Benchaib.
© ISTE Ltd 2015. Published by ISTE Ltd and John Wiley & Sons, Inc.

Other titles from

in

Electrical Engineering

2015

ROBYNS Benoît *et al.*
Energy Storage in Electric Power Grids

MEYNARD Thierry
Analysis and Design of Multicell DC/DC Converters using Vectorized Models

2014

BOILLOT Marc
Advanced Smart Grids for Distribution System Operators

2013

GALLOT-LAVALLÉE Olivier
Dielectric Materials and Electrostatic

GLAIZE Christian, GENIES Sylvie
Lithium Batteries and Other Electrochemical Storage

PÉRA Marie-Cécile, HISSEL Daniel, GUALOUS Hamid, TURPIN Christophe
Electrochemical Components

2012

BECKERS Benoit
Solar Energy at Urban Scale

FOULADGAR Javad
Electrothermics

GLAIZE Christian, GENIES Sylvie
Lead and Nickel Electrochemical Batteries

ROBOAM Xavier
Systemic Design Methodologies for Electrical Energy Systems

ROBOAM Xavier
Integrated Design by Optimization of Electrical Energy Systems

ROBYNS Benoît *et al.*
Electricity Production from Renewable Energies

SABONNADIÈRE Jean-Claude, HADJ-SAÏD Nouredine
Smart Grids

2011

GAO Fei, BLUNIER Benjamin, MIRAOUI Abdellatif
Proton Exchange Membrane Fuel Cells Modeling

SABONNADIÈRE Jean-Claude, HADJ-SAÏD Nouredine
Electrical Distribution Networks

LOUIS Jean-Paul
Control of Non-conventional Synchronous Motors

LOUIS Jean-Paul
Control of Synchronous Motors

MONMASSON Eric
Power Electronic Converters: PWM Strategies and Current Control

MULTON Bernard
Marine Renewable Energy Handbook

RAZIK Hubert
Handbook of Asynchronous Machine with Variable Speed

TRIGEASSOU Jean-Claude
Electrical Machines Diagnosis

ZAIM Mohammed El-Hadi, REZZOUG Abderrezak
Non-conventional Electrical Machines

2010

BERETTA Joseph
Automotive Electricity / Electric Drive Systems

BRUNET Yves
Energy Storage

DE FORNEL Bernard, LOUIS Jean-Paul
Electrical Actuators / Identification and Observation

JUFER Marcel
Electric Drive / Design Methodology

LE DOEUFF René, ZAÏM Mohammed El-Hadi
Rotating Electrical Machines

MARTINEZ-VEGA Juan
Dielectric Materials for Electrical Engineering

2009

HADJ-SAÏD Nouredine, SABONNADIÈRE Jean-Claude
Power Systems and Restructuring

HUSSON René
Control Methods for Electrical Machines

MOTTIER Patrick
LED for Lighting Applications

SABONNADIÈRE Jean-Claude
Low Emission Power Generation Technologies and Energy Management

SABONNADIÈRE Jean-Claude
Renewable Energy Technologies

2008

CRAPPE Michel
Electric Power Systems

MEUNIER Gérard
The Finite Element Method for Electromagnetic Modeling

2006

PRÉVÉ Christophe
Protection of Electrical Networks